Electrical Receptive Fields and Cortical Activation Spread in Response to Electrical Retina Stimulation. Assessment of Spatio–Temporal Resolution for a Retina Implant.

Dissertation

in partial fulfillment of the
requirements for the degree of

Doctor in Natural Science

by

Marcus Wilms

Department of Applied Physics / Neurophysics
Philipps-University Marburg

December, 2001

Elektrische rezeptive Felder und kortikale Aktivitätsverteilung nach elektrischer Reizung der Retina. Bestimmung der raum–zeitlichen Auflösung für ein Retina Implantat.

Dissertation

zur Erlangung des

Doktorgrades der Naturwissenschaften (Dr. rer. nat.)

dem
Fachbereich Physik
der Philipps–Universität Marburg
vorgelegt von

Marcus Wilms

aus Viersen

Marburg/Lahn im Dezember 2001

Abstract

Goal. Macula degeneration and retinitis pigmentosa are the most frequently diagnosed ailments in blind people. The former is the leading cause of blindness in the western world. To restore some vision to blind patients suffering from these conditions, several research groups jointly aim at developing a micro-electronic prosthesis. The goal is to electrically stimulate neurons in the retina, evoking activity in corresponding cortical neurons and hence pseudo-visual sensations in blind patients. This concept is based on the finding that patterns of simple visual sensations can be elicited in response to epi-retinal pattern electrical stimulation (Humayun et al., 1999). In order for a potential visual prosthesis to be of use to blind people, retinotopic activation of the cortex must be ensured. Moreover, a sufficient spatio-temporal resolution of electrical stimulation is required to provide for a satisfactory perception of a visual scene. As part of the effort in developing the visual prosthesis, prototype implants were tested and detailed studies were performed on the spatio-temporal resolution achievable with electrical retina stimulations.

Methods. At the present state of research, direct testing in human volunteers is ethically not acceptable. Therefore, we studied the spatio-temporal resolution of electrical retina stimulation in the anesthetized cat. We recorded neuronal activity in response to focal visual or electrical stimulation of the retina from visual cortical areas 17 and 18. Visual receptive fields (vRFs) were analyzed for retinal and cortical recording sites using a multi-focal visual stimulation approach. Electrical stimulations were carried out with epi-retinal fiber electrodes and prototype epi- and sub-retinal implants. In analogy to the receptive field concept in the visual domain, we derived electrical receptive fields (eRFs) as well. We compared electrical with corresponding visual RFs in order to assess the retinotopy of electrically evoked cortical activation. The spatial resolution of retinal stimulation was estimated from the location and width of cortical activity distributions (electrical point spread functions, ePSFs). Additionally, the overlap of ePSFs for adjacent retinal stimulation sites was assessed to investigate the retinal separation that may be cortically resolved ("minimum separabile"). Temporal resolution was assessed by the rise times of fastest response components of local field potentials as well as by the dependence between stimulation efficacy and mean rate of electrical stimuli.

Results. Retinal vRFs based on local field potentials match the corresponding retinal electrode locations very well. However, retinal vRFs based on spike activity are shifted distally with respect to the representation of the optic disk (N=7). *Retinotopy:* Cortical eRF-positions are similar to cortical vRF-positions. In particular, the retinotopic arrangement of cortical RFs is preserved for electrical stimulation. Location and width of ePSFs are distinct for retinal stimulation electrodes. *Spatial resolution:* We calculated the average full width at half height of ePSFs for local field potentials to $1.28\,mm\pm0.33\,mm$ cortex corresponding to $1.4°\pm0.4°$ visual angle (N=298, four cats). The width as well as the amount of overlap between ePSFs is smallest (i.e. spatial resolution highest) for near threshold stimulation currents. Minimum separabiles were $0.8°-2.0°$ for near threshold stimulation and $1.6°-4.3°$ for about tenfold threshold stimulation. *Temporal resolution:* Fastest signal components of local field potentials had rise times of $8-12\,ms$, depending on the stimulation current amplitude. Inter-stimulus delays of $16-24\,ms$, corresponding to a $40-60\,imp/s$ mean stimulation rate, should therefore be resolved by the cortex. Mean inter-stimulus times of as short as $12.5\,ms$ evoked significant modulations of cortical activity. Thus, even a stimulation rate of $80\,imp/s$ might be resolved cortically. Spike latencies increased with the mean electrical stimulation rate but hardly depended on the stimulation amplitude. This can be explained by a model of spike initiation that takes into account the relative refractory period of activated neurons. *Prototype testing:* Experiments with epi- and sub-retinal foil electrode arrays proved to be successful in demonstrating efficient and localized cortical activation. However, there is some evidence that epi-retinal electrical stimulation with flat electrodes tends to stimulate axons prior to somata.

Conclusion. The analyses of the width of ePSFs and of minimum separabiles lead to similar estimates for the spatial resolution. Based on these conservative estimates, the best spatial resolution is in the range of $0.8°$ visual angle. This would give the blind patient a visus of $1/48$. Temporal resolution of $40-60\,imp/s$ is achievable. We therefore expect a visual prosthesis based on electrical stimulation of the retina to fulfill the basic requirements of retinotopic activation of the visual cortex at a reasonable spatio-temporal resolution. Clinical experience with other neuro-prostheses (e.g. cochlear implant) indicates that the adjustment of the stimulation parameters in post implantation training can further improve the benefits to a blind patient.

Zusammenfassung

Einführung. Makula Degeneration und Retinitis pigmentosa gehören zu den häufigsten Ursachen für Blindheit. Aus diesem Grunde fördert die deutsche Bundesregierung die Entwicklung einer mikroelektronischen Sehprothese zur Wiederherstellung eines begrenzten Sehvermögens. Angestrebt wird die elektrische Reizung von retinalen Zellen. Dadurch sollen kortikale Neuronen über ihren normalen afferenten Eingangspfad aktiviert und Seheindrücke hervorgerufen werden. Dieses Konzept stützt sich auf die Beobachtung, dass einfache gemusterte Seheindrücke durch gleichzeitige elektrische Reizung an mehreren retinalen Orten ausgelöst werden können (Humayun et al., 1999). Damit die potentielle Sehprothese blinden Menschen einen Nutzen bringen kann, muss eine retinotope Aktivierung kortikaler Neurone gewährleistet werden. Außerdem muss eine ausreichende raum-zeitliche Auflösung von elektrischen Reizen möglich sein, damit der Patient einen befriedigenden Seheindruck hat. Im Rahmen der Entwicklung einer epi-retinalen Sehprothese wurden Implantat-Prototypen getestet und detailierte Studien zur raum-zeitlichen Auflösung elektrischer Reizungen der Retina durchgeführt.

Methoden. Im augenblicklichen Stadium der Forschung sind Funktionsprüfungen an freiwilligen Probanden ethisch nicht vertretbar. Darum wurden die Untersuchungen zur Retinotopie und raum-zeitlichen Auflösung elektrischer Reizungen der Retina an narkotisierten Katzen durchgeführt. Kortikale neuronale Aktivität nach visueller oder elektrischer Reizung der Retina wurde mit Mehrfachelektroden in den Arealen 17 und 18 des Sehkortex abgeleitet. Visuelle rezeptive Felder (vRF) wurden mit Hilfe von multi-fokalen visuellen Reizen für retinale und kortikale Ableitungsorte bestimmt. Elektrische Reize wurden mit epi-retinalen Faserelektroden sowie epi- und sub-retinalen Implantat-Prototypen appliziert. In Analogie zum visuellen rezeptiven Feld Konzept wurden elektrische rezeptive Felder (eRF) ermittelt. Elektrische und visuelle rezeptive Felder wurden verglichen, um die Retinotopie elektrisch evozierter Kortexaktivierung einzuschätzen. Anhand des Ortes und der Breite von kortikalen Aktivitätsverteilungen (ePSF) wurde die räumliche Auflösung bestimmt. Zusätzlich wurde der Überlappungsgrad von kortikalen Aktivitätsverteilungen in Beziehung zum Abstand der retinalen Reizorte gesetzt. Dies erlaubte die Bestimmung des retinalen Abstandes, der kortikal aufgelöst werden kann ("Minimum separabile"). Die zeitliche Auflösung wurde über die

Anstiegsdauer der schnellsten Antwortkomponenten lokaler Feldpotentiale bestimmt. Ausserdem wurde die Abhängigkeit zwischen der mittleren Reizrate und der Reizeffizienz untersucht.

Ergebnisse. Retinale vRFs, die auf lokalen Feldpotentialen basieren, stimmen sehr gut mit den korrespondierenden Elektrodenpositionen auf der Retina überein. Dagegen sind die aus Aktionspotentialen abgeleiteten vRFs oft distal von der Repräsentation des Sehnervkopfes versetzt. *Retinotopie:* Kortikale eRF-Positionen ähneln den kortikalen vRF-Positionen. Überdies ist die retinotope Verteilung kortikaler RFs für elektrische Reizung erhalten. Die Position und Breite von ePSFs sind unterscheidbar für retinale Reizorte. *Räumliche Auflösung:* Die mittlere Breite von ePSFs (volle Breite bei halber Höhe, lokale Feldpotentiale) war $1,28\ mm \pm 0,33\ mm$ Kortex bzw. $1,4° \pm 0,4°$ Sehwinkel (N=298, vier Katzen). Sowohl die Breite als auch die Überlappung von ePSFs sind am kleinsten – die räumliche Auflösung am höchsten – für schwellennahe Reizströme. Minimum separabiles waren $0.8° - 2.0°$ nahe der Reizschwelle und $1,6° - 4,3°$ für etwa zehnfachen Schwellstrom. *Zeitliche Auflösung:* Abhängig von der Reizstromstärke hatten die schnellsten Antwortkomponenten lokaler Feldpotentiale Anstiegszeiten zwischen $8 - 12\ ms$. Reizabstände von $16 - 24\ ms$ entsprechend einer Reizrate von $40 - 60\ imp/s$ sollten deshalb aufgrund der Anstiegssteilheit kortikaler Signale aufgelöst werden können. Mittlere Reizabstände von $12,5\ ms$ vermochten noch signifikante Modulationen kortikaler Aktivität auszulösen. Dies deutet auf kortikal auflösbare Reizraten bis zu $80\ imp/s$ hin. Die Latenzzeit kortikaler Aktionspotentiale steigt mit der Reizrate, ist aber nahezu unabhängig von der Reizamplitude. Dieser Effekt kann mit einem Modell der Aktionspotentialerzeugung erklärt werden, das die relative Refraktärzeit aktivierter Neurone berücksichtigt. *Testung von Implantat-Prototypen:* Mit epi- und sub-retinalen Folienelektroden konnten lokalisierte kortikale Aktivierungen erzeugt werden. Einige Indizien deuten darauf hin, dass flache epi-retinale Elektroden bevorzugt Ganglionzellaxone und nicht Somata erregen.

Schlussfolgerung. Die Analysen von ePSF-Breiten und Minimum separabiles für lokale Feldpotentiale ergaben vergleichbare konservative Einschätzungen für das räumliche Auflösungsvermögen. Es liegt im besten Fall bei etwa $0.8°$ Sehwinkel. Dieses Auflösungsvermögen würde dem blinden Patienten einen Visus von $1/48$ ermöglichen. Eine zeitliche Auflösung von $40 - 60\ imp/s$ erscheint möglich. Es ist daher zu erwarten, dass eine auf elektrischer Retinareizung basierende Sehprothese die Grundanforderungen für eine retinotope Kortexaktivierung bei einer akzeptablen raum-zeitlichen Auflösung erfüllt. Klinische Erfahrungen mit anderen Neuroprothesen (z.B. dem Cochlear Implantat) deuten darauf hin, dass die patientenspezifische Einstellung von Reizparametern nach der Implantation den Nutzen für den Patienten weiter erhöht.

Statement of originality

The animal experiments that provided the data for the investigations in this dissertation were jointly conducted, primarily with Dr. Thomas Schanze and Marcus Eger. The epi-retinal eye surgeries were often performed by PD Dr. med. Lutz Hesse. Sub-retinal surgery was carried out by Dr. med. Helmut Sachs. Except for the implantation of implant prototypes, the author was trained to perform all parts of the experiments self-dependently including animal anesthetics, surgery, intra-cortical recordings, and data analysis.

The author wrote about 30.000 lines of code for the generation and presentation of visual stimuli (in `PASCAL`) as well as for the analysis of recorded multi-channel data (in `IDL 5.4`, Research Systems Inc.). The maintenance and improvement of the data analysis programs were done in inspiring teamwork with Marcus Eger.

Small parts of the Results chapter intersect with a methodological paper submitted by Thomas Schanze, Marcus Wilms, Marcus Eger, and Reinhard Eckhorn. A paper comprising major parts of the results presented in this study is in preparation.

This thesis has not been submitted, either in whole or part, for a degree at this or any other university or institution.

Contents

1 Introduction

1.1 Normal vision

In normal vision, transparent optic structures, such as cornea and lens, focus visual objects sharply onto the retina of each eye. Light quanta traverse the entire transparent, multi-layered retina (0.4 mm thick; Boycott and Dowling, 1969) and are absorbed by rhodopsin molecules in the outer segments of the photoreceptors. In response to the absorption of single light quanta, rhodopsin molecules change their configuration (photo-isomerization) and trigger a cascade of intra-cellular reactions (Wald, 1968). In vertebrates, these ultimately lead to a graded membrane hyper-polarization. Successive retinal neurons, including horizontal, bipolar, and amacrine cells, further process the photoreceptor signal.

At the retinal output stage, ganglion cells generate action potentials ("spikes") from their pre-synaptic inputs. Ganglion cell axons form a layer of their own on top of the ganglion cell soma layer, directly beneath the inner retinal surface. These axons convey spikes towards the optic disk, which in cats is located about 15° nasal and 5° inferior from the area centralis. The area centralis is embedded in the macula region and provides for the highest spatial resolution. The optic disk is the output site of the eye. At this level, axons are equipped with a myelin sheath so that spike conduction velocity is increased (Rodieck, 1973). Myelinized axons form the optic nerves of either eye.

The optic nerves of both eyes terminate in the thalamic dorsal lateral geniculate nucleus ("dLGN"). Here, individual or small groups of optic nerve spikes can trigger the generation of dLGN spikes (Cleland et al., 1971). The dLGN relays incoming information via the optic radiation to the primary visual cortex. Subsequent anatomically or functionally segregated areas of the visual cortex process different stimulus aspects, such as stimulus form, color or movement direction. Besides an extensive divergence and convergence of neuronal connections, a complex network of feedback connections from the primary visual cortex to the dLGN exists as well as feedback from higher visual and non-visual areas (for details see Nicholls et al., 1992).

1.2   Impaired vision

The cortical areas mentioned above are essential for "normal" vision. Thus, impairment of one cortical area can deprive the cortex of a certain stimulus aspect (e.g. "motion"). In fact, studies of visual deficiencies after eye or brain injuries led to a better understanding of the neurophysiological correlates of vision (Zeki, 1993). Severe visual impairment or blindness results from an irreversible damage along the visual pathway. For example, damage may occur at the eye's optics level (e.g. cataract), at the retinal level (e.g. retinal dystrophia), or more centrally at the optic nerve level or in the visual cortex (e.g. brain tumor).

Outer retinal diseases are much more frequently diagnosed than central damage to the visual pathway. Macula degeneration and retinitis pigmentosa are among the diseases most often encountered. The former is the leading cause of blindness in the western world.

Macula degeneration typically leads to a progressive loss of the photoreceptors in the macula region. Central visual acuity is severely diminished as a secondary effect. This often results in legal blindness with only limited residual vision (Beers and Berkow, 2001). Apart from a variety of subtypes, the age-related macula degeneration (AMD) is most significant among the elderly. As the proportion of the elderly will increase significantly in the Western world, an increased incidence of age-related macula degeneration must be expected as well.

Retinitis pigmentosa is less common than age-related macula degeneration but it is the most frequently observed hereditary type of blindness (Zrenner et al., 1992). Apart from impaired night vision, a typical symptom is a mid-peripheral ring scotoma that gradually widens, affecting even central vision up to total blindness in later states of the disease (Beers and Berkow, 2001). Both macula degeneration and retinitis pigmentosa share the common feature of photoreceptor degeneration, leaving parts of the retina insensitive to light. However, despite a substantial loss of cells in all retinal layers, a large percentage of inner retinal neurons remain histologically intact (Santos et al., 1997). In particular, retinal ganglion cells that transmit pre-processed retinal activity to the brain are mostly left intact. The site of the damage restricts the possible methodology of treating the blindness.

1.3   Concepts for substituting visual function

Most concepts for substituting deteriorated visual function are based on the electrical stimulation of the remaining intact visual pathway. Electrical stimuli are meant to mimic normal neuronal inputs to subsequent visual processing. These approaches therefore intend to evoke "pseudo-visual" sensations. The

following paragraphs briefly introduce several of these concepts.

Concepts for substituting visual function after damage to the optic nerve or the Thalamus

If the optic nerve or thalamic level is injured, treatment is restricted to the intact cortical level. One approach is to electrically stimulate neurons in the visual cortex (reviews by Normann et al., 1996, 1999). Pioneering work in this field was done by Brindley and Lewin (1968) and Dobelle et al. (1974). They implanted arrays of 80 and 64 platinum disk electrodes into the sub-dural space over the occipital cortex of blind volunteers. The volunteers perceived small spots of light ("phosphenes"), as individual electrodes were driven by an external current supply. Inspired by their work, Schmidt et al. (1996) utilized penetrating electrodes in order to refine spatial resolution and reduce threshold currents for eliciting phosphene percepts. They found that intra-cortically applied stimuli resulted in a spatial resolution that was five times more accurate than with surface stimulation. Recently, Dobelle (2000) presented a portable artificial vision system based on cortical electrical stimulation with 64 sub-dural electrodes. One volunteer perceived localized phosphenes even though he had been blind for more than 20 years. After familiarizing himself with the implant, he was able to "scan" visual objects and could even count on the fingers of one hand. These results are amazing and encouraging. However, for this cortical stimulation approach, intra-cortical surgery is necessary. This not only increases considerably the risks of infection, but also poses ethical questions of manipulations in the cortex.

Concepts for substituting visual function after damage to the retina

In recent years several approaches were tested to assist blind patients with outer retinal degeneration diseases.

Some research groups focussed on the substitution of retinal function by replacing deteriorated outer retinal cells with intact sub-retinal transplants. Seiler et al. (1999) found that several weeks after the transplantation in rats normal photo-transduction processes were established. This is evidence that it might be feasible to transplant donated human retinal tissue into human eyes, replacing the function of degenerated neuronal cells.

Veraart et al. (1998) electrically stimulated the optic nerve of a blind patient suffering from retinitis pigmentosa. The volunteer perceived colored phosphenes when stimulated electrically, which were similar to those reported in studies with electrical stimulation in the visual cortex. The attributes of the phosphenes usually remained consistent throughout trials repeated over a short period of time.

Early experiments with epi-retinal electrical stimulation in cats were performed by Dawson and Radtke (1977). They were able to assess stimulation thresholds for evoked cortical activity to be in the range of 30–100 μA. Humayun et al. (1994) electrically stimulated the retina of rabbits and evoked localized retinal responses. They found the electrical charge densities at threshold stimulation to be within the safe limits for long-term electrical stimulation (100 μC/cm^2; cited in Humayun et al., 1994). Blind human volunteers reported moving and shaped phosphenes when stimulated epi-retinally with moving or elongated electrodes (Humayun et al., 1996). Moreover, perceptions of simple phosphene patterns could be achieved in response to epi-retinal pattern electrical stimulation (Humayun et al., 1999).

Inspired by these successes, the German government began funding a German Retina-Implant Project (BMFT, grant 01 IN 501 F). Joining their efforts, the research groups participating in the project aim at developing a microelectronic retinal prosthesis based on electrical stimulation of retinal neurons. Reviews were given for epi-retinal (Wyatt and Rizzo, 1996; Eckmiller, 1997) and sub-retinal (Zrenner et al., 1997) implant concepts.

The epi-retinal prosthesis

According to the epi-retinal approach, visual objects located in front of a patient will be "seen" by a small *camera* built into special glasses. An *encoder* performs simulated retinal operations on the video frames in real time and transforms the extracted stimulus information into a digital code (Eckmiller, 1997; Becker et al., 1997). A *sender* will transmit this data stream telemetrically into the eye via optical or inductive coupling. A *receiver* unit, either implanted into an artificial lens for inductive coupling or onto the peripheral retina for optical coupling, will decode image information and integrate stimulation energy from the signal. A *decoder* chip will be implanted into the lens capsule. It is supposed to generate spatio-temporal electrical stimuli from the received signal, and distribute them to epi-retinal *electrode contacts* embedded into a flat and flexible *stimulation unit*. Each retinal electrode contact is supposed to focally stimulate ganglion cells, and thereby transmit visual stimulus information from a well-defined field in visual space to the corresponding retinal representation of the visual field. The proposed retinal implant therefore replaces major optical and intra-retinal functions of the eye while directly generating meaningful retinal output to the cortex.

The sub-retinal prosthesis

In the sub-retinal approach electrical stimulation is applied from the subretinal space (Chow and Chow, 1997; Stett et al., 2000). A micro-photodiode array is implanted at the site of the deteriorated outer retina. When light

falls onto the array's photodiodes, nearby electrodes stimulate preserved inner retinal structures rather than ganglion cells (Santos et al., 1997). The elegance of this concept lies in its simplicity, since a retina encoder, as well as camera, sender, and receiver are obsolete. The pros and cons for the epi- and sub-retinal concept are discussed in more detail in chapter 4.7.

1.4   On this study

The study presented here was carried out as part of the BMBF-funded development of an epi-retinal prosthesis. Therefore, most data stems from epi-retinal electrical stimulation experiments. In some cases, sub-retinal electrical stimulations were performed in cooperation with other groups.

The work was motivated by the challenge to assess the potential benefits for a blind patient equipped with an epi-retinal prosthesis. In order for a potential visual implant to be of use to the blind patient, spatial relationships between stimulation sites must be preserved in their cortical representation (retinotopic stimulation). Additionally, cortical activations must be distinguishable for retinal stimulation sites (specific stimulation). Lastly, a sufficient spatio-temporal resolution of the evoked pseudo-visual perception is required. Knowledge of the stimulation parameters which govern the performance of the retinal prosthesis is influential on its design. Particularly, the spacing (spatial resolution) as well as the stimulus time course for individual electrode contacts (temporal resolution) must be carefully set to save stimulation energy, protect the patient from discomfort, and let the patient actually benefit from the prosthesis.

We studied the cortical representations of focal electrical epi- and sub-retinal stimuli in the cat, namely the spatio-temporal cortical activity distributions in areas 17 and 18 of the visual cortex. From the location, width, and overlap of activity distributions, we estimated the spatio-temporal resolution of electrical retina stimulation. Retinotopy and specificity of electrical stimulation were assessed by comparison of electrically evoked responses to those visually evoked.

Frequently used **abbreviations** as well as a **glossary** of important terms can be found at the end of this document.

2 Methods

2.1 General remarks

The cat experiments were conducted in accordance with the German animal welfare law, the guidelines of the European Community Council Directives (86/609/EEC) and the NIH Principles of Laboratory Animal Care (Publication 86–23, revised 1985). Preparatory and anesthetic procedures were as described in detail in Schanze et al. (2001). In the experiments, it was necessary to estimate distributions of cortical activity at high spatio-temporal resolution. Therefore, cortical activity was measured intra-cortically rather that with scalp electrodes. Electrical stimuli were applied with three types of retinal electrodes. For the in-depth analysis of cortical activity distributions and spatio-temporal resolution, we used an array of seven hexagonally arranged fiber electrodes with cone-shaped tips (Reitböck, 1983). In the framework of the Retina Implant project we tested cortical spread for implant prototypes as well. These were flat and flexible polyimide electrode arrays with either 30 planar electrodes implanted into sub-retinal space or 24 planar electrodes fixated onto the membrana limitans interna. Details on the stimulation electrodes are given in 2.5.1.

2.2 Anesthetic procedures, surgery, and animal care

Fiber electrode stimulation: A craniotomy over areas 17 or 18 of the visual cortex close to the vertical meridian was performed leaving the dura mater intact. Seven or sixteen recording micro-electrodes (Eckhorn and Thomas, 1993) were inserted about 1 mm into (layers 2–4 of) area 17 or 18 of the visual cortex. The electrode pitch was 0.5 mm for 7–electrode arrays and 0.305 mm for 16–electrode arrays. Epi-retinal electrical stimulation with fiber electrodes was performed by inserting a 7–electrode array through a scleral opening approximately 3 mm behind the temporal limbus. The electrodes were hexagonally arranged to provide for a two-dimensional stimulation and to minimize the scleral opening by a dense packing of electrodes (0.9 mm diameter of electrode array). Electrodes could be individually moved forward

and backward in the μm-range. This allowed the precise epi-retinal electrode positioning under visual inspection with an ophthalmoscope.

Epi-retinal implant stimulation: Experiments with epi-retinal polyimide foil electrode arrays (N=2) were performed in cooperation with Dr. med. Lutz Hesse (University Marburg, Eye Department). Eyes underwent a lentectomy and vitrectomy preceding the implantation. Implantation details were reported in more detail in Hesse et al. (2000). After positioning of the electrode structure at the suitable retinal position, the implant's fine wires to external current sources were fixated with tape near the eye lid. The implanted cats then were transferred from the dorsal position for eye surgery to their normal (ventral) position, which is more convenient for the preparation of the intra-cortical recordings. The cats' anesthetics were then maintained with isofluorane (0.5–1.5%, *Forene* by Abbot). Following a craniotomy (7 mm diameter) over the corresponding cortical area, a linear seven micro-electrode array was inserted into area 17. Spacing between recording electrodes was 0.75 mm. Cats recovered after about 1 day post experimentum. The stability of implant function was tested in consecutive experiments.

Sub-retinal implant stimulation: Experiments with sub-retinal polyimide foil electrode arrays (N=2) were performed in cooperation with Dr. med. Helmut Sachs (University Regensburg, Eye Department). Implantation was performed ab interno through a scleral incision approximately 6.5 mm behind the limbus. After a pars plana vitrectomy, the retina was locally elevated by injection of a bubble of *BSS* (a balanced salt solution by Alcon) distally from the target area near the area centralis. The retina then was incised at the distal end of the bubble. Through an additional scleral opening, the implant was advanced forward through the retinal incision towards the required subretinal position (Sachs et al., 1998; Kobuch et al., 1998). The cables of the implant were fixated with *histoacryl* at the scleral insertion site. To facilitate the preparation of the intra-cortical recording, the implanted cats were then moved from the dorsal position for eye surgery to their normal (ventral) position. Anesthesia was maintained with isofluorane. Following a craniotomy (7 mm diameter) over the corresponding cortical area, a linear 7–electrode array was inserted into area 17. Spacing between recording electrodes was 0.75 mm.

After experiments with sub-retinal polyimide foil electrode arrays and a few experiments with fiber electrodes (N=4), animals were sacrificed with an intra-venous injection of a curare derivative (*T61* by Hoechst Roussel Vet). Eyes were enucleated for histological analyses of the effects of electrical stimulation to the retinal tissue (e.g. for RCS-rats: Kohler et al., 2001). The acute experiments with fiber electrodes lasted for 47–84 hours. When animals were allowed to recover, experiments lasted for 10–20 hours.
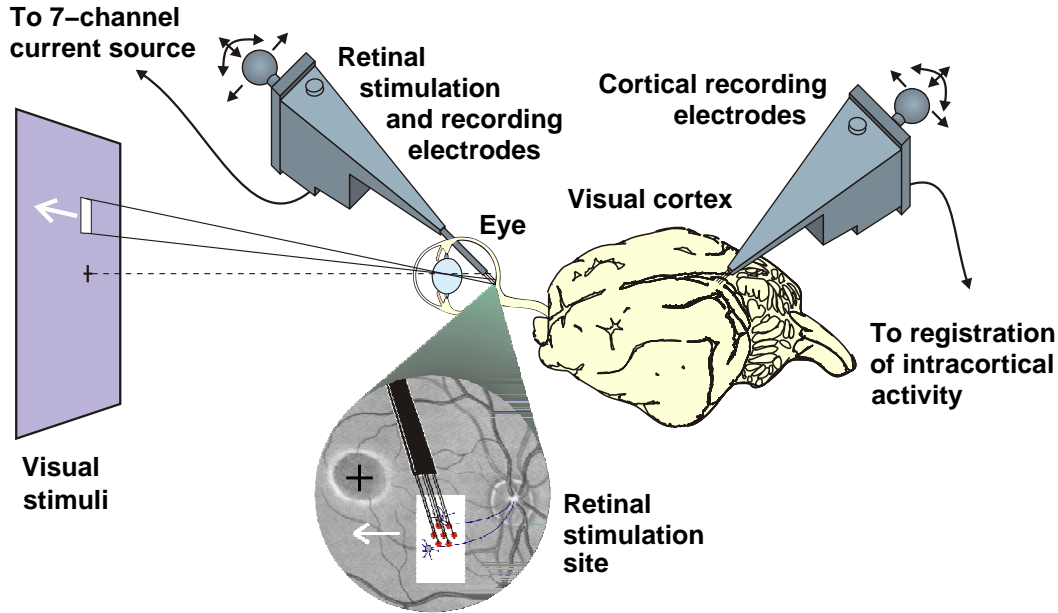
Figure 2.1: Setup for epi-retinal visual and electrical stimulation and intra-cortical recording in cat visual cortex (modified from Schanze et al., 2001).

2.3   Data recording and pre-processing

The experimental setup (Fig. 2.1) is described in Schanze et al. (2001). During the experiments, vital functions of the cat such as ECG, body temperature, and expiratory CO_2 content were monitored. Only if vital functions were normal and stable, data were recorded and considered for analysis.

Fiber Pt-W electrodes with 2–3 MΩ impedance at 1 kHz (Reitböck, 1983) were used for the recording of intra-cortical activity. Seven or sixteen electrodes were linearly arranged in a matrix which allowed electrodes to be moved individually back and forth (Eckhorn and Thomas, 1993). Recording electrodes were positioned over the cat's visual cortex area 17 or 18, typically at Horseley-Clarke positions A2–P5 and L0.5–L3 (area 17) or A3–P5 and L1–L5 (area 18). Recording electrodes were inserted into the cortex leaving the dura mater undamaged in all but one case. The insertion of each electrode was controlled by an audio signal from the electrode.

Generally, pre-amplified signals from the cortical recording electrodes were amplified and filtered to obtain local field potentials (LFP, low-pass filtered to 1–140 Hz, -3 dB at 12 dB/oct), multi-unit activity (MUA, 0.5–10 kHz band passed, full wave rectified and then low-pass filtered to 1–140 Hz, -3 dB at 12 dB/oct), and single unit activity (SUA, 0.5–10 kHz band passed, -3 dB at 12 dB/oct and subsequent window discrimination with 2 ms hold-off). These

signals were recorded at 500 Hz sampling rate using an AD-converter (CED 1401 Cambridge Electronic Design, maximum sampling rate 100 kHz) and stored on a personal computer hard disk for further off-line data analysis. The pitch of the cortical recording electrodes was chosen

- to be less than half that of the typical width of cortical activity distributions in order to detect them (spatial sampling theorem) and

- wide enough to sample a certain cortical space with a limited number of electrodes.

When the 7–electrode cortical recording matrix was used, electrode pitch was chosen to be 0.5 mm, thus sampling 3 mm of cortex. With the 16–electrode cortical recording matrix, electrode pitch was lowered to 0.305 mm, thus sampling 4.575 mm of cortex at higher spatial resolution.

2.3.1 Suppression of stimulation artifacts

The electrical stimulation inevitably induces strong electrical artifacts that are volume conducted to the cortical recording sites. The impulse response of the recording filters then occludes neuronal activity of short latencies depending on the stimulation current amplitude, duration and the filter characteristics. In order to assess neuronal activity with latencies below 10 ms (primarily early SUA and MUA), we recorded broad-band signals (1–4000 Hz) at 20 kHz sampling rate. In the broad-band signal, the recorded stimulation artifacts were temporally more constrained because of the higher cutoff frequency. Due to the AD-converter bandwidth of 100 kHz, five channels could be recorded at a time. After the experiment, stimulation artifacts were camouflaged in the broad-band data by substituting artifact data samples by 1–2 ms samples of adjacent time windows.

In some experiments, we used the 16–electrode cortical recording matrix and did not sample broad-band signals. We intentionally sacrificed the detection of early cortical responses for a higher spatial resolution available with 16 densely spaced recording electrodes.

2.3.2 Pre-processing of broad-band recording data

Local field potentials (LFP) and multi unit activity (MUA) were generated off-line by convolution of the artifact suppressed broad-band signal with the impulse responses of the laboratory hardware filters (Eger, 2001).

Extraction of single unit activity (SUA) from neuronal recordings is an intricate task. One electrode usually records the superposition of spike activities from several neurons. However, while recorded spikes are uniformly sized and/or shaped for individual neurons, the recorded spike form differs for

different neurons due to the variable distance to the recording electrode. This can be used to differentiate between the contributions of individual neurons by analyzing the form of spikes. The quality of this kind of "spike sorting" depends on the signal-to-noise ratio of the recording as well as on the amount of temporal overlap of spikes (Abeles and Goldstein, 1977). We extracted SUA from high-pass filtered (500–1000 Hz) artifact suppressed broad-band data using an amplitude thresholding approach: First, local data peaks of a certain width were detected by the analysis of the first and second derivatives of the signal time series. In a second step, the peaks were sorted into ranges of amplitudes and stored into event data files. However, it cannot be ruled out that one sorted spike population comprised more than one spiking neuron. Within this limitation, these neuronal units were regarded as "SUA".

To illustrate how delicate the task of spike sorting can be, Fig. 2.2 shows a 40 ms sequence of a high pass filtered cortical responses to multi-focal visual stimulation. The diagram depicts signal deflections ("spikes") of different shape and amplitude. However, these spikes code different stimulus attributes, as revealed by a cross-correlation analysis between separated spike trains and the stimulus (for explanations refer to section 2.4).

Fig. 2.3 illustrates the results of artifact elimination, off-line LFP generation, high pass filtering, off-line MUA generation as well as spike detection. Shown are averaged cortical responses (PSTHs) to electrical stimuli with Gamma distributed inter-stimulus intervals. Note the strong stimulation artifact in the first two milliseconds of the *recorded broad-band signal* after the stimulus onset. The first cortical response can already be observed as a positive signal deflection ("spike") after 3.4 ms time to peak (i. e. time between stimulus onset and maximum response signal deflection). A second response is seen at 5.0 ms time to peak and probably a third one at 6.3 ms time to peak. The peaks at latencies of 9.4 ms and later are averaged stimulation artifacts of consecutive stimuli. The cortical response in the *artifact suppressed signal* is unchanged. Note that the stimulation artifacts at latencies of 9.4 ms and later disappeared. Spikes are highlighted in dark yellow, and low frequency signal components in light blue. Low-pass filtering of the artifact suppressed signal yields the *LFP* signal. LFPs were inverted so that neuronal excitation can be observed as downward signal deflections. High-pass filtering of the artifact suppressed signal (*HP signal*) is the basis for the generation of the *MUA* signal as well as for spike detecting and sorting. Black arrows in the LFP and MUA signal point at the maximum of first excitatory response components. The LFP and MUA signal is shifted with respect to the broad-band signal due to the causal filter operations. The spikes detected in each trial are marked in piled rows in the *spike raster plot*. Note the cluster of spikes at the position of the second response (5.0 ms time to peak). The first response (3.4 ms time to peak) was harder to detect in the broad-band data. Spike frequency does
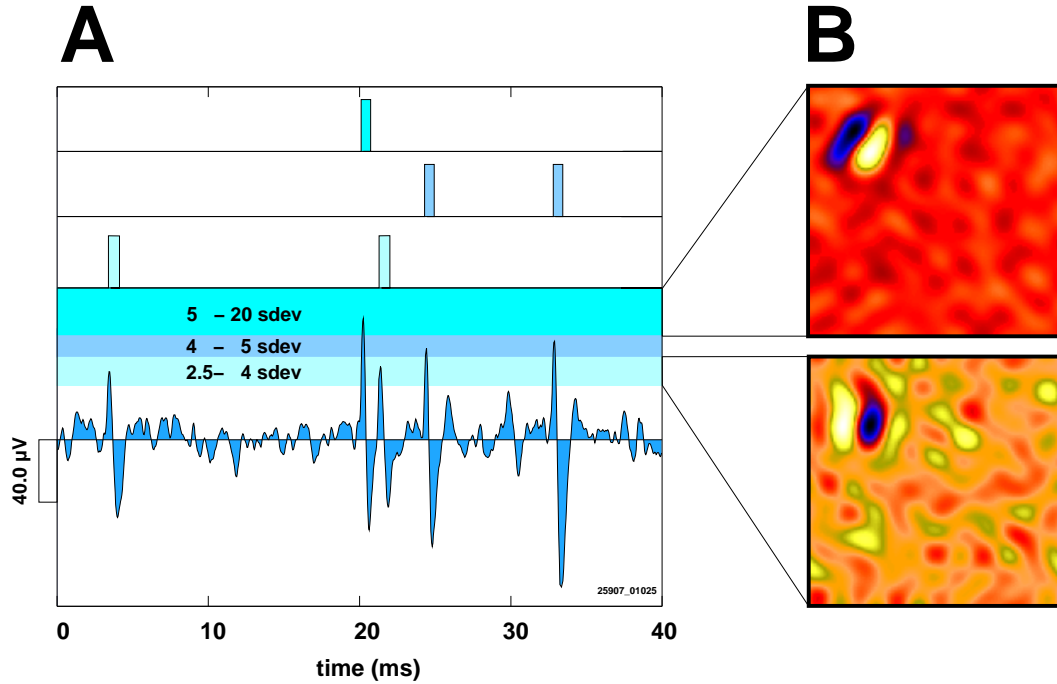
Figure 2.2: Spike sorting separates "one" cortical broad-band signal into three SUA components. **A)** 40 ms sequence of high-pass filtered cortical responses to multi-focal visual stimulation exhibits spiking activity of different recording amplitudes. The spikes are sorted into three single units by amplitude thresholding to multiples of the signal standard deviation (*sdev*). **B)** A subsequent cross correlation analysis between the separated spike trains and the visual stimulus reveals distinct visual receptive field properties (switched polarities and different orientations) for two of the separated spike populations.

not change within the entire duration of the measurement indicative of nearly stationary recording conditions. Therefore, the *spike frequency* histogram does not obscure time-variant cortical SUA.

2.4   Visual receptive field measurement

Visual receptive fields (vRFs) of retinal and cortical neurons can be assessed by probing the neuron's responsiveness to short flashes of single small light spots at densely spaced positions in visual space. This concept corresponds to a linear system identification task. In noiseless technical systems, the system's response to a single stimulation impulse fully describes the transfer function of the system. Even though the retina and cortex are non-linear systems (e.g. due to neuronal threshold mechanisms) recorded population responses behave in a more linear way since they comprise a linear superposition of
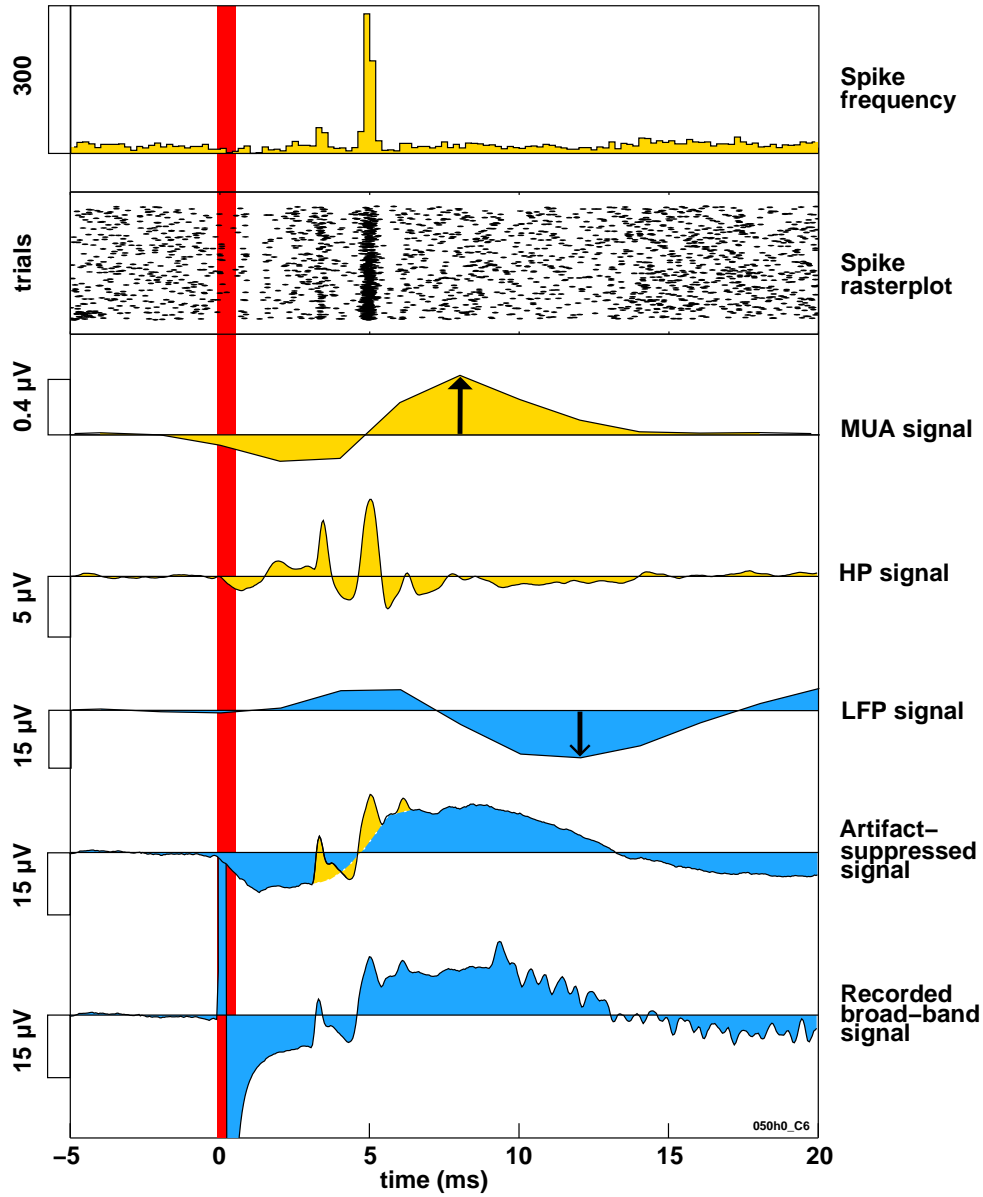
Figure 2.3: Demonstration of the different steps of data processing by averaged cortical responses. Electrical stimuli with Gamma distributed inter-stimulus intervals were applied at 39.7 imp/s mean stimulation rate (N=5100, 40 μA single biphasic stimuli, 0.4 ms duration). **From bottom to top:** *Recorded broad-band signal*. The cortical response is unchanged in the *artifact suppressed signal*. Averaged spikes are highlighted in dark yellow and low frequency signal components in light blue. *LFP signal*, the *HP signal*, and *MUA signal* are generated by off-line filtering of the artifact suppressed broad-band signal. Black arrows in the LFP and MUA signal point at the first excitatory response components. The spikes detected in every trial are marked in consecutive rows in the *spike raster plot*. Frequencies of detected spikes can be estimated by the *spike frequency* histograms.

many neuronal processes. Therefore a linear approximation is valid for the estimation of receptive fields of population responses. Moreover, recordings from neurons show an extensive background activity which is not related to the visual stimulus. Therefore, averaging of impulse responses is necessary to yield the deterministic stimulus–response relation. In practice, the estimation of vRFs is performed reversely since one is interested in the stimulation history preceding a neurons' response (Bialek et al., 1991). On the contrary, forward approaches focus on the response following the stimulus.

In our experiments, a set binary pseudo random sequences drives the luminance at certain coordinates on a computer monitor in front of the animal (Eckhorn et al., 1993). For the study presented here, two standard procedures were developed: "sparse noise" and "dense noise" stimuli based approaches.

2.4.1 The "sparse noise" approach

In the "sparse noise" approach, two-dimensional visual stimuli ("frames") consisted of single ("sparse") rectangular light spots on a dark background. The position of the light spot changed randomly every 40 ms. Thus, after some time, every position on the monitor had been active in one stimulation cycle time. Repetitions of this cycle were used to enhance the signal-to-noise ratio of the cross correlation maps between stimulus and response. The advantage of this approach is that the stimulus energy is high, due to the strong luminance contrast of the light spot against the dark background. However, if the spatial resolution of the stimuli is increased, i.e. more spot positions per length are allowed, the cycle time increases quadratically with the resolution enhancement. Moreover, if the spot size is reduced, the stimulus energy decreases, requiring more repetitions of the stimulation cycle. In addition, with just one active light spot at a time, spatial interactions between multiple stimulus positions, i.e. higher order cross correlations cannot be studied.

2.4.2 The "dense noise" approach

In the "dense noise" approach, multi-focal ("dense") visual stimulation was used (see inset in Fig. 2.6). Stimulation was at up to 101 Hz and maximum contrast of a 21 inch computer monitor positioned at a distance of 130 cm in front of the animal. Multi-focal pseudo random stimuli were based on binary m–sequences (Sutter, 1987, 1992; Reid et al., 1997; Reich et al., 2000; Sutter, 2001) and were generated using a feedback shift register algorithm (Williams and Sloane, 1976; Borish and Angell, 1983). Each square light spot (about 1° side length) on an imaginary 28x28 grid was driven by a cyclically shifted version of the same pseudo-random m–sequence of 4095 steps. For that reason, approximately one half of all grid positions were active in each stimulus frame.

The grid dimension was set to 28x28 in order to allow a cyclical shifting step width of five (28*28=784 starting positions equally distributed on the 4095 stimulus frames of one m–sequence). Thus, starting positions for m–sequences at any two grid positions were separated by multiples of five time steps, i.e. by multiples of about 50 ms when the stimulation was at 101 Hz. Since response durations are generally longer than 50 ms, starting positions for m–sequences were randomly addressed to grid positions. Due to the randomized addressing and the fact that autocorrelations of m–sequences are zero at all non-zero shifts (Williams and Sloane, 1976), spatio-temporal contiguousness of stimuli was very low. Each multi-focal m–sequence was presented up to 45 times (total duration 30 min) to improve averaged cross correlations between stimulus and response. However, in cases of good recording signal-to-noise ratio (e.g. $S/N > 4$), a single presentation was sufficient to assess RF-centers and -sizes, reducing the measurement time to 41 s. Cross correlations between stimulus (m–sequence) and response yielded vRFs for each recording channel. The use of cyclically shifted sequences at all grid positions considerably reduced the expense for calculating the cross correlations between all pairs of recording and stimulation channels (Reid et al., 1997).

One advantage of the "dense noise" approach is that in principle, a nearly complete characterization of the vRFs is possible since the temporal stimulus statistics are "white" for every spot location. Cross correlations between stimulus sequences have peaks at temporal delays that are beyond the systems' memory for most pairs of stimulation sites. Moreover, the cycle time does not depend on the spatial resolution of the stimulus grid, making it more appropriate for high spatial resolution tasks. However, "dense noise" stimuli are much less effective in driving cortical neurons (Orban, 1984). The enormous amount of stimulus presentations at each spot position compensates for the much lower stimulus effectivity. E.g., for the 28x28 stimulus grid and a given stimulation duration, in the m–sequence based "dense noise" approach each spot position is stimulated 392 times more often than in the "sparse noise" approach.

2.4.3   Visualization of visual receptive fields

In the experiments, monocular vRFs were coarsely estimated with a hand held lamp projected onto a tangent screen. For the detailed and standardized estimation of basic vRF-properties such as position, size, and subfield structure, the "dense noise" approach was used more often than the "sparse noise" approach. The "dense noise" approach was preferred mainly because of the higher spatial resolution. Apart from the spatial resolution, however, both approaches gave similar results, when directly compared in the experiments.

Fig. 2.4 illustrates the procedure of calculating vRFs. In this example,
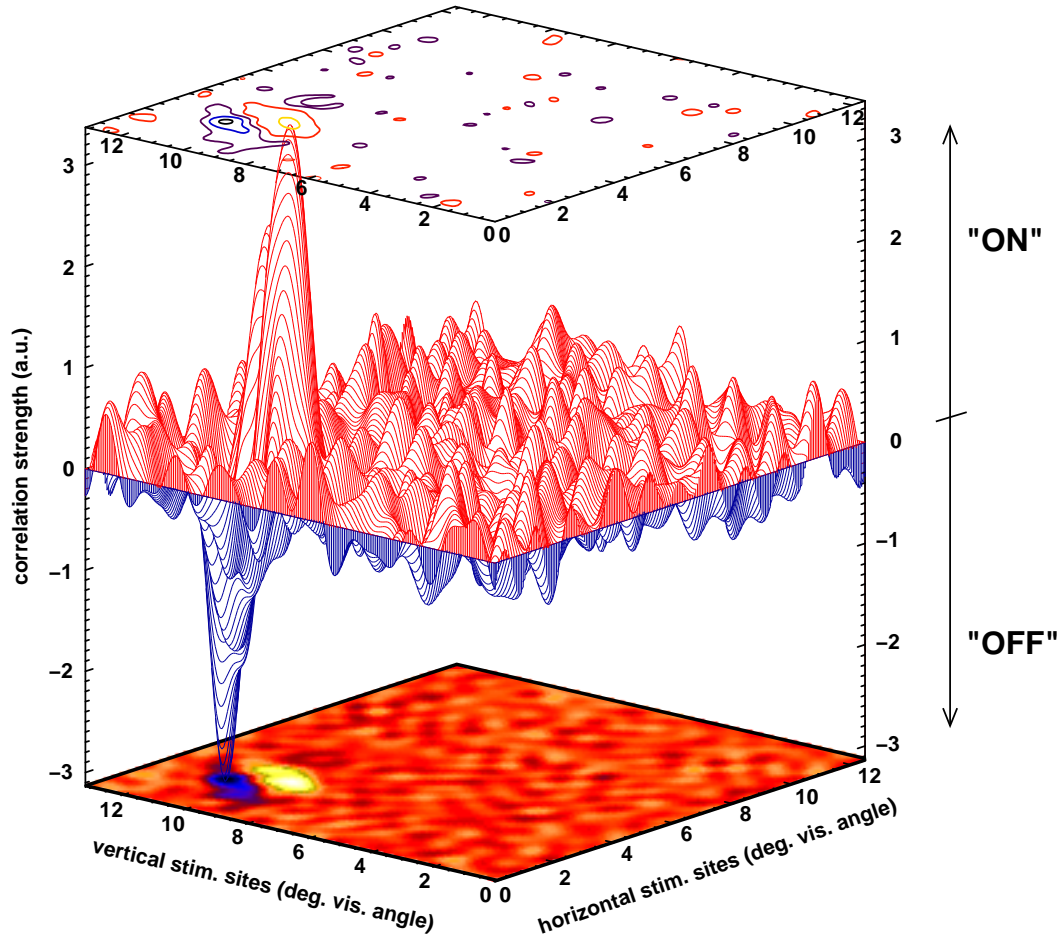
Figure 2.4: Visualization of a visual receptive field. Cortical MUA was recorded in response to a multi-focal visual stimulus. The correlation strength between the stimulus and cortical MUA exhibits localized excitatory "ON" (positive peak and bright colors) and inhibitory "OFF" (negative peak and dark colors) subfields.

cortical MUA was recorded in response to a multi-focal visual stimulus given at 25 Hz. One stimulation cycle of 4095 stimuli was presented in 164 seconds. The mean cross correlation strength (temporal lag 30–40 ms) between a visual stimulus sequence and the cortical response was plotted for each stimulation site (horizontal and vertical stimulation site). The initial spatial sampling of 28x28 visual stimulation sites was eightfold interpolated by zero-padding in the frequency domain (Elliott and Rao, 1982) in order to yield a smoothed vRF structure at a 224x224 resolution. Negative correlation values indicate that the cortical response was anti-correlated to the respective visual stimulus sequence. In other words, at negative peak positions, the cortical response was correlated with the complement of the binary sequence, i.e. the "OFF"-stimulus. On the contrary, high positive correlation values indicate that the
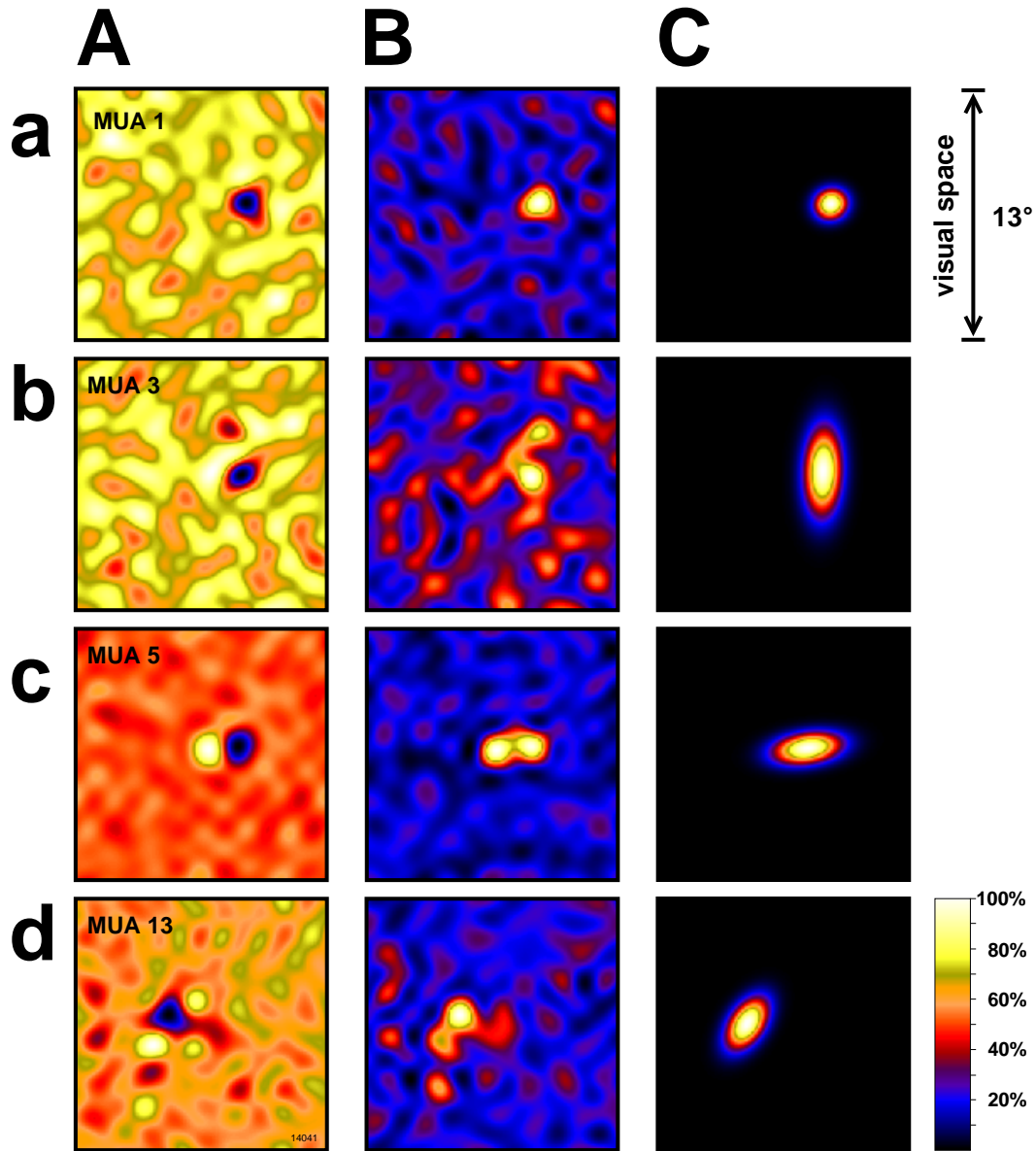
Figure 2.5: Visual receptive fields (vRFs) of four cortical multi unit responses (MUA, **a–d)**) after visual stimulation (centered about 7.5° below area centralis, N=92160 at each grid position, T=30 min) with a multi-focal visual pseudo-random stimulus. Stimuli were based on binary m–sequences given at 101 Hz frame rate on a computer monitor. Correlation strength between stimulus site and response is color-coded for each map separately. **A)** Cross correlation maps for the two-dimensional stimulus sequence and four cortical responses. The maps were interpolated and low pass filtered to pronounce the receptive field structures. Note the bimodal topography most prominent in MUA 5. **B)** Rectified vRF-maps. **C)** Fitting two-dimensional Gaussian envelopes into the rectified vRF-maps allows the estimation of vRF-center and -size of bimodal vRFs.

recorded cells primarily respond to "ON"-stimuli.

Correlation strengths are color-coded in the bottom plane of the plot. This type of plot visualizes the spatial structure of vRFs, in particular the existence of bipolar ON/OFF-profiles ("subfields"). Visual receptive subfields are indicative of simple cells which prefer a localized and oriented edge of light. To obtain the position and -size of vRFs with subfields, vRF-maps were rectified and then fitted with two-dimensional Gaussian envelopes (Fig. 2.5).

On top of Fig. 2.4, contours of selected cross correlation levels appear as closed lines. This vRF-representation was used to compare vRF-locations for multiple recording electrodes. For this purpose, contours at a 90% level of the vRF-amplitude were superimposed for all available recording electrodes. Fig. 2.6 demonstrates this technique for an experiment where 15 recording electrodes were available. Visual RFs could be calculated for 11 electrodes in this example.

By recording retinal activity with the stimulation electrodes, vRFs were estimated for the retinal stimulation sites as well. A comparison of the relative locations of retinal and cortical vRFs indicated whether cortical activation was expected to be close to or distant from cortical recording sites. In addition to the vRF-center and vRF-size, orientation and direction of movement tuning was estimated using computer controlled bright bar stimuli.

2.5 Electrical stimulation

2.5.1 Stimulation electrodes

Retinal electrical stimuli were applied extracellularly in close proximity to the neuronal target cells. When during a stimulus pulse an electrical charge is passed, the working potential across the metal/electrolyte interface changes. This brings into play electrochemical reactions at the interface which are determined by the voltage, the electrolyte composition, as well as the metal type and surface structure of the stimulation electrode (Loeb, 1989; Kossler, 1998). Tissue-destroying reactions (e.g. forming of gaseous H_2 or O_2) have to be excluded so that stationary stimulation conditions and a long-term stable electrical stimulation can be guaranteed (McCreery et al., 1995, 1997). In order to control the actual electrical charge injected by the electrode, we used biphasic, charge-balanced current pulses.

Three types of electrical stimulation electrodes were used (Fig. 2.7). For the in-depth analysis of cortical activity distributions and spatio-temporal resolution of electrical retina stimulation, we used quartz-isolated platinum-tungsten fiber electrodes (Fig. 2.7 A). Fiber electrodes had cone-shaped tips of 20–25 μm diameter and 200–500 kΩ impedance at 1 kHz (Reitböck, 1983). Seven fiber
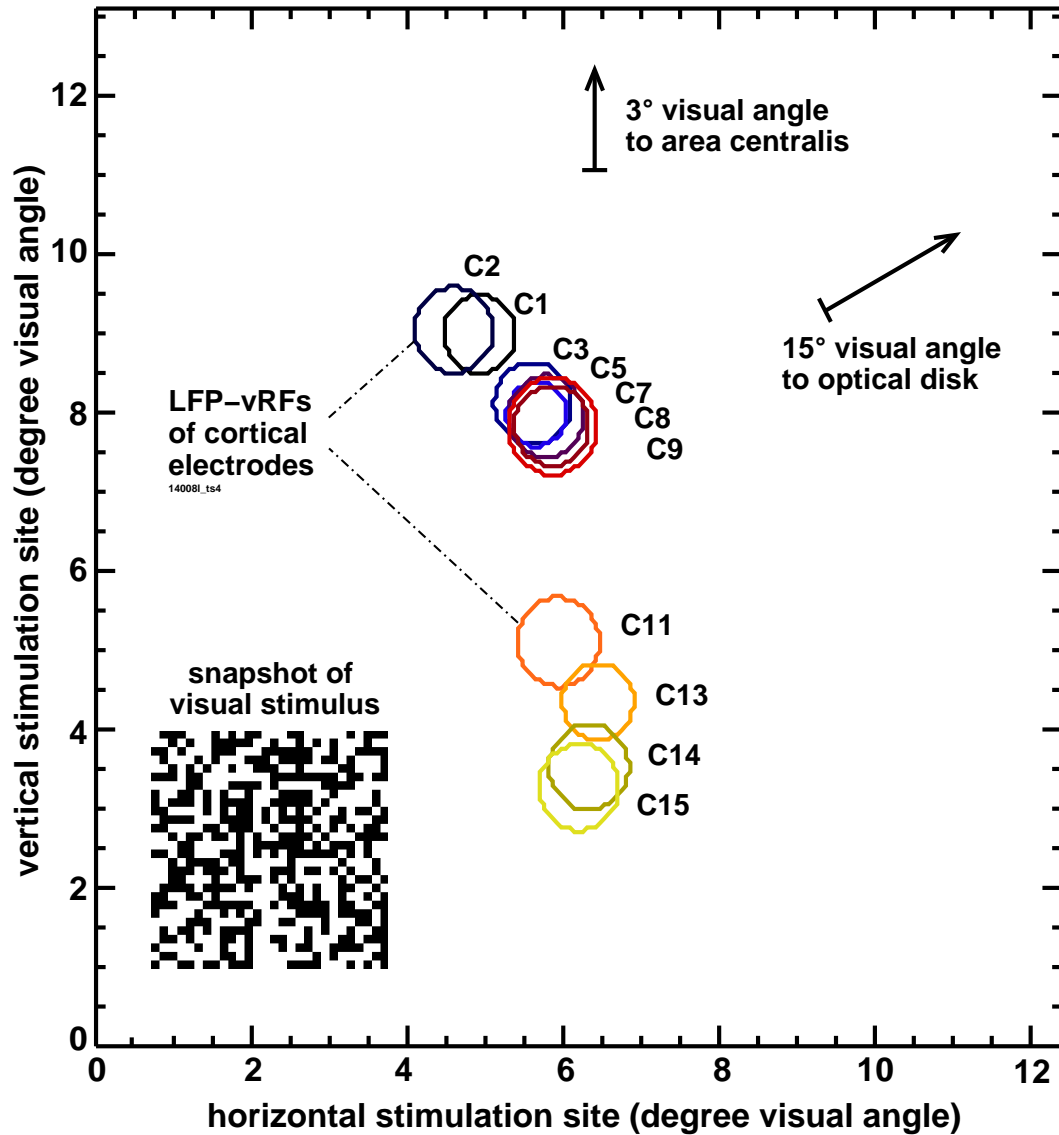
Figure 2.6: Visual receptive fields (vRFs) generated from multiple cortical population responses (LFP, C1–C15) to visual stimulation with a multi-focal pseudo-random stimulus (centered about 7.5° below area centralis, N=92160 at each grid position, T=30 min). The coordinate system demarcates the region in visual space covered by the visual stimuli. One of the 4095 different stimuli is plotted to the lower left. Area centralis was approximately at 6.5° horizontal and 14° vertical with respect to the coordinate system. Circles indicate positions of vRFs for the cortical recording sites. Visual RFs are drawn as contours on a 90% level of respective Gaussians fitted to the cross correlation maps between stimulus and response.

electrodes were hexagonally arranged in a matrix similar to the recording electrode matrix. Each retinal electrode could be individually moved back and forth. Additionally, the whole matrix could be moved spherically around the electrodes' point of insertion into the eye (Schanze et al., 1998). The electrodes were advanced towards the retina under visual inspection with an ophthalmoscope. In addition, an audio control of the electrode signal was available during electrode positioning. When the electrode touched the retinal surface, vigorous spike activity was regularly observed in response to the fundus light of the ophthalmoscope. Retinal stimulation electrodes had to be carefully positioned in close proximity to the retinal receptive fields of the cortical recording electrodes (area 17/18 vRFs of para-central eccentricities have a diameter of approximately $1° − 3°$ corresponding to 0.2–0.6 mm on the retina). Additionally, tight electrode contact to the retina was crucial for effective stimulation. Elevating the electrode tip by 50 μm from the retinal surface reduced the response strength to 50% (Schanze et al., 2001). In each experiment with fiber electrodes, at least two different retinal stimulation areas were tested by shifting the electrode array.
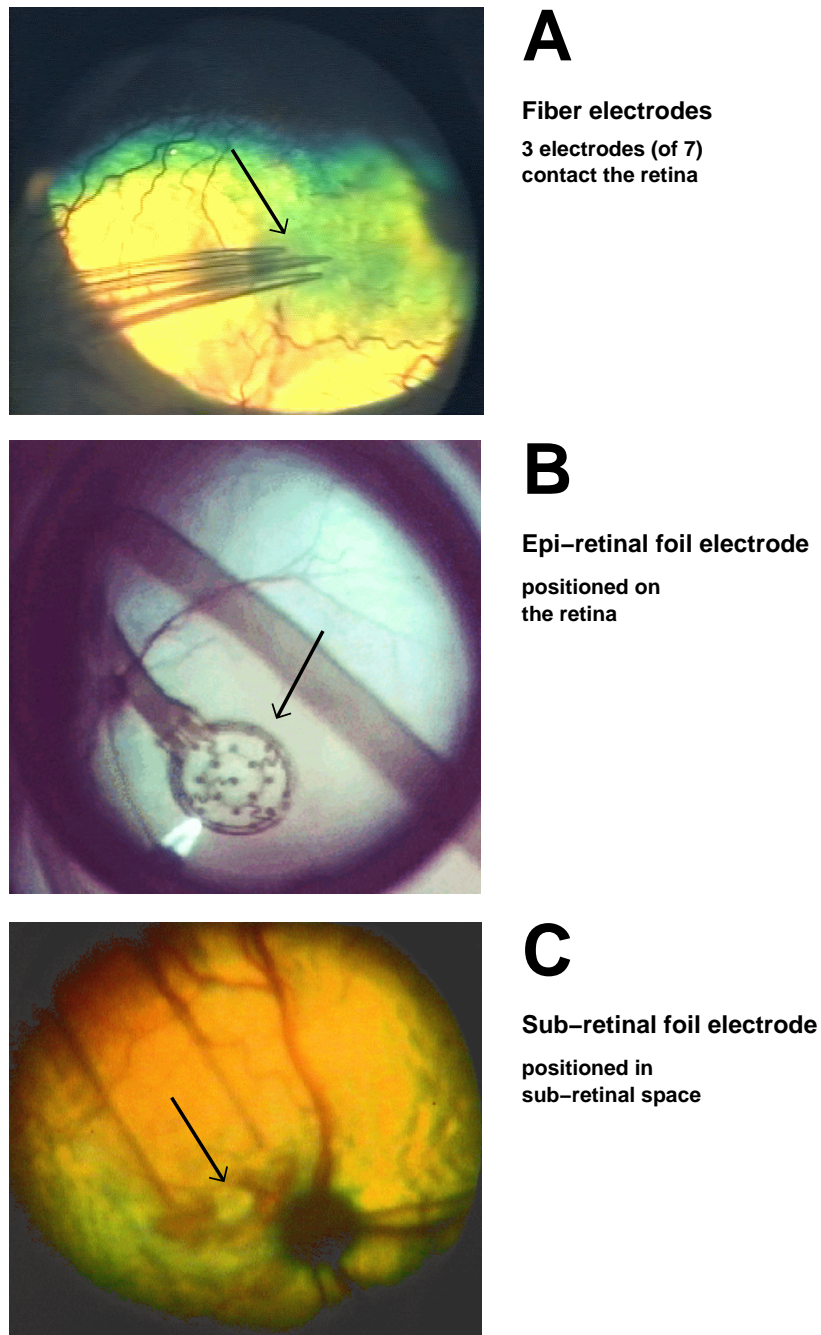
In the framework of the Retina Implant project we estimated cortical activity distributions for two different implant prototypes as well. One prototype was a flat polyimide electrode array with 24 planar electrodes designed for epiretinal implantation onto the membrana limitans interna (Fig. 2.7 B, IBMT St.Ĩngbert). Each electrode array comprised concentric bipolar Pt-Ir-electrodes with 0.75 mm spacing on a rectangular array (Stieglitz et al., 2000). Electrode contacts had 110–140 kΩ impedance at 1 kHz.

The other implant prototype used was a flat polyimide electrode array with 30 planar electrodes designed for implantation into the sub-retinal space (Fig. 2.7 C, NMI Reutlingen). Each electrode array consisted of six rows of 50 μm square TiN electrode contacts with 100 μm spacing. Rows of electrodes were separated by 100 μm, 200 μm, 400 μm, 800 μm, and 1600 μm, respectively. Electrode contacts had 8–10 kΩ impedance at 1 kHz (Nisch, 2001).

2.5.2 Generation of electrical stimuli

Up to four electrical stimulation channels could be supplied simultaneously by our digital-to-analog converter. In order to distribute these stimuli to up to seven retinal stimulation electrodes available with the hexagonally arranged fiber electrode array, a fast multiplexer was developed, built, and tested according to a concept by Thomas Schanze (Fig. 5.1 and Fig. 5.2). The combined setup for electrical stimulation consisted of:

- a *personal computer* generating and sending spatio-temporal waveforms

A

Fiber electrodes

**3 electrodes (of 7)
contact the retina**

B

Epi–retinal foil electrode

**positioned on
the retina**

C

Sub–retinal foil electrode

**positioned in
sub–retinal space**

Figure 2.7: In situ photographs of the three different types of stimulation electrodes used in this study. **A)** Hexagonally arranged Pt-W fiber electrodes with cone-shaped tips (Neurophysics Marburg, three out of seven are shown). **B)** 24 concentric bipolar Pt-Ir-electrodes for epi-retinal stimulation (IBMT St. Ingbert). **C)** 30 TiN-electrodes for sub-retinal stimulation (NMI Reutlingen).

- a *digital-to-analog converter* producing four-channel spatio-temporal voltage patterns

- a *multiplexer* distributing the four-channel input to eight-channel spatio-temporal voltage patterns

- a *voltage-to-current converter*

- *epi-retinal stimulation electrodes* (Fig. 2.7 A and B).

Electrical stimuli for sub-retinal stimulation (Fig. 2.7 C) were delivered by means of a commercial current source.

For each measurement the electrical stimulation consisted of a set of different randomly presented stimuli. By testing different stimuli randomly interleaved rather than sequentially, instationarities of the recording affected all stimulus conditions equally, thus easing the interpretation of stimulation effects. For a given waveform, typically, different stimulation electrodes, amplitudes or rates were chosen. Waveforms were single or bursts of biphasic charge-balanced impulses of variable duration and amplitude. Temporal separation between stimuli jittered between 150–500 ms to avoid input rhythmicity. Stimulus conditions were repeated one hundred or more times. This facilitated the averaging of cortical responses for individual stimulus conditions.

In order to mimic normal retinal activity, in some measurements, stimulus statistics were adapted to those naturally found. The Poisson model is the simplest model for neuronal spike statistics. It states that the probability function for spike occurrence only depends on the mean spike rate. In particular, spikes are independent of each other. According to the model, intervals between directly following spikes are exponentially distributed and the number of spikes in a time interval is Poisson distributed. However, the validity of this model is limited, since spikes are not exactly independent from each other (Berry II and Meister, 1998). This is due to the refractory characteristics of spiking neurons: Shortly after the neuron spiked, the probability of a subsequent spike is strongly reduced but recovers thereafter. To provide for natural stimulus statistics, we therefore generated electrical stimuli with Gamma distributed inter-stimulus intervals that account for the refractory period of spiking retinal cells. Stimuli with Gamma distributed inter-stimulus intervals were applied at various mean stimulation rates for the analysis of rate dependent cortical activation (Rieke et al., 1997).

Effectivity of stimulation and threshold stimulation current was assessed by the cortical responses to pseudo-random uni-focal activation with varying stimulus amplitudes typically ranging from 5–100 μA. Details on stimulus features as well as time stamps for stimulations were logged for off-line data analysis.

2.6   Data analysis

2.6.1   Averaged cortical responses

For this study, cortical responses to electrical stimuli were averaged over identical stimulus conditions (Peri Stimulus Time Histograms or "PSTH", see Fig. 2.3) to increase the signal-to-noise ratio of our data. Data were tested for instationarities by moving window analyses (LFP, MUA) or spike raster plots (SUA).

Major response characteristics investigated in this study were the response latency and the amplitude of the first excitatory signal deflection after the stimulus. Latencies for LFP and MUA responses were defined as the temporal delay between stimulus onset and excitatory response maximum. When multiple excitatory peaks were encountered, the first peak was taken. For SUA, latency was defined as the temporal delay between stimulus onset and mean arrival time of the first spike. When multiple spikes were elicited, the latency of the first spike was considered.

The amplitude of a cortical signal depends on the spatial distance between the neuronal current sources and the recording electrode tip. In addition, the impedance of the recording electrode influences the signal gain as well: Higher impedances yield greater signal amplitudes. This gain factor affects the recording of all neuronal signals, independent of the electrode tip's distance to specific neuronal current sources. In order to separate these independent effects in the PSTH, the cortical signals were normalized to the signals' standard deviation in a corresponding time window before stimulus onset. This procedure facilitated the comparison of (normalized) signal amplitudes from different recording channels. A reduced normalized signal amplitude thus is indicative of an increased distance between the neuronal current source and electrode tip.

2.6.2   Cortical activity distributions

The amplitudes of normalized averaged cortical responses to electrical stimuli were plotted against the cortical recording electrode separations. This yielded cortical activity distributions or "electrical cortical point spread functions" (ePSF). It often was possible to fit ePSFs by Gaussians weighted with the standard deviations of the underlying PSTH amplitudes to obtain a quantitative measure of the ePSF width and position relative to the recording sites. Only those Gaussians that obviously fitted the ePSFs ($p<0.05$, Chi-square-test) were included. When ePSFs were multi-peaked, Gaussians were fit to the envelope of the activity distribution. The widths of ePSFs were defined as the full width at half height (FWHH) of the Gaussian fits.

Since cortical activity was sampled with a linear array of recording electrodes, two-dimensional ePSFs were cut along the recording array's plane. Therefore, the width of ePSFs were estimated from projections onto the recording array's plane. However, the profile of an approximately Gaussian ePSF is radial-symmetric. Without loss of generality, the Gaussian can be centered at the coordinate origin, and be written as

$$f(r) = \frac{1}{\sqrt{2\pi}\sigma} \ \exp(-\frac{r^2}{2\sigma^2}). \tag{2.1}$$

Any linear section through this Gaussian is well defined by its distance d to the center of the Gaussian. Thus, the section's profile may be obtained by means of the coordinate transformation

$$r^2 = \rho^2 + d^2, \tag{2.2}$$

where ρ is measured along the section. $\rho = 0$ denotes the center of the section's profile. The coordinate transformation yields

$$f(\rho) = \frac{1}{\sqrt{2\pi}\sigma} \ \exp(-\frac{\rho^2 + d^2}{2\sigma^2}), \tag{2.3}$$

$$f(\rho) = \frac{1}{\sqrt{2\pi}\sigma} \ A(d, \sigma) \ \exp(-\frac{\rho^2}{2\sigma^2}), \tag{2.4}$$

with

$$A(d, \sigma) = \exp(-\frac{d^2}{2\sigma^2}). \tag{2.5}$$

Thus, the section's profile is a Gaussian with a reduced amplitude that depends on the distance d and has the same FWHH as in the radial-symmetric distribution (equation 2.1). Consequently, the FWHH of an ePSF can be assessed from its section provided by the linear recording electrode configuration.

The temporal evolution of ePSFs was studied as well. For this purpose, ePSFs were calculated for consecutive time windows, color-coded, and plotted on a two-dimensional plane. Similarly, cortical visual point spread functions (vPSF) were determined from the data recorded for the generation of the vRF maps.

2.6.3 Cortical activation overlap

To address the question, which retinal distance between two electrical stimulation sites might be separable in the cortex, the overlap of ePSFs for pairs of stimulation electrodes was analyzed. After fitting the ePSFs with Gaussians, spatial separability was assumed if 50% of their respective amplitudes were above their mutual point of intersection. One of the Gaussians was shifted

to the position which fulfilled the given constraint. The cortical separation of the shifted Gaussians was called *"minimum separabile"* in cortical coordinates (Fig. 2.8 A-C). This procedure takes into account the width as well as the amplitude of ePSFs.

Since the vRFs of retinal stimulation sites were known, cortical separations of ePSFs could be related to corresponding separations in visual space.

By this procedure, a "local cortical magnification factor" could be estimated as the separation of two ePSFs in cortical coordinates divided by the separation of vRFs of the corresponding retinal electrodes (Tusa et al., 1979). The ratio of the minimum separabile and the local cortical magnification factor for the respective pair of retina electrodes allowed to estimate the minimum separabile or angular resolution in degrees visual angle (Fig. 2.8 D).

2.6.4   Electrical receptive fields

In correspondence to the receptive field concept in the visual domain, we defined the retinal area which is capable of modulating cortical neuronal activity when stimulated electrically as "electrical receptive field" (eRF). Based on the same data as for calculating ePSFs, eRFs were constructed from the early response components of cortical LFP signals. For each cortical recording channel we estimated the stimulation efficiency from the normalized response amplitudes elicited by each retinal stimulation electrode. The eRF positions and sizes were determined using two-dimensional Gauss fits of the response amplitudes at the retinal sampling points of each eRF-map. This procedure is exemplified in the Results chapter (Fig. 3.4).

2.6.5   Temporal resolution of electrical retina stimulation

A series of measurements was performed to address the question of the achievable temporal resolution with electrical retina stimulation. Three approaches were tested. The first assesses the fastest response components of cortical LFP to electrical stimuli. Since the initial response component is characterized by a steep rise, rise times were evaluated for different stimulation conditions. For this purpose, LFP-PSTHs (normally sampled at 2 ms temporal resolution) were interpolated by splines in order to obtain a 0.1 ms temporal resolution. Rise times were defined as the time between the end of the residual stimulation artifact and the peak position of the first response component. Peak positions were automatically identified by a peak detection algorithm. The estimated temporal resolution was defined as twice the rise time.

In a second approach, analyses were done on SUA, since the assessment of temporal resolution involves mainly temporal aspects of the cortical signal.
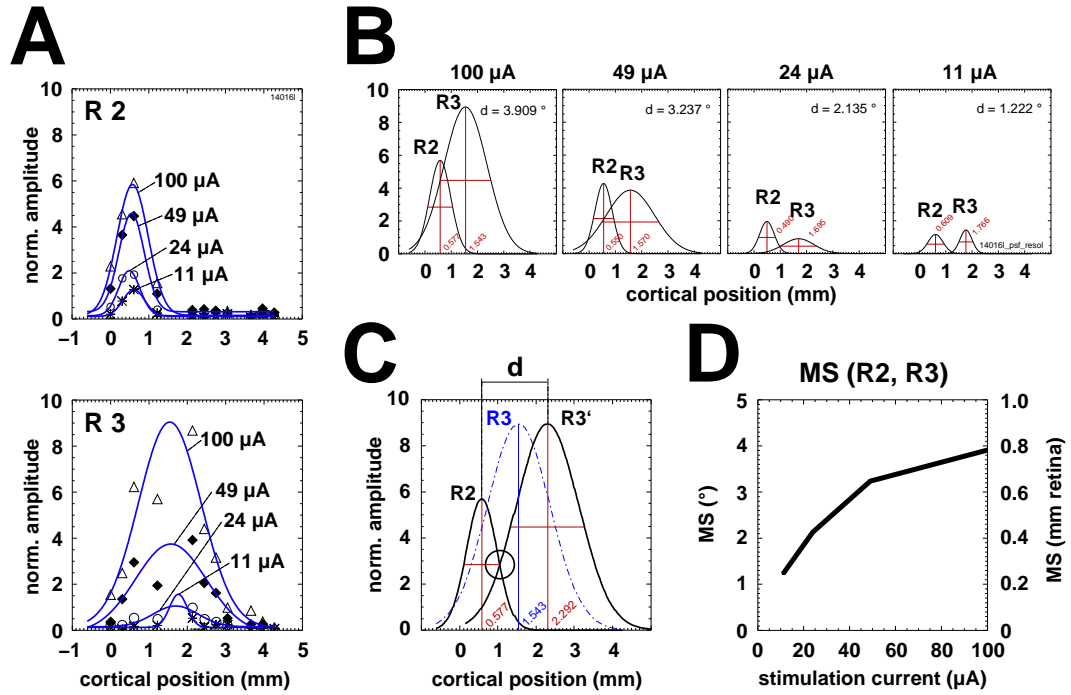
Figure 2.8: **A)** Cortical ePSFs for two stimulation electrodes (R2 & R3) and four different stimulation currents. Electrical PSFs are based on the early LFP response component. Stimulation electrodes were separated by 0.45 mm on the retina, corresponding to 2.2° in visual space. The data was fitted with weighted Gaussians. **B)** For each stimulation current, ePSFs for R2 and R3 are superimposed to illustrate the amount of overlap of cortical spread. **C)** For each pair of stimuli the separation **d** of the Gaussians that would yield their mutual point of intersection below their respective half heights was estimated. **D)** Since the vRFs of the retinal stimulation sites are known, the separation **d** for each two ePSFs can be related to the corresponding separation in visual space and in the retina ("minimum separabile", "MS"). The minimum separabile mostly increases with higher stimulation currents. Lowest minimum separabiles were found for stimulation just above threshold.

SUA gives temporally more precise evidence. Therefore, in some experiments, cortical SUA was studied in dependence of the mean rate of electrical stimuli with Gamma distributed inter-stimulus intervals. Mean temporal intervals between electrical stimuli could be resolved if a significant number of spikes could be evoked.

A third approach for the assessment of temporal resolution is based on the duration of the excitatory phase of cortical responses to electrical retina stimulation.

3 Results

3.1 General remarks

This study is based on data from experiments on nine cats. Five experiments were performed with fiber electrodes and four experiments with flat electrode arrays (prototypes of a visual implant). Five to sixteen recording channels were available in each experiment. We tested at least two stimulation electrode array positions in each experiment with fiber electrodes. On average, five of seven stimulation electrodes were effective in activating cortical cells within reach of the recording electrodes (N=50 effective stimulation sites). In experiments with flat electrode arrays, about 20% of stimulation electrodes were effective in driving neurons at the recording sites (N=20 effective stimulation sites). The apparently lower effectivity can be attributed to the larger dimensions of the foil implants which, according to the retino-cortical magnification factor, covered a relatively large cortical area. However, given a limited number of cortical recording electrodes, we restricted the recording sites to a narrow cortical area in order to properly sample individual cortical activity distributions.

3.2 Properties of evoked cortical responses

In the best cases thresholds for cortical activation with single electrodes were as low as 2.5 μA for epi-retinal stimulation with fiber electrodes and below 6.25 μA for (epi-retinal) stimulation with flat polyimide electrode arrays (single biphasic impulses of 0.4 ms total duration, leading cathodic phase). In most cases, a stimulation current of 40 μA is sufficient for eliciting cortical responses, when retinal stimulation sites are within the receptive fields of cortical recording electrodes. Moreover, the threshold current can be reduced by rapid sequences of charge-balanced biphasic stimuli (Schanze et al., 2001).

Cortical LFP and MUA responses often consist of multiple excitatory peaks between 15 and 80 ms with a slow inhibitory component thereafter (Fig. 3.1). However, in other recordings cortical LFP and MUA response time courses are single-peaked and temporally constrained to about 30 ms, when stimulation is just above threshold. When burst-like responses occur, the first inhibitory com-
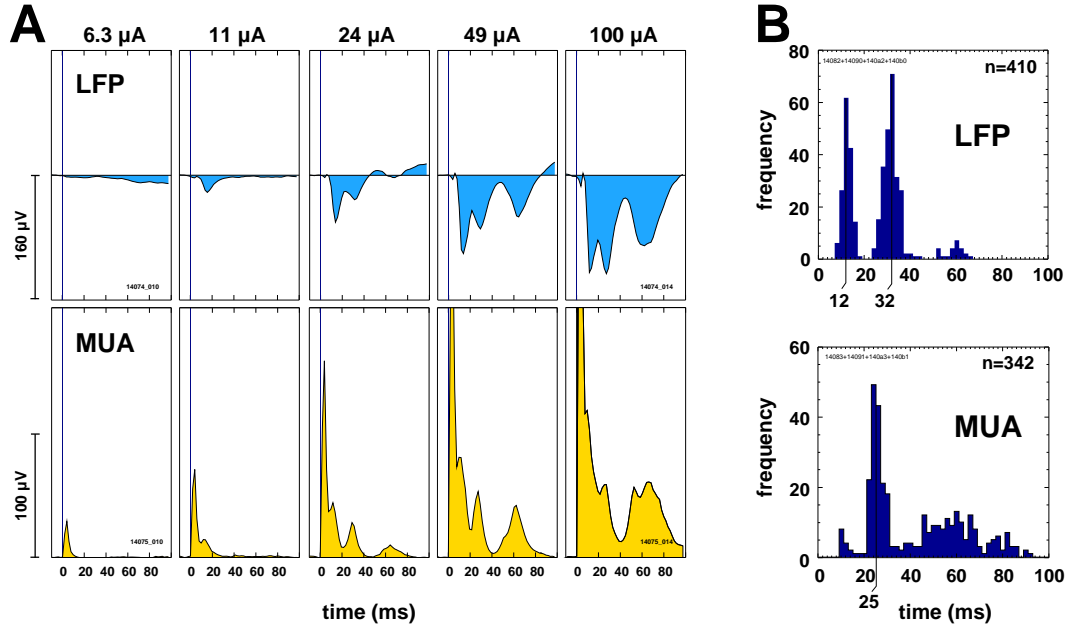
Figure 3.1: Temporal multi-peaked cortical responses to electrical retina stimulation. **A)** Shown are PSTHs for LFP and MUA responses to electrical stimuli with different stimulation currents as indicated on top of the plots. The stimulation artifact is most prominent in the MUA between 0–10 ms. Note that at just above threshold level (11 μA) stimulation evokes only the early response component. At higher stimulation currents, consecutive response components appear. The strong stimulus artifact often occludes the early MUA response component. **B)** Time-to-maximum histograms for LFP and MUA responses to strong electrical stimuli (100 μA).

ponent often is absent or camouflaged by excitatory signal deflections. Typically, burst-like activities form with increased strength of electrical stimulation. Low stimulation currents elicit only early response components, whereas the second and third component appears consecutively at higher stimulation currents (Fig. 3.1). Peak latency distributions are therefore often multi-peaked with up to three peaks. The first excitatory LFP component peaks after 10–20 ms, the second after about 32 ms, and the third after about 60 ms. MUA response components peak at shifted latencies with respect to LFP components. At the point when retino-cortical signal transduction forms the early response components, intra-cortical processing has not yet shaped spatial activity distributions. For this reason, early response components are further analyzed for the estimation of cortical spread after retinal stimulation. Since the early MUA response was often occluded by the stimulus artifact (in experiments were no broad-band recording was performed), the early LFP response component was studied in more detail.
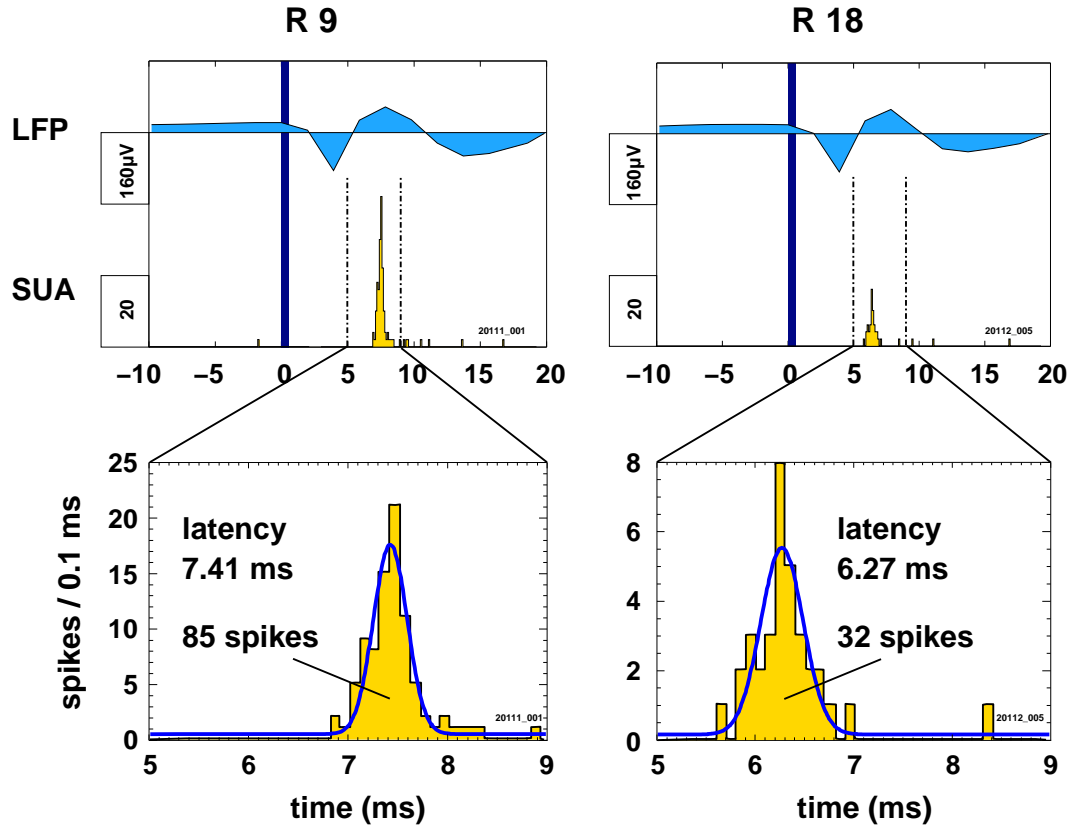
Figure 3.2: PSTHs (N=201) of cortical population responses (LFP) and single unit activity (SUA) after para-central epi-retinal electrical stimulation with an implanted polyimide foil electrode array (IBMT, St. Ingbert). 100 μA stimulation impulses were delivered with a leading cathodic phase and 400–500 ms inter-stimulus delay (dark column). PSTHs are shown for one cortical recording site and two different stimulation electrodes (**R 9** & **R 18**) that were separated by 1.7 mm on the retina along the axon fibers. Spike latency distributions are plotted at higher temporal resolution in the bottom row. The probability of eliciting a spike was 42 % for stimulation with electrode **R 9** and 16 % for stimulation with electrode **R 18**. Note that the average latency for evoked spikes differs for the two retinal stimulation electrodes.

Individual cortical neurons are activated with about 3.4–9.0 ms latency. Fig. 3.2 shows latency distributions for the spike activity of one cortical neuron. Interestingly, this neuron can be driven by two retinal stimulation electrodes separated by 1.7 mm along the retinal axon fibers. However, the latency distributions exhibit distinct mean latencies that differ by 1.14 ms. As the stimulation electrode closest to the optic disk yields a smaller latency than the electrode stimulating more distally along the axon, the latency shift can be attributed to the additional intra-retinal conduction time.

If the stimulation electrodes are placed between the vRFs of cortical recording sites and the optic disk ("proximal stimulation"), effectivity of stimulation often is higher than for positioning of stimulation electrodes beyond the vRFs ("distal stimulation").
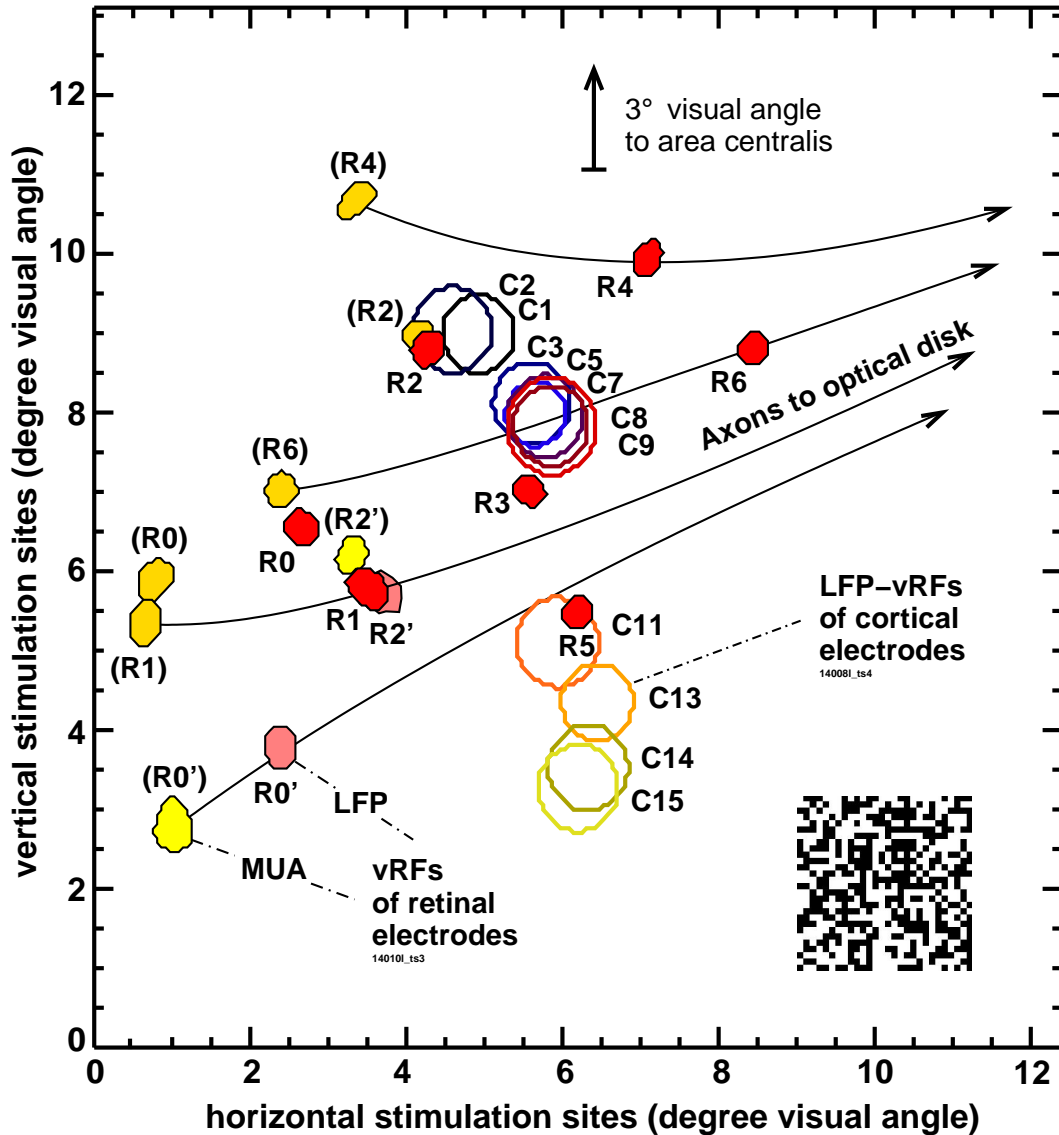
3.3 Visual receptive fields

In contrast to cortical vRFs, vRF positions of retinal electrodes are distinct for LFP and MUA signals. LFP-based vRFs of retinal electrodes are located at positions very close to the electrode positions that were manually back-projected onto a tangent screen. However, MUA-vRFs are always distal from LFP-vRFs (N=5) or approximately at the same site (N=2) but never proximal with respect to the optic disk. This is demonstrated in Fig. 3.3. Superimposed on the cortical vRFs (C1–C15, Fig. 2.6), retinal LFP-vRFs are plotted as filled red circles (R0–R6). The positions of the LFP-vRFs clearly resemble the hexagonal stimulation array geometry, which is slightly stretched due to the angle under which the electrodes approach the retina. MUA-vRFs could be calculated for five retinal stimulation electrodes. They are plotted as dark yellow filled circles (annotation in brackets). MUA-vRFs are located to the left side of LFP-vRFs, i.e. distal with respect to the optic disk. In one case LFP- and MUA-vRFs are at the same location (R2). After 23 hours, a second measurement of retinal vRFs produced vRFs that were shifted with respect to the earlier measurement (LFP-vRFs plotted as filled pink circles, MUA-vRFs as filled yellow circles). However, the separations of LFP- and MUA-vRFs are similar compared to those in the first measurement.
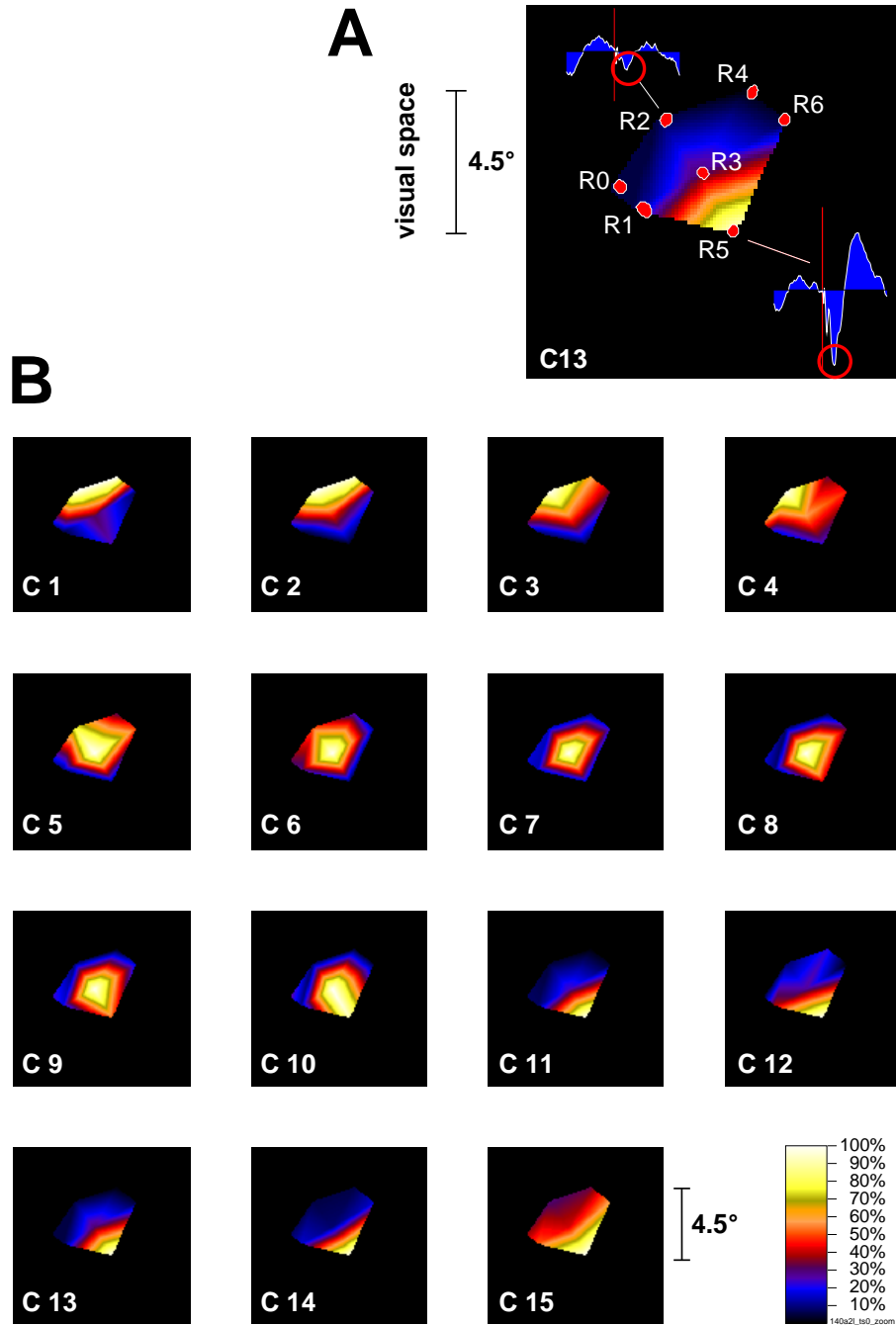
3.4 Electrical receptive fields

The estimation of cortical eRFs was possible, when a sufficient number of closely spaced retinal stimulation sites was capable of evoking cortical responses . This was the case for experiments with epi-retinal fiber electrodes, in which stimulation electrodes could be iteratively placed in close proximity to the retina at sites corresponding to those of cortical recordings. The centers of the LFP-vRFs of retinal electrodes closely resembled the actual electrode position (section 3.3) and were taken as the retinal "electrical sampling points" of cortical eRFs.

Fig. 3.4 shows linearly interpolated eRF-maps for 15 cortical recording electrodes after color-coding the cortical response strength (early response amplitude of LFP) to each of the retinal electrical sampling points. The upper right plot illustrates this procedure on a magnified scale. Note that with each consecutive recording electrode number (C1–C15) the eRF-center (yellow and

Figure 3.3: Visual receptive fields (vRFs) of retinal and cortical population responses (LFP) (stimulation details as in Fig. 2.6). Filled red and pink circles denote LFP-vRFs, filled dark and light yellow circles denote MUA-vRFs of retinal electrodes. Open greater circles indicate positions of vRFs for cortical recording sites. Sizes of vRFs are drawn as contours on a 90% level of vRF peak amplitudes. Note that retinal MUA-vRFs are always located distally with respect to the optic disk or at the same location as LFP-vRFs. Black arrows indicate the assumed trajectories of ganglion cell axons.

Figure 3.4: Electrical RFs for cortical recording electrodes. **A)** Amplitudes of the early LFP response component (red circles in the signal insets) were taken to construct electrical receptive fields. Linear interpolation was performed between the seven spatial sampling points of the hexagonal stimulation matrix (R1–R6). The black background corresponds to the coordinate system in Fig. 3.3. **B)** Note the downward shift of eRFs in visual space for consecutive recording electrodes from the upper left (C1) to the lower right (C15) plot. Recording electrodes C1–C15 were inserted in a posterior-anterior direction along the vertical meridian in area 18.
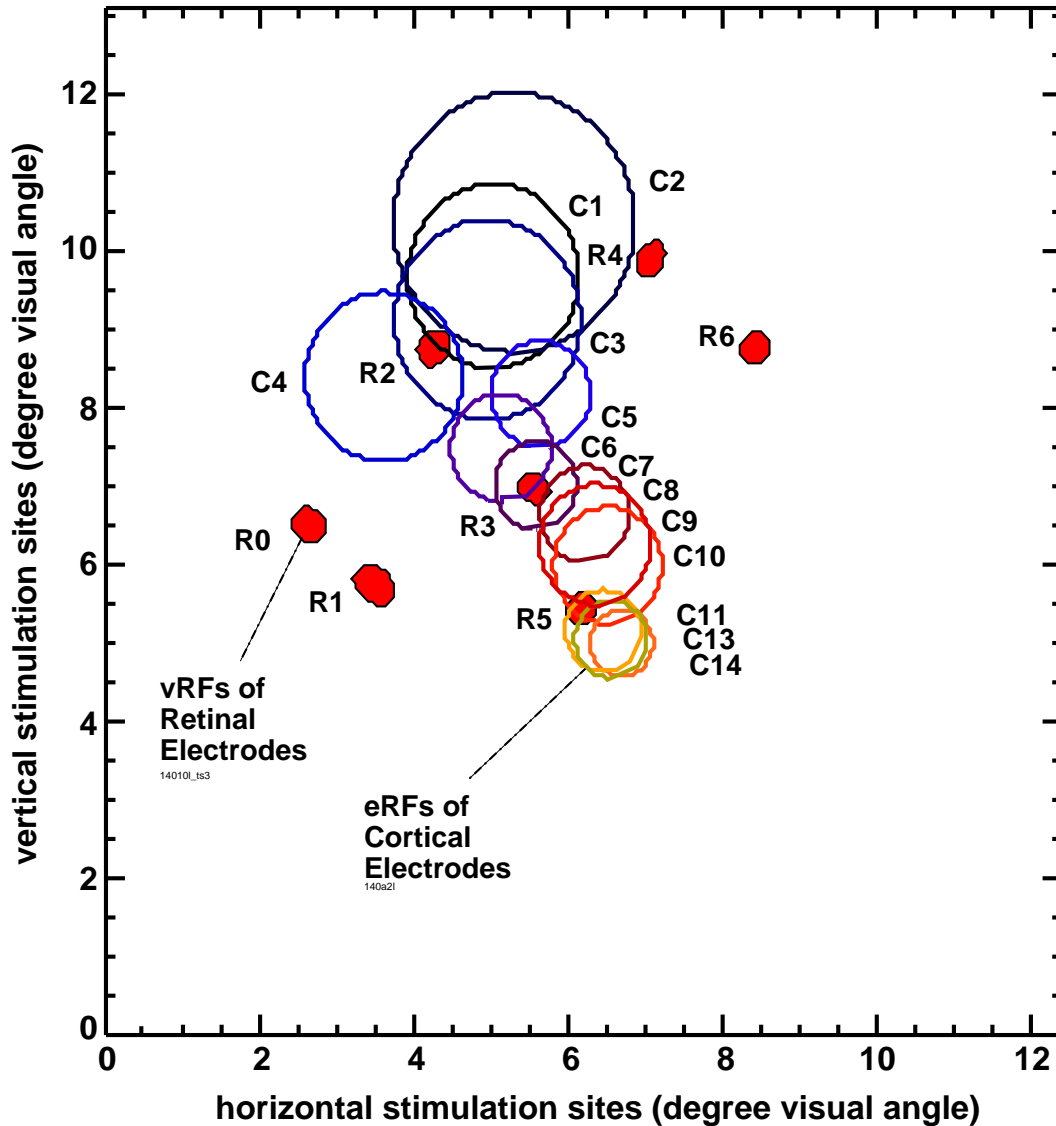
Figure 3.5: Superimposed electrical RFs for cortical recording electrodes. Amplitudes of the early LFP response component were taken to construct interpolated electrical receptive fields for each recording electrode (C1–C14, cf. Fig. 3.4). Two-dimensional Gaussians were fit through seven spatial electrical sampling points (taken from the LFP-vRFs of retinal stimulation sites, e.g. **R0**). The Gaussians were constrained to be symmetric in order to save one degree of freedom in the fitting algorithm. Shown are the contours at a 90% level of the fit maximum (fitting for recording electrode C12 and C15 did not converge). Note the downward shift of eRFs for consecutive recording electrodes from the upper left (C1) to the lower right (C15) plot. A similar shift is observable for the corresponding vRFs of the same recording electrodes (Fig. 3.3). Recording electrodes C1–C15 were inserted in a posterior-anterior direction along the vertical meridian in area 18. The coordinate system shows the entire field mapped visually. The area centralis was approximately located at 6.5° horizontal and 14° vertical.
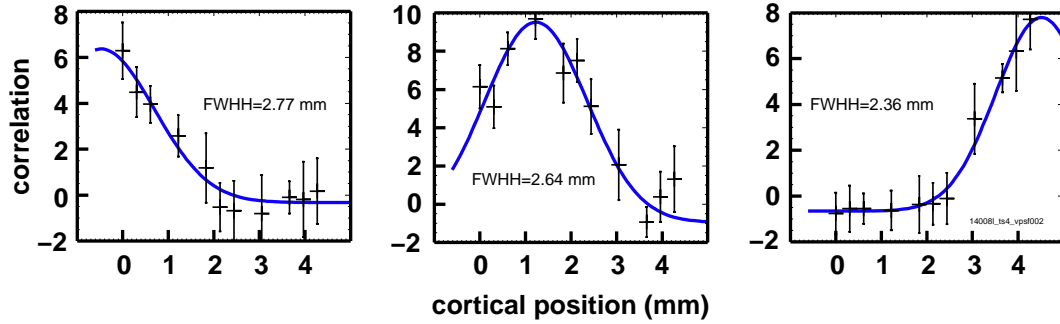
Figure 3.6: Visual PSFs for cortical population responses (LFP) after para-central visual stimulation with a multi-focal random visual stimulus sequence (N=92160 stimuli given at each grid position and at maximum contrast of the monitor, pitch of stimulus grid was 1°, T=30 min duration of presentation). Stimuli were based on binary m–sequences given at a 101 Hz frame rate.

white colors) shifts downward in visual space. Recording electrodes C1–C15 were inserted in a posterior-anterior direction along the vertical meridian in area 18. Thus, the vRFs of the recording electrodes shift downwards, too, as can be verified in (Fig. 2.6).

The estimation of eRF-positions and -sizes was possible after two-dimensional Gaussian fitting over the seven retinal sampling points of each eRF-map (not the interpolated map). Cortical eRFs are retinotopically arranged and show similar topographic relations as their visual equivalents (Fig. 3.5). The average absolute misalignment of eRFs with respect to their vRF counterparts in the RF plot shown in Fig. 3.3 is 1.07° ± 0.45° (n=10 pairs of v/eRFs).

3.5 Cortical visual point spread functions

For reference, cortical visual point spread functions (vPSF) were calculated from the data recorded for generation of the vRF maps. Fig. 3.6 shows three vPSFs for visual stimuli at the center of three cortical vRFs. Visual PSFs often are broader than the corresponding ePSFs (section 3.6.1).

3.6 Spatial resolution of electrical retina stimulation

3.6.1 Cortical ePSFs

We estimated cortical ePSFs for LFP, MUA, and SUA data. The method is exemplified in Fig. 3.7. Shown are PSTHs of five simultaneously recorded LFP, MUA, and SUA responses to focal electrical stimulation of the retina (C1, C3,
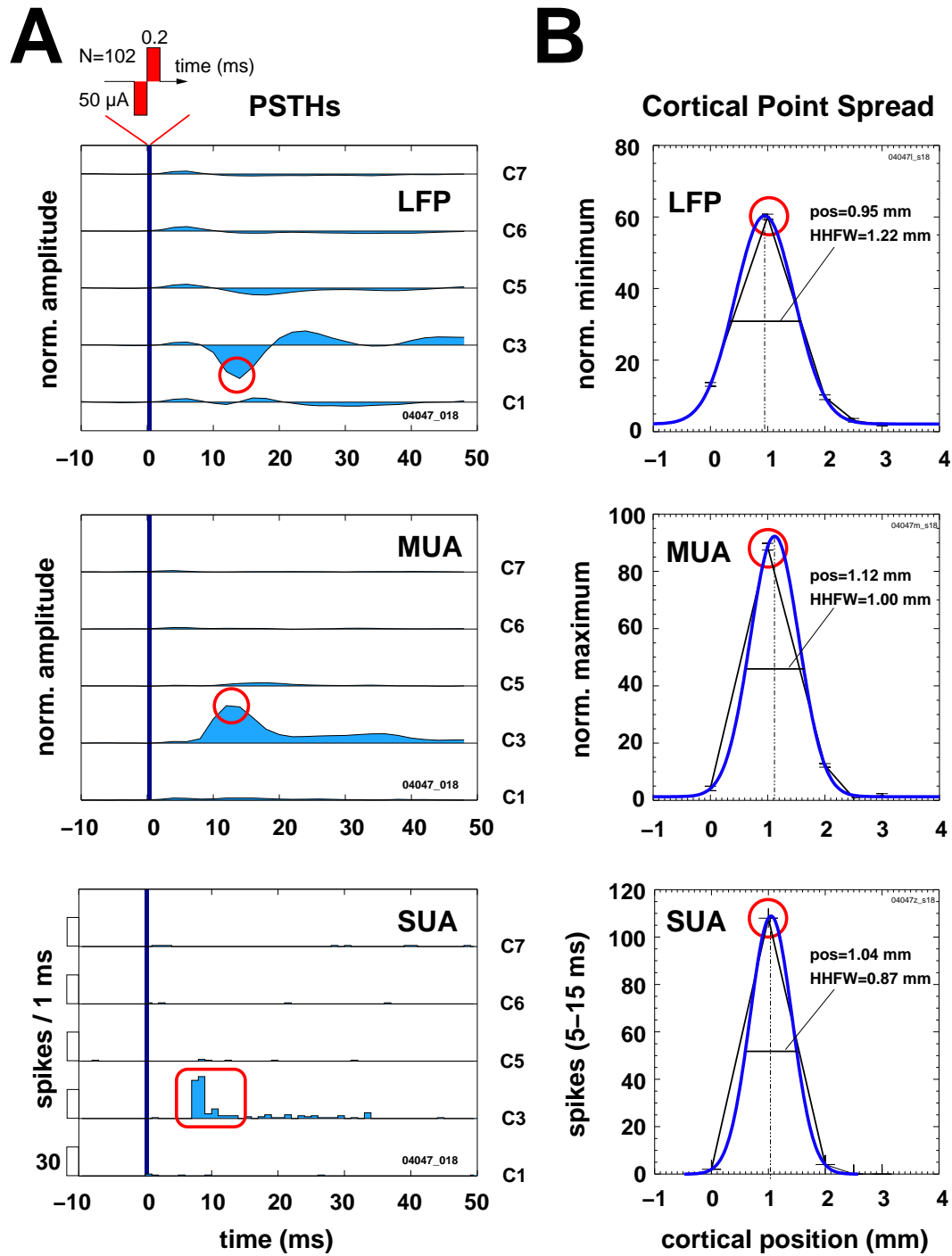
Figure 3.7: Cortical electrical point spread to focal electrical retina stimulation detected with different spatio-temporal resolution (para-central stimulation, N=102). **A)** PSTHs for LFP, MUA, and SUA data (off-line filtered broad-band signals). Red circles mark early cortical excitatory activation. Note the inhibitory response component most prominent in the LFP. The recordings were done with a linear array (C1, C3, C5, C6, C7). **B)** From the PSTHs, ePSFs are estimated by the averaged first response amplitudes (LFP, MUA) and spike counts (SUA), respectively.

C5, C6, C7). From the average amplitudes of the first response components, ePSFs are calculated (shown to the right). Generally, LFP-based ePSFs are wider than MUA- or SUA-based due to the size of the spatial integration field (Schanze, 1995). In addition, MUA-ePSFs and SUA-ePSFs are mostly less smooth than LFP-ePSFs. This can be attributed to the better signal-to-noise ratio for LFP data, because LFP averages over more cortical units.

Fig. 3.8 depicts cortical ePSFs in area 18 measured simultaneously for seven retinal stimulation electrodes and five different stimulation current amplitudes. Plots are schematically positioned according to the hexagonal geometry of the stimulation electrodes. In the experiment, ganglion cell axons were directed approximately from the left to the right side of the plot. Positions of vRFs for retinal and cortical electrodes are as in Fig. 3.3. Note that the stimulation electrodes evoke distinct ePSFs that differ in shape, cortical position, width, and amplitude. In particular ePSFs are retinotopically arranged. Stimulation of the lower retina (upper field of view (R2 and R4)) results in activation of more posterior and the stimulation of the upper retina (lower field of view (R1 and R5)) in activation of more anterior cortical neurons in area 18.

Cortical ePSFs are single-peaked at threshold level. However, with increased stimulation current, ePSFs sometimes become multi-peaked with one or two additional side lobes (Fig. 3.9). For a single retinal stimulation site, peaks in ePSFs are fixed to cortical positions. Shifting the retinal stimulation sites results in either slight shifting of ePSF-peaks or formation of adjacent peaks. Hence, high activation peaks are also fixed with respect to the cortical recording array.

The width of ePSFs is taken from the full width at half height (FWHH) of Gaussian fits to ePSFs (section 2.6.2). The average width of ePSFs is (1.28 $\pm$ 0.33) mm cortex (N=298 ePSFs, 4 cats) (Fig. 3.10). The width of ePSFs depends on the stimulation current with higher currents affecting more cortical space, thus yielding broader ePSFs.

Retinal stimulation was performed at $4° - 9°$ eccentricity in most experiments. Within this range and number of experiments (N=9), there was no systematic influence of stimulation eccentricity on the width of ePSFs.

3.6.2 Dynamics of cortical ePSFs

Plotting color-coded ePSFs for consecutive time windows (section 2.6.2) exhibits the dynamics of ePSFs. Fig. 3.11 shows time resolved ePSFs for the same data as in Fig. 3.8. The initial cortical response is spatially well localized at the entry site of cortical afferents (t = 10–20ms). On the other side, later response components exhibit broad and non-localized ePSFs (t = 30–70 ms). Electrical PSFs therefore tend to overlap strongly for later response components. The transition from localized to non-localized ePSFs occurs in a
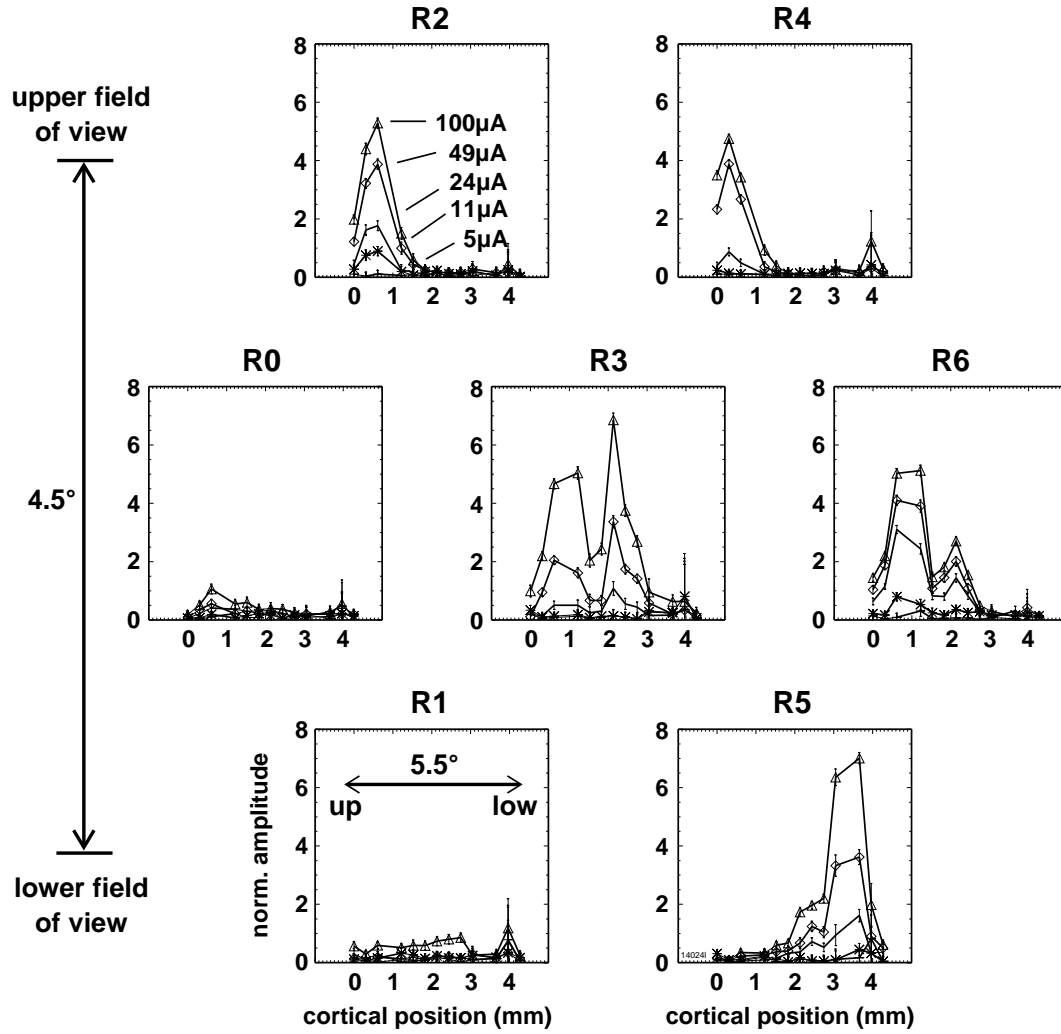
Figure 3.8: Electrical PSFs for cortical population responses (LFP) after paracentral electrical stimulation with seven electrodes (N=101). Plots are schematically positioned according to the hexagonal stimulation electrode geometry. Each ePSF is plotted against the cortical recording electrode positions (C1–C15 in Fig. 3.3). Error bars indicate standard deviations of the amplitudes in the underlying PSTHs. Leftmost peaks correspond to upper, rightmost peaks to lower positions in visual space.
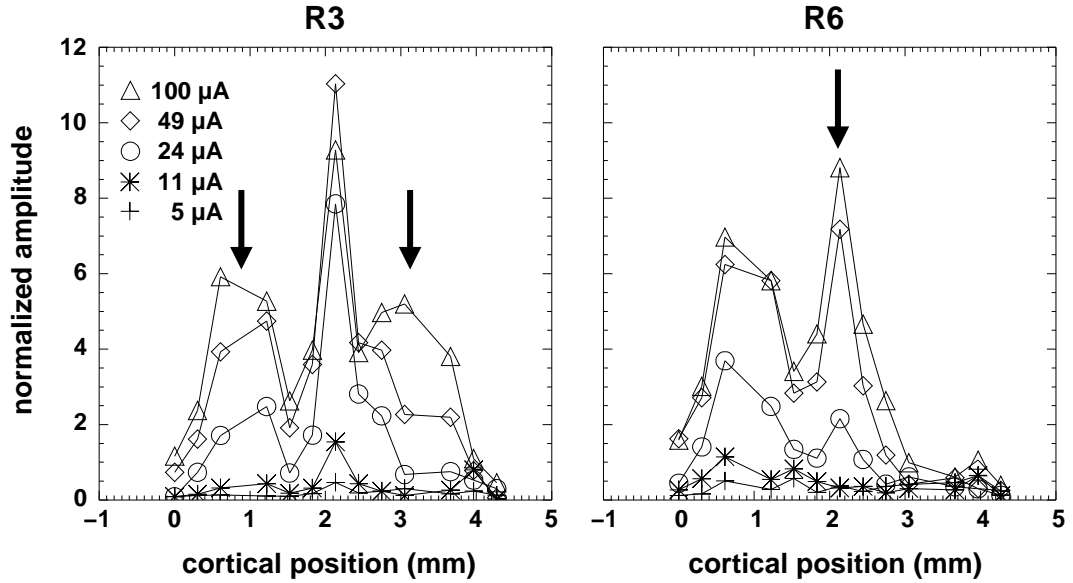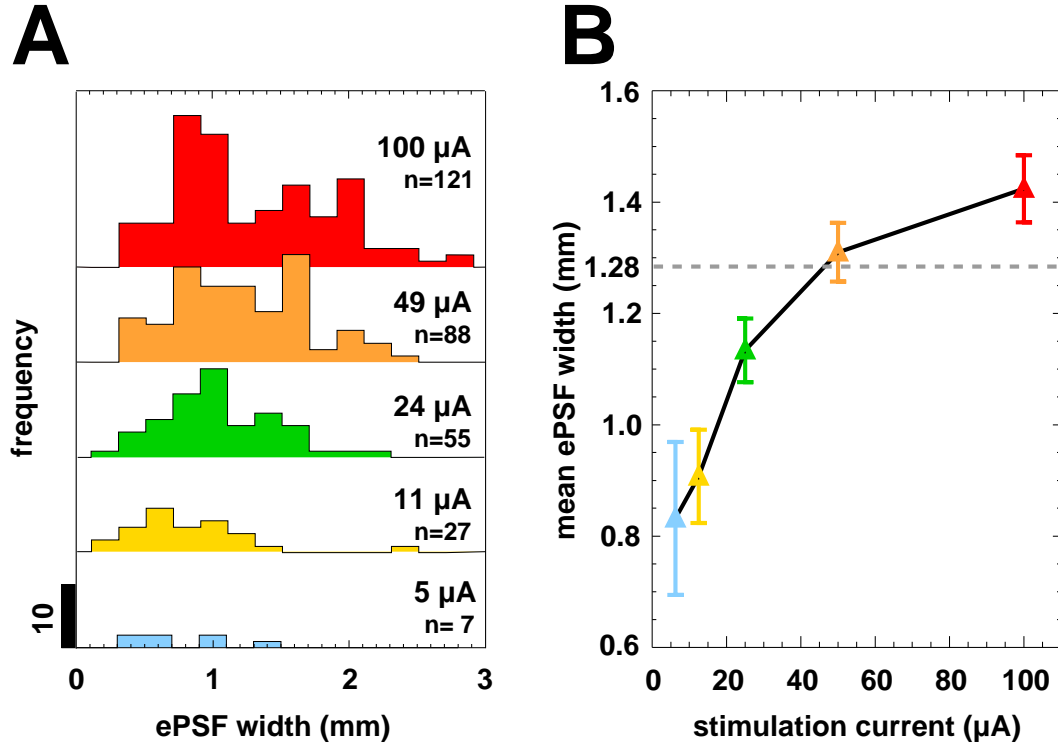
Figure 3.9: Electrical PSFs for cortical population responses (LFP) after para-central electrical stimulation (N=101) with five different current amplitudes at two retinal positions (R3 & R6). Cortical ePSFs are single-peaked at threshold level. However, with increased stimulation current, ePSFs become multi-peaked with one or two additional side lobes as indicated by the arrows.

step-like fashion between 20–30 ms after the stimulus. With increasing stimulation current, the transition from localized to non-localized ePSFs becomes more evident. Fig. 3.12 shows that for just above threshold stimulation (11μA) the ePSF is rather localized. At higher stimulation currents, the point spread for the initial response component becomes slightly broader (see Fig. 3.10) and non-localized ePSFs occur at 20 ms temporal offset to the initial response.

3.6.3   Minimum separabiles

To address the question of separability of electrical retina stimulations, minimum separabiles were estimated from the overlap of ePSFs for pairs of epi-retinal stimulation electrodes (section 2.6.3). Minimum separabiles depend on the stimulation current, with a strong increase between 11 μA (threshold level) and 24 μA and a weaker increase for amplitudes of 24 μA to 100 μA (Fig. 3.13). The data suggests that with epi-retinal stimulation an angular resolution of 2° is possible. In best cases angular resolution drops to about 1.6° for stimulation well above threshold (tenfold threshold level) and to $0.8° - 2.0°$ for stimulation at threshold level. 76% of all ePSFs analyzed had minimum separabiles between $1.6° - 4.3°$ (N=137).

Figure 3.10: **A)** Histograms for the width of ePSFs calculated from cortical population responses (LFP) to para-central electrical stimulation with fiber electrodes in 298 stimulation sessions (n=101 stimulations each) in 4 cats. The width of ePSFs were taken from the full width at half height of Gaussian fits to ePSFs. Histograms are shown for 5 μA (blue), 11 μA (yellow), 24 μA (green), 49 μA (orange), and 100 μA (red). **B)** The mean width of ePSFs increases with increasing stimulation current (0.2 ms dual polarity, cathodic phase first). Error bars indicate the standard deviation of means (standard error).

3.7 Temporal resolution of electrical retina stimulation

3.7.1 Analysis of response rise times

The duration of the steep rising phase of the initial LFP response component was analyzed. In a total of 6825 PSTHs from N=13 measurements (5 stimulation currents, 7 stimulation electrodes, and 15 cortical recording electrode signals), 17% (N=1164) had a significant ($S/N > 4$) early response component and were included in the analysis. Fig. 3.14 A shows the distributions of rise times for the five stimulation currents tested. The rise time distributions are broadly tuned and do strongly overlap. However, the mean rise time depends on the stimulation current (Fig. 3.14 C). The mean rise time for the 100 μA
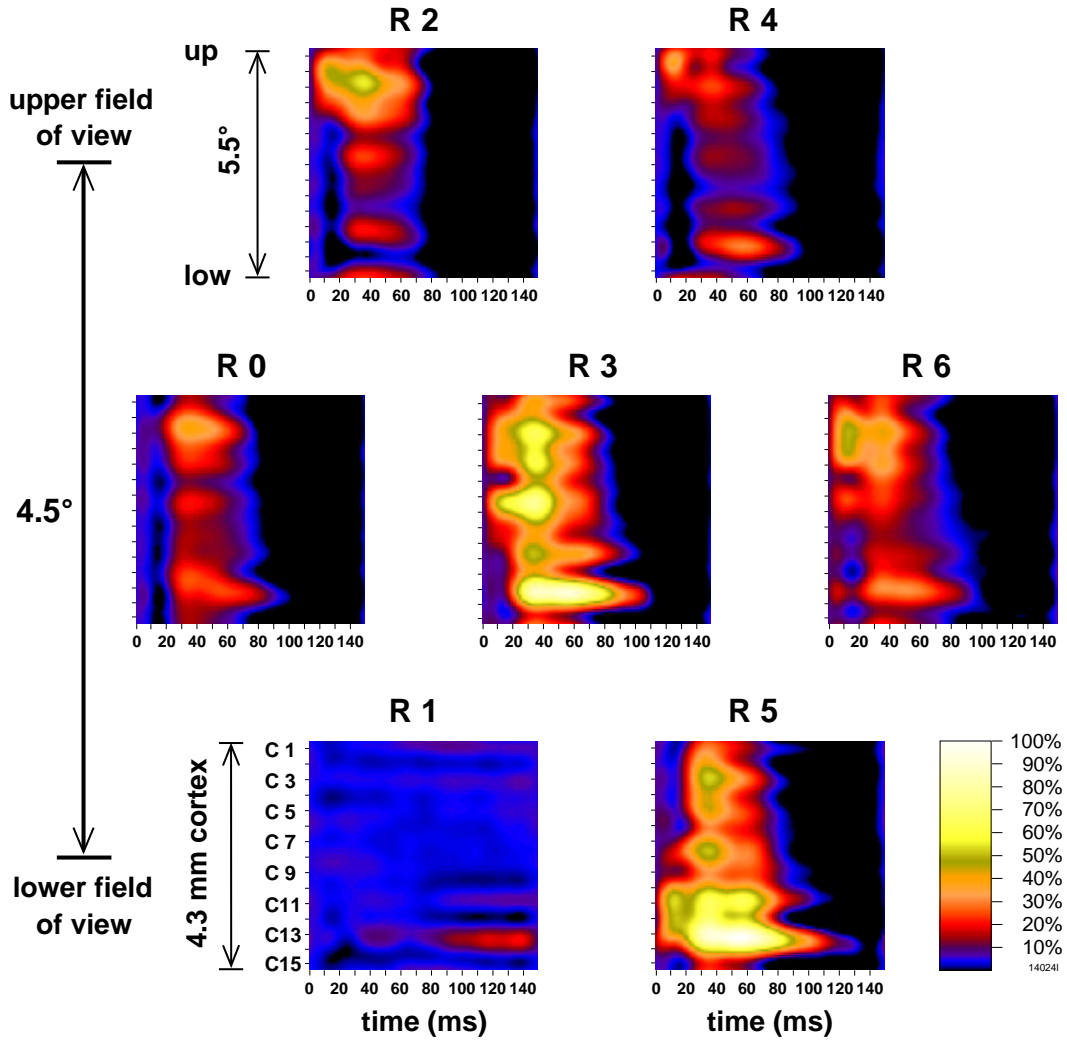
Figure 3.11: Spatio-temporal evolution of cortical ePSFs for cortical population responses (LFP) after epi-retinal para-central electrical stimulation (N=101) with a hexagonal 7–electrode array. Normalized response amplitudes were calculated and color-coded for consecutive time windows and plotted on a two-dimensional plane. Each plot shows the evolution of cortical point spread in response to electrical stimulation with one retina electrode as indicated on top of each plot. Stimulation and recording electrode numbers correspond to those in figure 3.3. Note that early response components arrive after 10–20 ms and are often more localized compared to the consecutive response components.
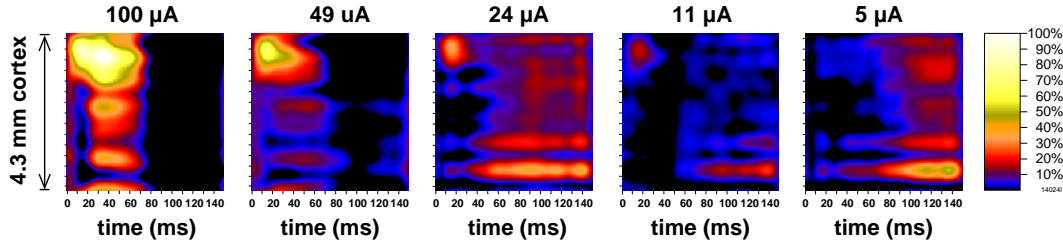
Figure 3.12: Spatio-temporal evolution of cortical ePSFs for cortical LFP responses after epi-retinal para-central electrical stimulation (6° from area centralis, N=101 stimuli). Stimulation current was decreased from well above threshold (I=100 μA, left) to sub-threshold level (I=5 μA, right). Note the occurrence of activity side bands 20 ms after the initial response to strong stimulation.

stimulation is significantly shorter than for 49 μA (t-test, $p < 0.1$) as well as for 24 μA, 11 μA, and 5 μA, respectively (t-test, $p < 0.0005$). Fig. 3.14 B demonstrates examples of the data analyzed. Of LFP-PSTHs the first 30 ms after the stimulus are plotted for 100 μA, 49 μA, 24 μA, and 11 μA stimuli, respectively. Responses are plotted on a normalized scale for an easier comparison of the temporal aspects. The first negative signal deflection reflects the residual stimulation artifact. The artifact is seen at the same latency for all stimulation currents. Without scaling, artifacts would differ in amplitude according to the stimulation strength. Depending on the stimulation current amplitude, first cortical responses peak after about 14–18 ms. Note that for the higher stimulation currents (100 μA and 49 μA), a subsequent response component appears. Rise times are in the range of 8–12 ms, depending on the stimulation current (Fig. 3.14 C).

### 3.7.2 Dependency between stimulation rate and efficacy

In correspondence to the visual "critical flicker frequency" (CFF), the maximum frequency of electrical stimulation capable of modulating neuronal activity was estimated.

In a series of measurements, the mean stimulation rate of electrical stimuli with Gamma distributed inter-stimulus intervals (N=5100) was varied systematically between 5–73 impulses/s (section 2.5.2). Cortical spikes can be observed in a narrow time window after the stimulus that differs for the different experimental conditions (see Discussion). The average number of evoked spikes in this time window decreases with increasing mean stimulus rate. Fig. 3.15 shows this relationship for data from five measurements in three cats. The absolute spike counts in a narrow time window (highlighted in Fig. 3.15 B) are corrected for an estimated number of "spontaneous spikes" that would have occurred without stimulation. The latter is taken from a corresponding
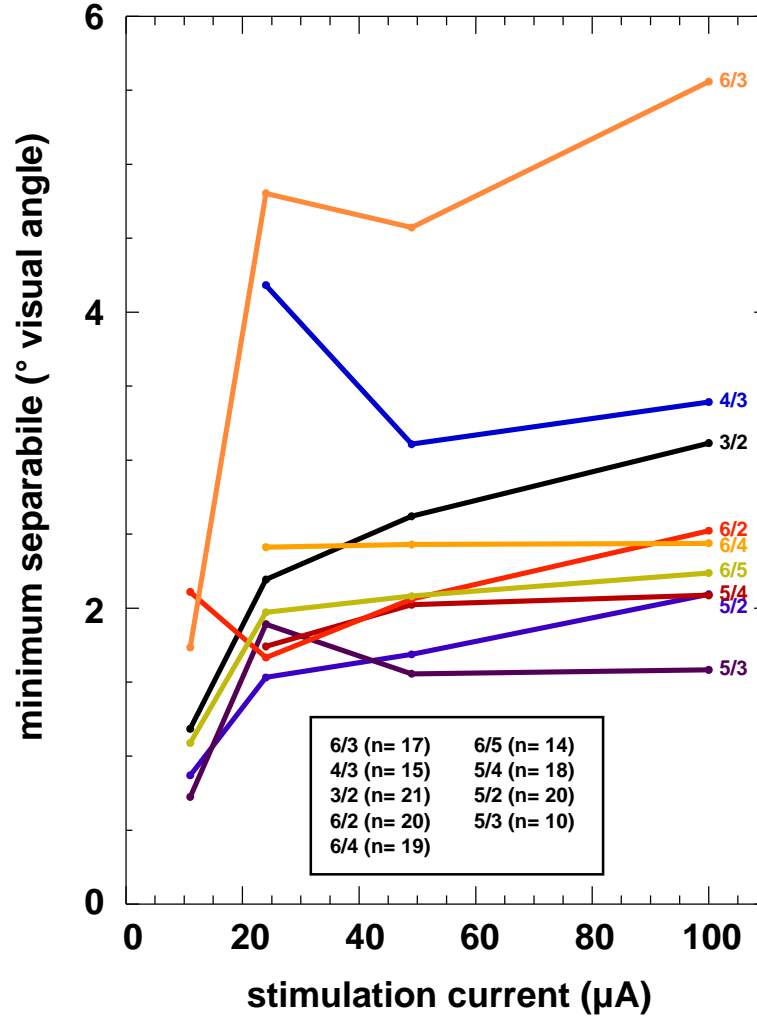
Figure 3.13: Minimum separabile depending on the stimulation current (data based on N=154 ePSFs, calculation of minimum separabiles described in Methods). Graphs are plotted for all pairs out of five efficient retinal stimulation electrodes. The electrode pair R2 and R4 yields minimum separabiles of up to 18° (N=26, not shown)).

time window before the stimulus and accounts for the background activity that is superimposed on the evoked spike activity. In order to compare spike counts from different recording conditions (i.e. different experiments and cats), corrected spike counts were normalized to the respective background activity. Thus an ordinate value of one indicates that in the specified time window twice as many spikes are found than in the background activity ($S/N = 2$). As can be seen in Fig. 3.15 A, this is true at mean stimulation rates above 60 imp/s for most recordings. The blue curve is based on SUA from a recording site that does not optimally match the stimulation electrode position. The
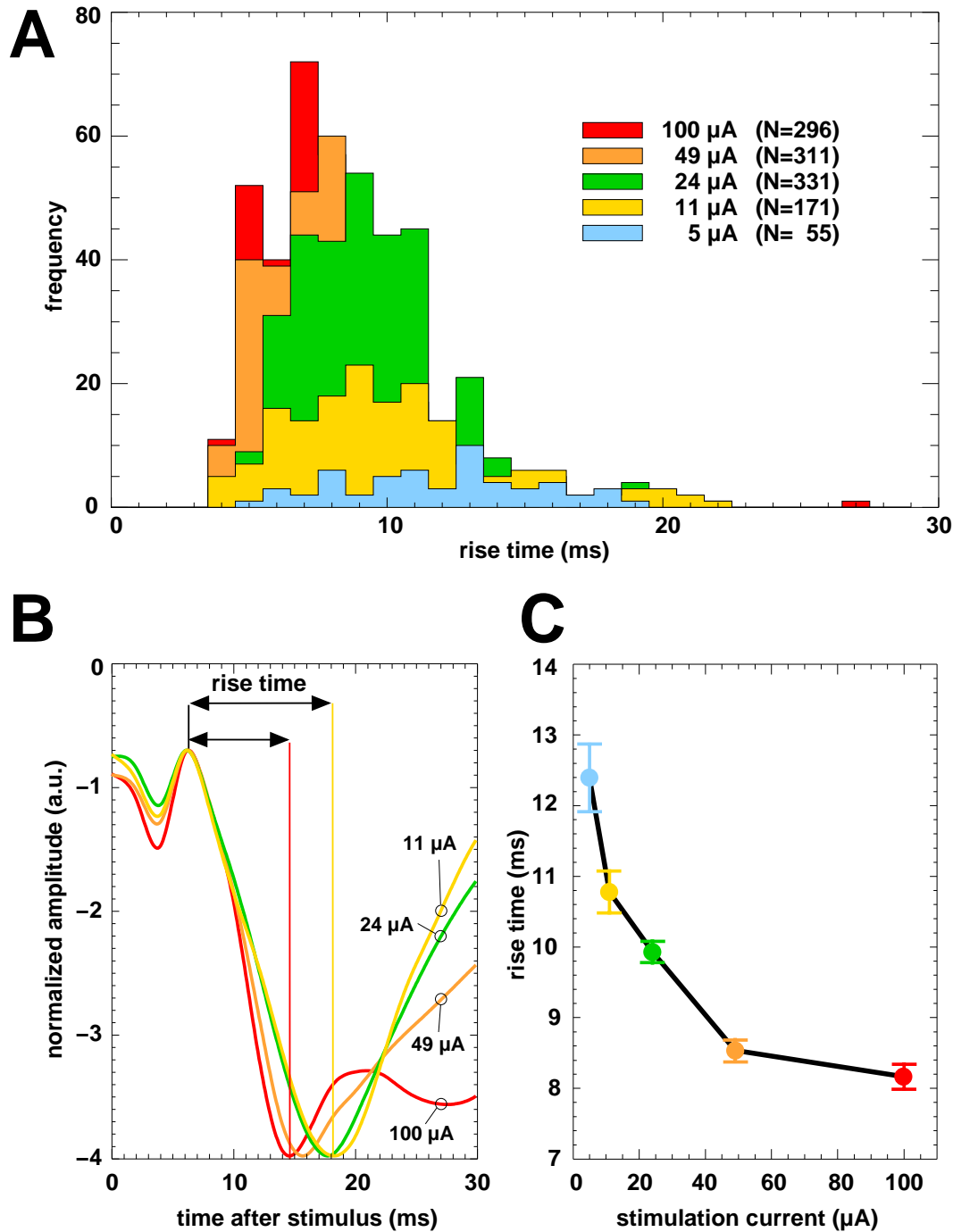
Figure 3.14: Rise times of significant ($S/N > 4$) early response components of LFP-PSTHs (N=1164) were analyzed. **A)** Shown are rise time-histograms for five stimulation currents (see inset). **B)** Example for the estimation of rise times for different stimulation amplitudes (colors as in A). Note that the cortical response peaks earlier for high stimulation currents (14–18 ms). **C)** Summary tuning curve for the mean rise time from the distributions shown in A. The rise time declines for increasing stimulation current. Error bars indicate the standard deviation of means (standard error).
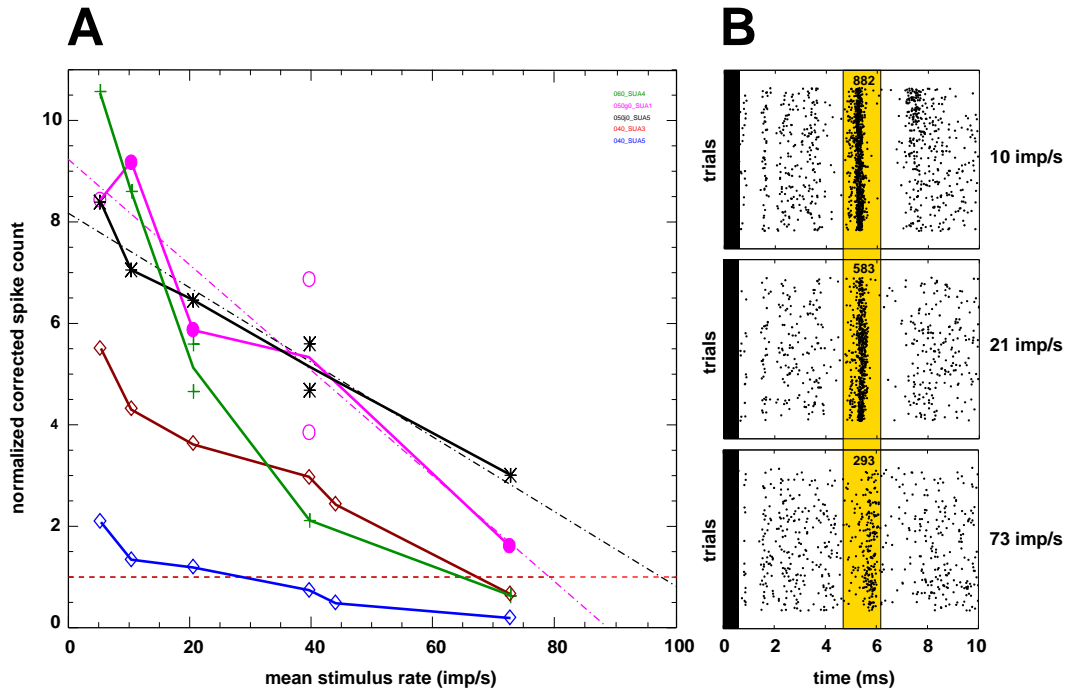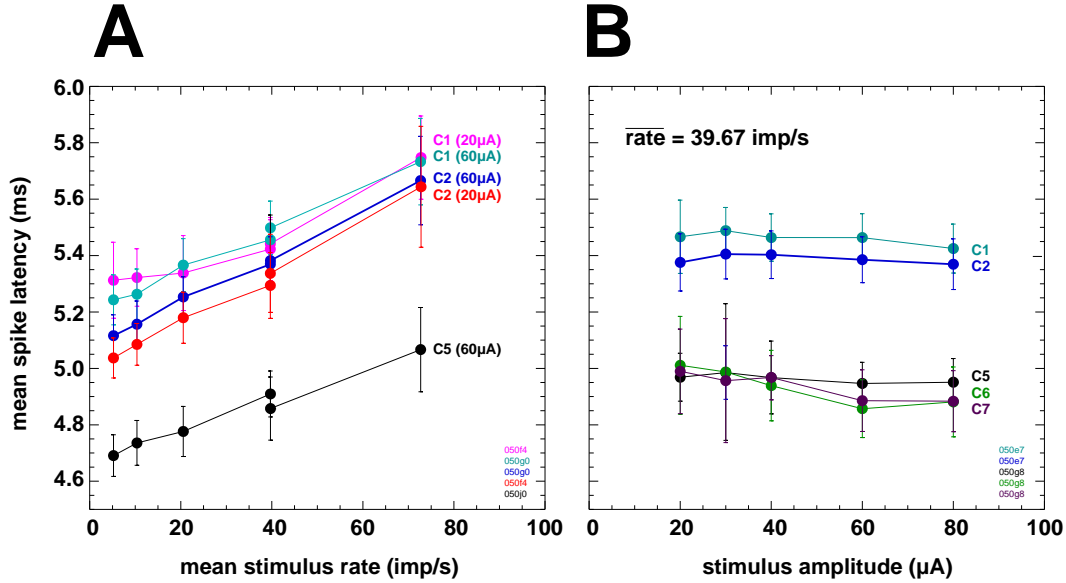
Figure 3.15: **A)** Dependence of the spike count on the mean stimulation rate of electrical stimuli with Gamma distributed inter-stimulus intervals (N=5100). The spike counts observed in a narrow time window after the stimulus are corrected for an estimated number of "spontaneous spikes" that would have occurred without stimulation. The horizontal red line marks the level at which twice as many spikes are found as in a window before the stimulus (S/N=2). **B)** Example raster plots for three different mean stimulation rates. The number of spikes found in the analysis window (highlighted in dark yellow) is given on top of each raster plot. Dots between $0-4ms$ after the stimulus result from residual stimulation artifacts and do not reflect neuronal activity. Note the slightly delayed occurrence of spikes in the high stimulation rate case.

SUA upon which the brown curve is based was simultaneously recorded and matched the stimulation site better, yielding a higher stimulation effectivity. In two measurements (magenta and black curves) even the highest stimulation rate tested (73 imp/s) yields spike counts that are well above the background level. Linear fits of these curves traverse the threshold level above 80 imp/s stimulation rate.

3.7.3 Precision of electrically evoked cortical responses

Let us take a closer look at the timing and precision of evoked spikes. In Fig. 3.15 B we can observe that the spikes are slightly delayed in the high stimulation rate condition (lower raster plot). In Fig. 3.16 A mean spike la-

Figure 3.16: **A)** Dependence of the spike latency on the mean stimulation rate of electrical stimuli with Gamma distributed inter-stimulus intervals (N=5100). The upper (colored) graphs represent data from electrical stimulation at one retinal stimulation site. Latencies are slightly shifted with respect to each other for different recording sites and amplitudes. The lower (black) line represents data from a stimulation 3.2° (approximately 0.64 mm retinal distance) closer to the optic disk. The latency therefore is reduced due to the spared intra-retinal travel time. **B)** Only weak dependence of the spike latency on the stimulation amplitude can be observed.

tencies are plotted against the mean stimulation rate for three neurons. Error bars indicate the standard deviation of the latency distributions. The upper four graphs represent data from two SUAs that were recorded in two measurements with 20 μA and 60 μA stimuli, respectively. The lower (black) curve represents data from a stimulation site 3.2° (approximately 0.64 mm retinal distance) closer to the optic disk. The latency therefore is reduced due to the spared intra-retinal travel time. Given that the conduction velocity is approximately 1–2 m/s for the unmyelinated axon fibers in the retina (Stanford, 1987), this accounts for a 0.32–0.64 ms short cut. Obviously, the mean spike latency correlates with the mean stimulation rate in a linear fashion with higher stimulation rates yielding higher latencies. Additionally, the width of latency distributions slightly increases with the stimulation rate as can be seen from the amplitude of the error bars. However, mean spike latencies are similar for 20 μA and 60 μA stimulation amplitudes (upper four graphs).

Interestingly, the amplitude of electrical stimuli has only little or no effect on the spike latencies. Fig. 3.16 B shows the mean latency of spikes for different stimulation amplitudes. The mean stimulation rate was kept at 39.7 imp/s for

all measurements. The blue and the black curves in Fig. 3.16 B correspond to the blue and black curves in Fig. 3.16 A. Little or no effect can be observed on the mean spike latency.

Fig. 3.17 demonstrates the findings for the narrowly distributed latencies of one recording site. Again, electrical stimuli with Gamma distributed inter-stimulus intervals were applied (N=5100). In Fig. 3.17 A the mean stimulus rate is increased from 5.2 imp/s in the upper plot to 72.7 imp/s in the bottom plot. The current amplitude for single biphasic stimuli is kept constant at 60 μA. As expected from the previous results, the narrowly distributed spike latencies systematically shift towards higher values for increasing mean stimulus rates. The maximum shift is 0.55 ms in this rather typical example. In Fig. 3.17 B, the stimulus amplitude is varied from 80 μA in the upper plot down to 20 μA in the bottom plot. 10 μA stimuli did not evoke any spikes. The mean stimulation rate is kept constant at 39.7 imp/s. No shift is observable in the latency. The plots marked with an asterisk are based on measurements with identical stimulation conditions and exhibit mean latencies that match very well.

## 3.8 Testing of epi-retinal prototype implants

Epi-retinal stimulations with flat polyimide foil electrode arrays (Fig. 2.7 B, IBMT St. Ingbert) were successfully performed on two cats. Mapping of visual cortical receptive fields was not possible directly after the surgical implantation procedure.

In one experiment, electrical stimulation with single biphasic anodic stimuli of 25 μA amplitude and 400 μs total length was sufficient to evoke cortical potentials that could be registered at the cortical recording sites. In the other experiment, 6.25 μA stimulation was clearly above threshold.

Single cortical spikes could be driven with two stimulation electrodes (Fig. 3.2, R9 and R18). Latencies for these spikes depend on the stimulus channel. Spikes that were elicited by retina electrode R9 have latencies of about 7.50 ms, whereas those elicited by retina electrode R18 are seen after only 6.25 ms. The temporal delay of spikes elicited by R9 can be explained by an additional intra-retinal travel time.

Earliest evoked LFP responses peak between 10–20 ms after stimulation onset. This latency is similar to latencies for epi-retinal electrical stimulation with fiber electrodes (Fig. 3.18).

Activation is achieved exclusively by a spatially constrained set of stimulation electrodes. Efficient retinal stimulation sites demarcate an elongated eRF (highlighted yellow) slightly differing for cortical recording sites. The elongated axis is oriented approximately along the axon fibers. Cortical ePSFs are relatively broad for some of the efficient stimulation electrodes with occasional
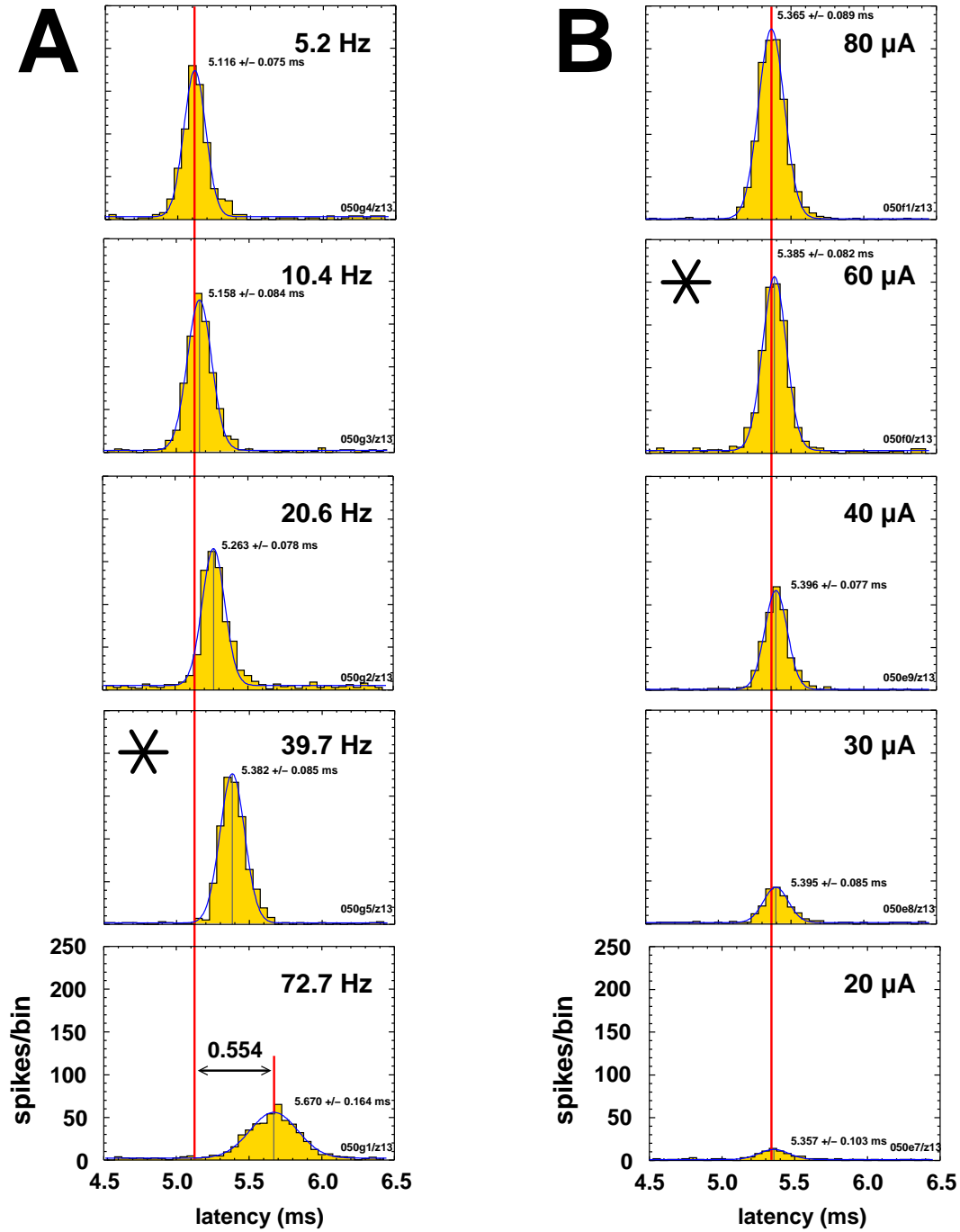
Figure 3.17: **A)** Example for the dependence of the spike latency on the mean stimulation rate of electrical stimuli. Stimuli had Gamma distributed inter-stimulus intervals (N=5100). Spike PSTHs for one cortical recording site are shown. The current amplitude for single biphasic stimuli was 60 μA. The mean stimulus rate is increased from 5.2 imp/s in the upper plot to 72.7 imp/s in the bottom plot. The narrowly distributed spike latencies shift systematically towards higher values for increasing mean stimulus rates. **B)** Spike PSTHs for the same cortical recording site as in A are shown. Here the mean stimulus rate is 39.7 imp/s and the stimulus amplitude is varied from 80 μA in the upper plot down to 20 μA in the bottom plot. 10 μA stimuli are sub-threshold (not shown). No dependence on the stimulation amplitude can be observed. The plots marked with an asterisk have identical stimulation conditions.

sharp peaks (Fig. 3.20 B). In the two experiments with epi-retinal prototype implants, ePSF-widths were within the range of those found with epi-retinal fiber electrode stimulation.

3.9   Testing of sub-retinal prototype implants

Sub-retinal stimulations with flat polyimide foil electrode arrays (Fig. 2.7 C, NMI Reutlingen) were successfully performed on two cats. Mapping of visual cortical receptive fields, though, was not possible in these experiments. However, one cortical recording site showed visually evoked potentials when the eyes were stimulated with a full field visual stimulus. Electrical stimulation with single biphasic anodic stimuli of 50 μA amplitude and 1 ms total duration evoked cortical potentials that could be registered at a subset of recording sites. Fig. 3.19 summarizes the stimulation success for one experiment. Three rows of five boxes are depicted schematically indicating the positions of the corresponding stimulation electrodes on the retina. The horizontal electrode separation is 0.1 mm, while the vertical electrode separation is 0.1 mm between the top and middle row, and 0.2 mm between the middle and bottom row. The top row is at the distal end of the implant. Three more proximal rows of electrodes did not activate cortical units at the recording sites (not shown). The upper left electrode was damaged during the implantation surgery and did therefore not work during the experiment. Electrode contacts were $7° - 8°$ nasal and $2° - 3°$ superior of the area centralis. Each box contains PSTHs of six cortical recording electrodes (C1, C3–7). Downward deflections indicate cortical activations. As can be observed in the plot, cortical activation can only be achieved by a certain subset of "efficient" electrodes that are grouped closely together at top left forming an elongated eRF approximately along the axon fiber orientation (highlighted yellow). The initial stimulation artifact is present at all recording positions. At some recording positions, early cortical activations occur as downward deflections shortly after the artifact (10–20 ms). This latency corresponds to similar delays after epi-retinal electrical stimulation with fiber electrodes. Later response components (20–60 ms) can be seen at more recording positions than early response components, which is indicative of a broadened cortical spread of activity.

Cortical ePSFs can be estimated from the LFP responses as shown in Fig. 3.20 C. In the two experiments, ePSFs had a similar width as for epi-retinal stimulation width fiber electrodes.
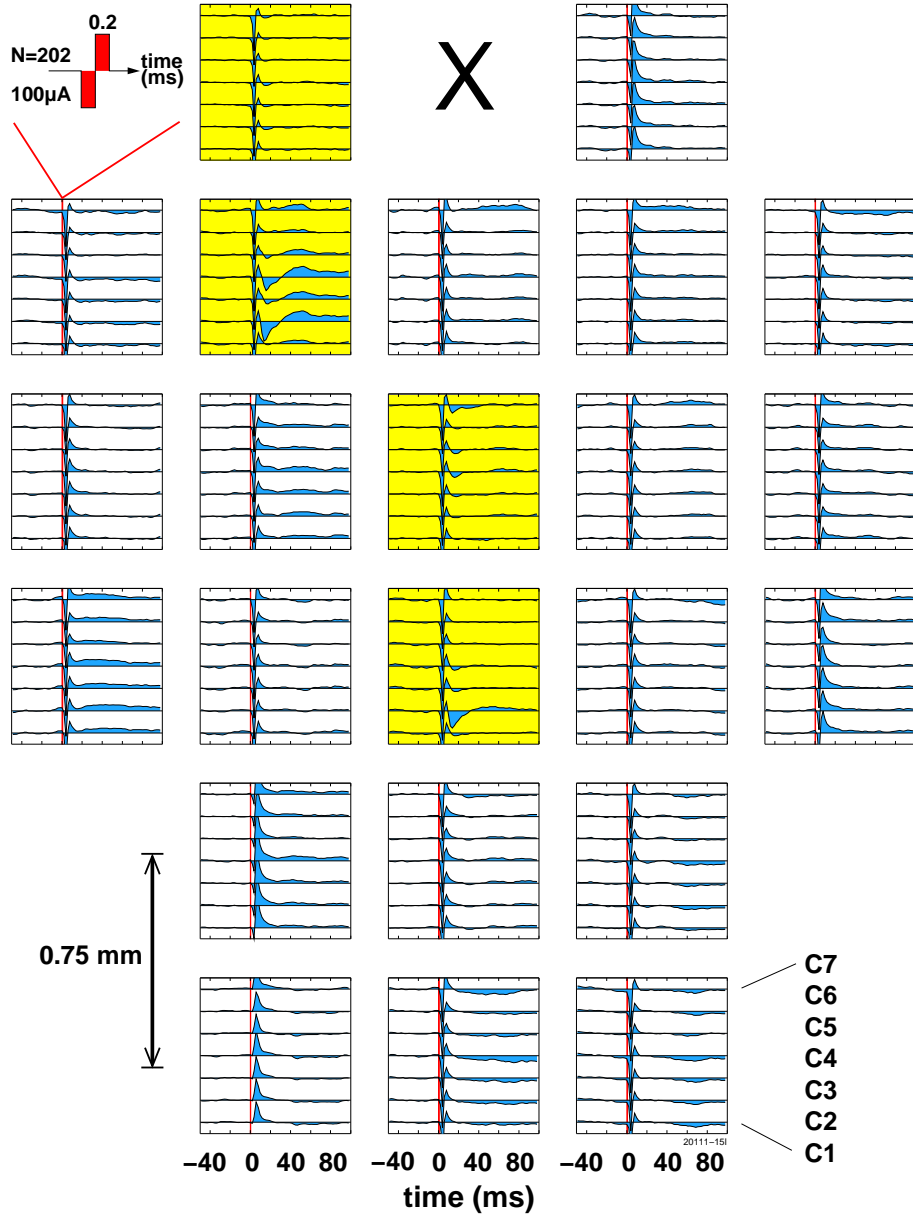
Figure 3.18: PSTHs of cortical population responses (LFP) after para-central epi-retinal electrical stimulation (N=202) with an implanted polyimide foil electrode array (IBMT St. Ingbert). The electrode array extended from the optic disk to the area centralis. Electrode contacts had a 750 μm spacing on a rectangular grid. Box positions schematically indicate the positions of the stimulation electrodes. The electrode contacts on top touched the area centralis, those at the bottom were placed at the edge of the optic disk. Thus, ganglion cell axons extended from top to bottom of the plot. Each box contains PSTHs of seven cortical recording electrodes (C1–C7). After an initial stimulation artifact which is present at all recording positions, earliest cortical activation can be seen as downward deflections shortly after the artifact. Note that cortical activation can only be achieved by a certain sub-set of "efficient" electrodes that are grouped together forming an elongated eRF (highlighted yellow).
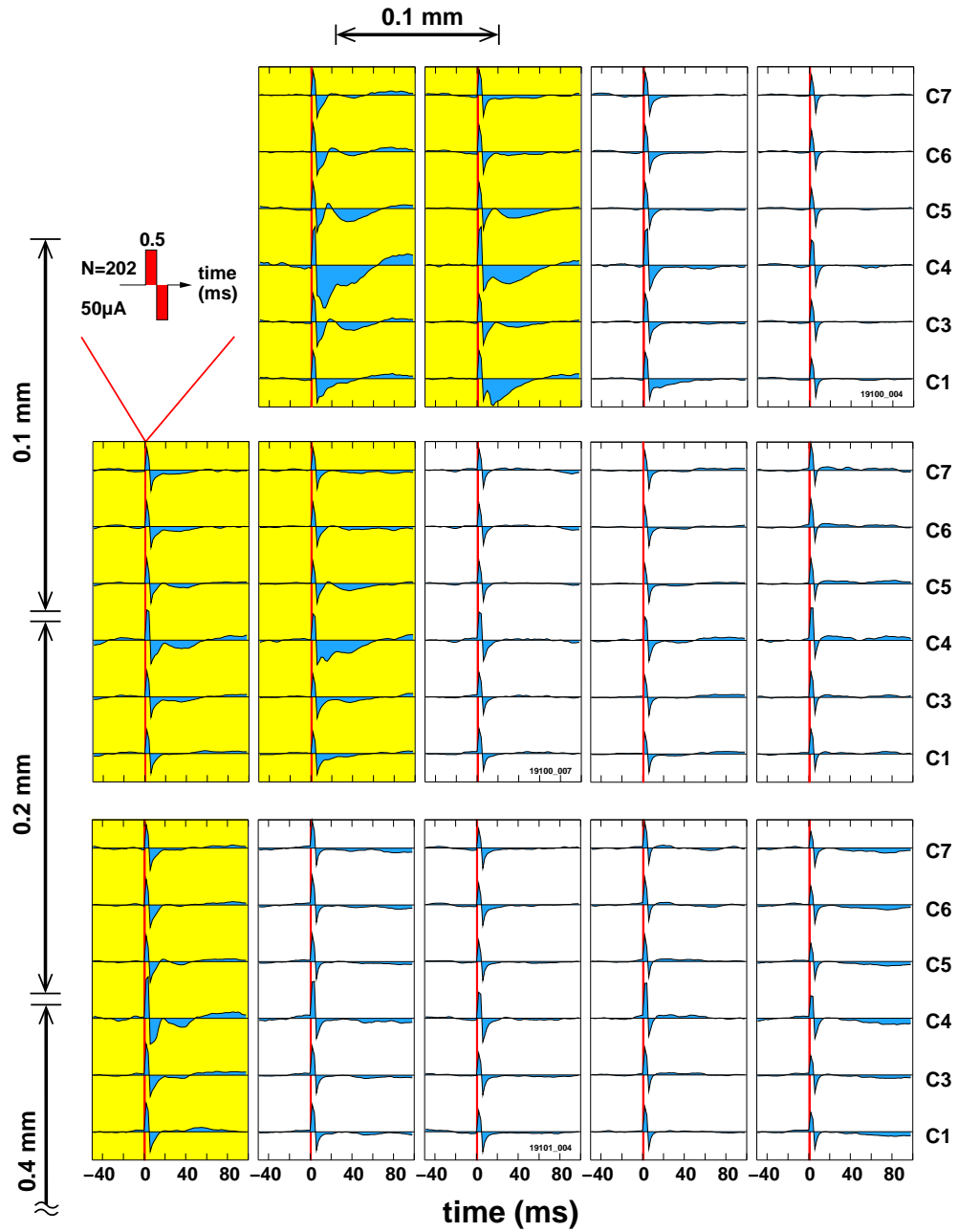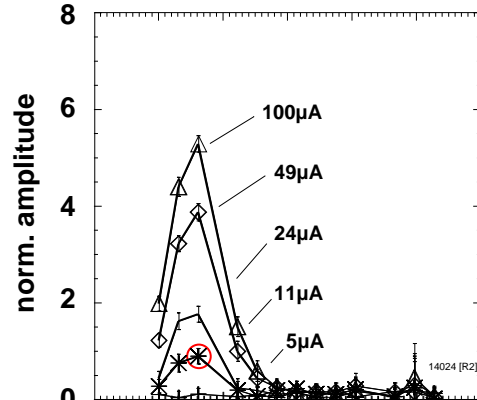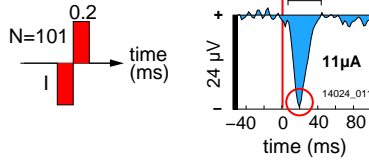
Figure 3.19: PSTHs of cortical population responses (LFP) after para-central sub-retinal electrical stimulation (N=201) with an implanted polyimide foil electrode array (NMI Tübingen). Three rows of five boxes are depicted schematically indicating the positions of the corresponding stimulation electrodes on the retina. Electrode contacts were $7° - 8°$ nasal and $2° - 3°$ superior of the area centralis. Each box contains PSTHs of six cortical recording electrodes (C1, C3–C7). Downward deflections indicate cortical activations.
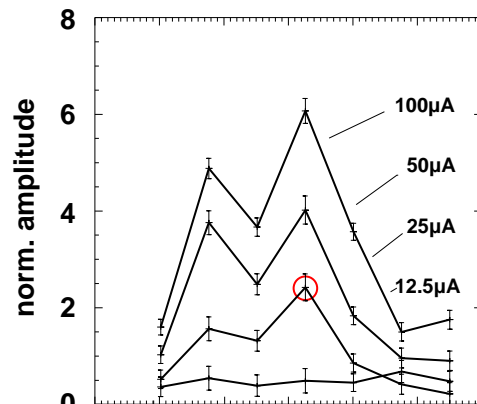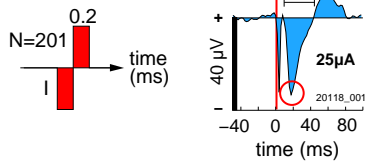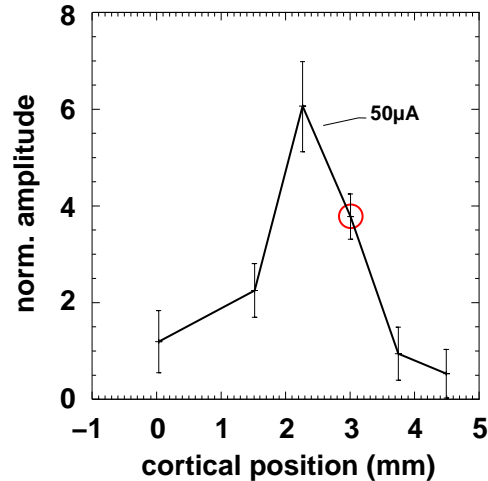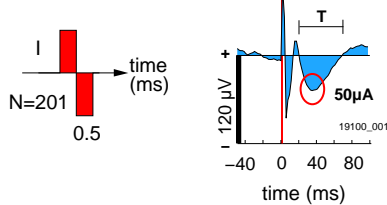
Figure 3.20: Examples of ePSFs of cortical population responses (LFP) after para-central epi-retinal electrical stimulation with **A)** fiber stimulation electrodes (Marburg), **B)** an epi-retinally implanted polyimide foil electrode array (IBMT St. Ingbert), and **C)** a sub-retinally implanted polyimide foil electrode array (NMI Tübingen). Distributions of cortical activity are shown for several stimulation current amplitudes (A, B). Typical cortical responses are depicted to the right. Normalized responses (red circles) for the generation of ePSFs were taken from the first response component after the stimulation artifact.

3.10 Stimulation with fiber electrodes and implants

Fig. 3.20 compares ePSFs for epi-retinal fiber electrode stimulation (A), epi-retinal foil electrode stimulation (B), and sub-retinal foil electrode stimulation (C). Typical cortical LFP responses are depicted for each stimulation type. The duration T of the excitatory phase of the cortical response is marked with a horizontal bar. For just above threshold stimulation, T typically lies between 35–45 ms. However, the duration T can rise significantly for higher stimulation amplitudes (Fig. 3.1).

4 Discussion

4.1 General remarks

In order to assess the potential benefits for a blind patient equipped with a retinal prosthesis, we studied the cortical representations of focal electrical epi- and sub-retinal stimuli in the cat, namely the spatio-temporal cortical activity distributions. We estimated the spatio-temporal resolution of electrical retina stimulation from the location, width, and overlap of activity distributions. Retinotopy and specificity of electrical stimulation were assessed by comparison of electrically evoked responses to those visually evoked.

Retinal vRFs based on LFP match the corresponding retinal electrode locations very well. However, retinal vRFs based on spike activity are shifted distally with respect to the representation of the optic disk (N=7). Cortical eRF-positions are similar to cortical vRF-positions. In particular, the retinotopic arrangement of cortical RFs is preserved for electrical stimulation. Location and width of ePSFs are distinct for retinal stimulation electrodes. We calculated the full width at half height of ePSFs for local field potentials to $0.92° \pm 0.15°$ (N=7) near threshold stimulation and $1.58° \pm 0.49°$ (N=121) at about tenfold threshold stimulation. Average full width at half height was $1.28\ mm \pm 0.33\ mm$ cortex corresponding to $1.4° \pm 0.4°$ visual angle (N=298, four cats). Correspondingly, the amount of overlap between ePSFs of retinal stimulation sites was smaller (i.e. spatial resolution higher) for low stimulation currents (N=154 pairs of ePSFs tested): Minimum separabiles were $0.8° - 2.0°$ for near threshold stimulation and $1.6° - 4.3°$ for about tenfold threshold stimulation.

The fastest signal components of local field potentials had rise times of $8 - 12\ ms$ depending on the stimulation current amplitude. Inter-stimulus delays of $16 - 24\ ms$ corresponding to a $40 - 60\ imp/s$ mean stimulation rate should therefore be resolved by the cortex. Mean inter-stimulus times of as short as $12.5\ ms$ evoked significant modulations of cortical activity. Thus, even a stimulation rate of $80\ imp/s$ might be resolved cortically. Spike latencies increased with the mean electrical stimulation rate but did barely depend on the stimulation amplitude. This can be explained by a model of spike initiation that takes into account the relative refractory period of activated neurons.

Experiments with epi- and sub-retinal foil electrode arrays proved to be

successful in demonstrating efficient and localized cortical activation. But several lines of evidence indicate that epi-retinal electrical stimulation with flat electrodes tends to stimulate axons prior to somata.

4.2 Electrical retina stimulation with fiber electrodes and prototype implants

Experiments with epi- and sub-retinal prototype implants proved to be successful in demonstrating efficient and localized cortical activation. Retinal and cortical responses to visual stimuli vanished immediately after the implantation. Most probably the retina was traumatized during the eye surgery. When cats were allowed to recover from the surgery, visually evoked responses could be verified on subsequent days after the implantation. Based on our experience with fiber electrode stimulations, it was still possible to position the recording array over cortical sites that roughly corresponded to retinal stimulation sites. Hence electrically evoked activity could be recorded and permitted the estimation of ePSFs.

More detailed studies on the response characteristics and spatio-temporal resolution of electrical retina stimulation were carried out with fiber electrodes. The implantation surgery was atraumatic and fiber electrodes could easily be repositioned during the experiment. Additionally, individual tight electrode contacts onto the retina could be ensured and fine tuned under visual inspection. Because of this, fiber electrode experiments facilitated the detailed analysis of ePSFs and eRFs.

4.3 Cortical evoked response characteristics

4.3.1 What is stimulated?

In our epi-retinal stimulations, we elicited none, one or more than one cortical spike per stimulus when stimulation was sub-threshold, supra-threshold or activating different populations of retinal cells, respectively. However, when burst stimuli were applied (i.e. electrical biphasic stimuli in rapid succession at about 2.5 kHz, N=1 observation), evoked cortical spike latency patterns tended to be more complex than after single electrical stimuli. They revealed up to six spike clusters within a 5 ms time interval (data not shown).

For the epi-retinal approach one expects that maximally one spike can be evoked per stimulus and ganglion cell. This is due to the (relative) refractory period of the ganglion cells (Nicholls et al., 1992) which is longer (ca. 10 ms) than the typical duration of electrical stimulation impulses (0.4 ms). For electrical burst stimuli, however, any of the N impulses within a burst can be

supra-threshold. Additionally, consecutively evoked spikes can be temporally integrated at subsequent synapses. Both mechanisms yield a differentiation of spike latencies into the contributions of specific burst-impulses and hence yield more complex spike latency patterns.

Principally, spikes can be elicited in rapid sequences as long as the inter-stimulus delays exceed the refractory period of the stimulated cells. The recorded data shows that efficient stimulation of cortical neurons is constrained to inter-stimulus times larger than 12.5 ms. At this time scale it seems feasible to mimic the physiological statistics of retinal output by the generation of complex ganglion cell activity patterns. If sub-retinal stimulation is applied, the still intact retinal network is activated and can produce bursting activities at the retinal output layer (Stett et al., 2000). Since the intensity of a visual stimulus is rate-coded in normal vision, epi- and sub-retinal electrical stimuli can code intensity or contrast information by means of the stimulation rate.

In some cases single cortical spikes could be driven with two stimulation electrodes. The stimulation electrodes were positioned along the same retinal axon fiber originating from a ganglion cell within the cortical neuron's RF. This indicates that epi-retinal stimulation was axonal for at least one of the stimulation electrodes. From the difference between spike latencies and the known electrode separation along the axon, we estimated the intra-retinal conduction velocity. For example, Fig. 3.2 is based on an experiment in which stimulation electrodes R9 and R18 of an epi-retinal implant were separated by 1.7 mm. The evoked spike latencies differed by 1.14 ms. This leads to an intra-retinal conduction velocity of 1.49 m/s which is in good agreement with data from Stanford (1987) who reported conduction velocities between 1–2 m/s.

Nowak and Bullier (1997a) addressed the problem whether axons or cell bodies are activated by electrical stimulation. They compared the chronaxies for axonal and soma electrical stimulation in cortical gray matter by anti-dromic activation and intra-cellular current injection, respectively. They report that chronaxies for axonal stimulation were very similar to those for post-synaptic potentials after extracellular electrical stimulation. On the contrary, chronaxies for soma stimulation were 40 times higher. This indicates that axons and not cell bodies are the neuronal elements activated after electrical stimulation of gray matter. With epi-retinal stimulation, stimuli are applied to a highly segregated, laminar structure with ganglion cell axons being closer to the stimulation electrode tip than somata. This also supports the notion that axons are more likely to be stimulated.

4.3.2   Precision of electrically evoked cortical responses

In our data, latencies for cortical spikes were between 3.4–9.0 ms and were narrowly distributed with an absolute width of 0.5 ms or less (Fig. 3.17). Lee

et al. (1977) demonstrated that the conduction time for a spike in a retinal ganglion cell to its cortical target is between 4.5–7.5 ms for X or Y cells. Our conduction times for axonally evoked spikes were even lower (e.g. see first spike in Fig. 2.3), since a fraction of the intra-retinal travel time, which can easily add up 1–3 ms depending on the stimulation eccentricity, is spared (Stanford, 1987). Latencies beyond the range given above by Lee et al. (1977) can be attributed to the occasional recording from neurons at subsequent steps of cortical signal processing. In this case, additional temporal delays comprise post-synaptic spike initiation times (about 0.4 ms), mono-synaptic delays (0.6–1.05 ms), and di-synaptic delays (1.05–2.4 ms) (Ferster and Lindström, 1983). Moreover, Eger (2001) argued that epi-retinal electrical stimulation can simultaneously excite magno- and parvo-cells, which show distinct latencies in a similar range. Due to the reliability and precision of the excitation (in some cases one spike for every stimulus within $\pm$ 0.3 ms), activated neurons carry a large amount of information about the stimuli (Eger, 2001).

In addition to the retinal position, spike latencies depend on the mean electrical stimulation rate but not on the stimulation amplitude. For higher mean stimulation rates, cortical spike latencies are delayed and have an increased variability (Fig. 3.16 A and Fig. 3.17 A). This effect cannot be explained by an apparent decrease of stimulation efficacy per se, since spike latencies are not changed with different stimulation amplitudes (Fig. 3.16 B). A similar effect has been reported by (Stone and Hoffmann, 1971). They electrically stimulated in the optic chiasm of anesthetized cats and recorded evoked pre- and post-synaptic activity in the dLGN. Compared to a stimulation at 1 imp/s, a stimulation at 100 imp/s caused an increase in spike latency, and in the variability of the spike latency. The latency of the pre-synaptic signal, however, was unchanged. This indicates that the rate-dependent change in the post-synaptic spike latency may be attributed to the spike initiation mechanism.

These somewhat surprising latency-effects can be explained by the influence of the refractory period of spiking neurons on the efficiency of stimuli. When the mean electrical stimulation rate is elevated, i.e. the mean inter-stimulus interval lowered, an increasing number of electrical stimuli falls into absolute refractory periods of activated neurons and hence fails to be efficient. This reduces the total yield of evoked spikes. At intermediate inter-stimulus intervals (10–50 ms), electrical stimuli tend to fall into the relative refractory periods of activated neurons. Refractory neurons are excited if the extracellular stimulation potential exceeds the slowly recovering threshold potential of the neuron. However, due to the negative slope of the threshold potential, the probability that a stimulus excites the neuron increases with the duration of the stimulus. The threshold potential "approaches" and traverses the extra-cellular voltage drop caused by the stimulation, thus favoring a delayed response. This effect is barely visible at low stimulation rates, since most inter-stimulus intervals

are longer than the refractory period.However at high stimulation rates the excitation delay becomes evident.

When the stimulation amplitude is increased, more retinal ganglion cells are simultaneously activated, because the electrical field depolarizes a wider retinal area (Schanze et al., 1997). A contiguous population of ganglion cells projects to a contiguous population of target cells in the dLGN and the cortex. Thus, with higher stimulation amplitudes activating more neurons, lateral connections among target cells can support the cooperative activation of dLGN cells by means of spatial summation. This increases the probability of the generation of post-synaptic dLGN spikes, which are detected as first spikes in the input layer 4 of the primary visual cortex. However, the latency of the first spike is only weakly affected. Temporal summation of pre-synaptic dLGN inputs has no effect due to the simultaneity of the afferent input. The latency of first cortical spikes is therefore not influenced by temporal summation at the dLGN level.

The classical view of retinal stimulus encoding states that ganglion cells encode their inputs by their output firing rate (Meister and Berry, 1999). Due to the variability of the neuronal firing rate, this coding scheme requires a considerable time for information processing (Mountcastle et al., 1962). However, stimulus specific cortical responses have been found as soon as 40 ms after the stimulus (Celebrini et al., 1993). To overcome the limitation of a short information processing time, temporal codes have been proposed that take into account the timing of first cortical spikes. Rullen and Thorpe (2001) showed that natural visual stimuli could be reliably extracted from a population of ganglion cell spike trains by means of the rank order of first spike arrival times. By appropriately arranging spatio-temporal electrical stimuli, rank orders of evoked first spikes could be specifically set within a population of cortical neurons. Given that the latency of cortical spikes can be influenced by the stimulation rate, information may be encoded in the spike arrival times by a modulation of the mean stimulation rate, too.

4.3.3 Multi-peaked averaged cortical responses

Multiple peaks were often observed in the PSTHs of cortical population responses (Fig. 3.1). This repetitive excitatory activity may be caused by intracortical feedback loops in response to electrical stimuli. Moreover, the activation of segregated retino(-thalamo)-cortical pathways may account for burst-like responses due to distinct latencies for magno-, parvo- and conio-pathways. However, Nowak and Bullier (1997b) (and earlier work by Kirk et al., 1975) found that retino-geniculate conduction times differed between retinal cell types: On average, Y axons transfer information to the cortex 3.5 ms faster

than X axons, and X axons 6 ms faster than W axons. Troy and Lennie (1987) pointed out that the conduction advantage of the Y pathway is small compared to the variability in latency of reliable detection of a visual stimulus and therefore of minor importance for visual perception. Baseler and Sutter (1997) and Klistorner et al. (1997) identified distinct magno- and parvo-cellular contributions to the multi-focal VEP in human volunteers. The parvo-cellular component was delayed by about 20 ms. Magno- and parvo-cellular cortical input may account for the first and second excitatory peak in the observed multi-peaked PSTHs. Conio-cell activities as well as the activation of intra-cortical feedback loops may contribute to the later response components.

In some recordings, the polarity of cortical LFP responses was inverted with respect to the other recording sites (Mitzdorf and Singer, 1978). In these cases, electrodes had always been inserted into deeper cortical layers as noted in the experiment protocols. However, excitatory and inhibitory responses could be identified by the analysis of spike activity simultaneously recorded by the same electrode (MUA and SUA).

4.3.4   Properties of visual receptive fields

Fig. 4.1 shows a schematic representation of the pattern of fiber bundles in the central part of the right retina of a cat (modified from Stone and Holländer, 1971). Each bundle consists of a number of axons, each arising in individual ganglion cells and projecting to the optic disk. The visual stimulus used for assessing vRFs was projected on a retinal area highlighted by the light blue rectangle. Contours of cortical vRFs (as in Fig. 2.6) are projected onto corresponding retinal locations (small colored circles) and appear upside down with respect to the representation in the visual space. Axons originating in the vicinity of the cortical vRFs are highlighted in dark blue.

Visual RFs of cortical recording sites sometimes showed a non-conformal visuotopic organization. Some adjacent cortical recording sites have vRFs that strongly overlap, others are clearly separated. This has been observed by others as well (Das and Gilbert, 1997; Normann et al., 2001) and may reflect the patchy organization of the visual areas (e.g. bands of ocularity in cat area 18).

The vRFs of retinal electrodes were distinct for LFP and MUA signals (Fig. 3.3). LFP-vRFs closely resembled the stimulation array's geometry. In comparison, MUA-vRFs were shifted to more distal locations with respect to the optic disk. The connection lines between corresponding LFP- and MUA-vRFs were oriented similar to the axons at this retinal location (compare highlighted axon bundles in Fig. 4.1 to those in Fig. 3.3). Since the LFP signal is band-limited to 1–140 Hz, LFP-vRFs are not influenced by the vigorous retinal spike activity. Most probably, retinal LFP reflects local intra-retinal
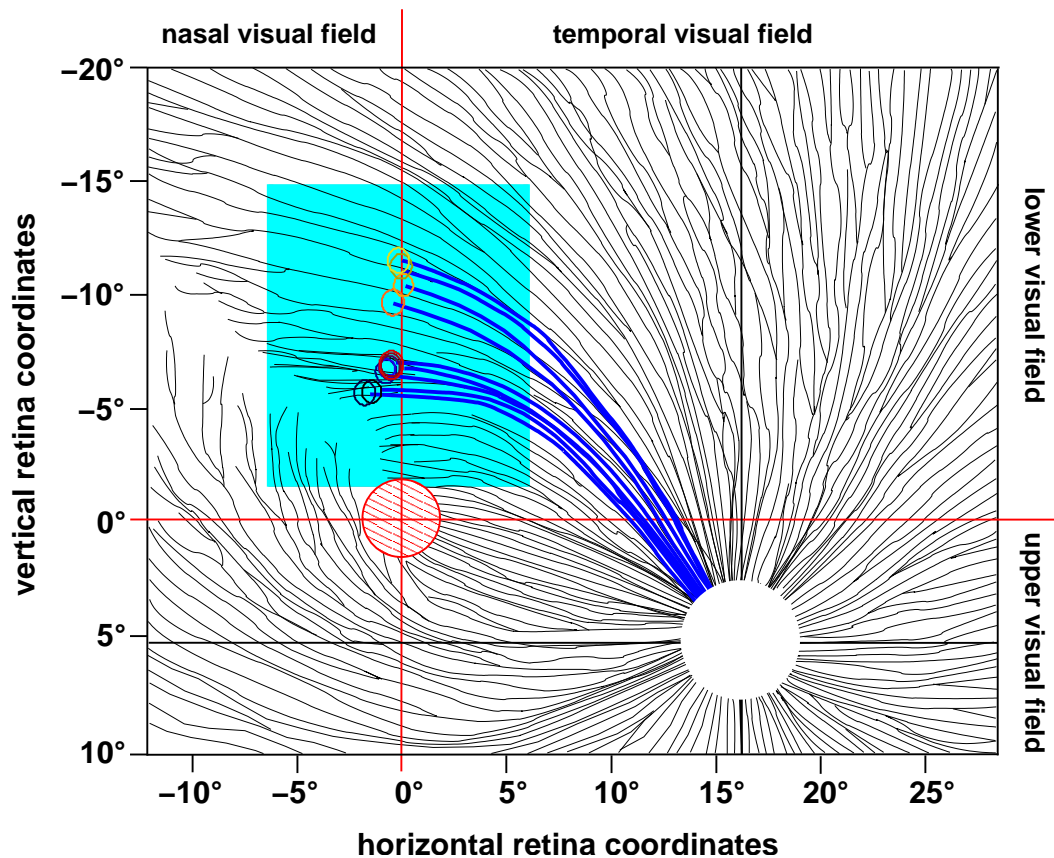
Figure 4.1: A schematic representation of the pattern of fiber bundles in the central part of the right retina of a cat. Each bundle consists of a number of axons, arising in individual ganglion cells and projecting to the optic disk (white circle in the lower right quadrant) (modified after Stone and Holländer, 1971). The red hatched circle marks the area centralis. The visual stimulus used for assessing vRFs fell on a retinal area highlighted by the light blue rectangle. Contours of cortical vRFs are projected onto corresponding retinal locations (small colored circles). Due to the geometry of the projection, vRFs are plotted upside down with respect to the representation in visual space (same vRFs as in Fig. 2.6). Note the orientation of axons originating in the vicinity of the vRFs (highlighted dark blue).

activity generated by photoreceptors, horizontal cells, bipolar cells, or amacrine cells. These neurons can produce slow graded potentials within the frequency range of the LFP signal. Graded potentials, however, are rather localized. This suggests that LFP-vRFs are located at the actual position of the retinal electrode. But MUA reflects the density of spike activity. The shift of MUA-vRFs to more distal locations is therefore indicative of the recording of spikes from axons originating in more distal somata. This is illustrated in Fig. 4.2. The figure shows interpolated cross correlation maps between a multi-focal
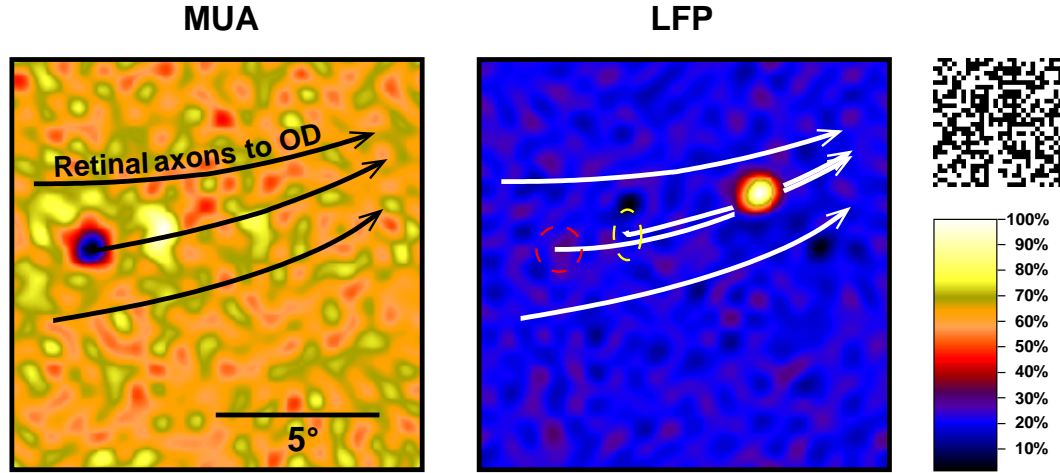
Figure 4.2: Example of interpolated cross correlation maps between a multi-focal visual stimulus and the simultaneously recorded MUA and LFP response of one retinal electrode. Stimulation details as in Fig. 2.6. Arrows indicate the assumed trajectories of ganglion cell axons to the optic disk (OD). Dashed circles indicate positions of MUA-vRFs superimposed on the LFP-vRF map.

visual stimulus and the simultaneously recorded MUA and LFP response of one retinal electrode (R6 in Fig. 3.3). The direction to the optic disk (OD) is indicated by the arrows. One MUA-vRF is located at the far left (dark patch) and a second, less pronounced about 2.1° further proximal with respect to the optic disk (white patch). The neurons responsible for the two MUA-vRFs have opposing characteristics: one group of neurons prefers an "OFF–ON" step in luminance ("ON"-cells), the other an "ON–OFF" step ("OFF"-cells). The LFP-vRF is shifted about 4.1° further proximally. Corresponding neurons prefer the "OFF-ON" luminance step. According to the explanations aforementioned, the retinal electrode was located at the position reflected in the LFP-vRF. The two MUA-vRFs indicate that "OFF"- and "ON"-ganglion cells at the retinal MUA-vRF locations generated spikes in response to the visual stimulus. These in turn were detected when the spikes passed the retinal recording site along their respective axon.

Despite a continuous intra-venous medication with a muscle relaxating agent, residual eye movements were evident in shifted vRFs of retinal and cortical recording sites. However, the relative positions of retinal LFP- and MUA-vRFs were unchanged for small eye movements (up to 3°), indicating that the locations of the retinal electrode tips were stable with respect to the retina. Most probably, retinal electrode tips were passively moved along with the eye movement due to their tight contact with the retina.

4.3.5   Properties of electrical receptive fields

The LFP-vRFs of retinal stimulation electrodes were taken as the "sampling points" for cortical eRFs. The analysis of cortical eRFs is thus based on the assumption that visual and electrical stimuli presented at the position of retinal LFP-vRFs stimulate the same cortical cells. However, as mentioned before, vRFs of retinal stimulation electrodes do not necessarily coincide with the actual sites of retinal activation. In particular, separations of stimulation sites along the retinal axons are more prone of misjudgments than those perpendicular to the axon orientation. Therefore, the estimation of eRF-locations is more precise in perpendicular than in parallel direction relative to axons. In most experiments, the cortical recording electrode array was oriented roughly in parallel to the vertical meridian. Because of this, the corresponding vRFs of the cortical electrodes were oriented perpendicularly to axons at the eccentricities used. Thus, we chose an electrode configuration that minimized the influence of the uncertainty of the exact stimulation site on the eRF estimation.

The estimation of eRFs was constrained by the limited number and the geometry of retinal stimulation electrodes. Seven electrodes were available with the fiber electrode array. However, estimated eRFs could be compared to corresponding vRFs (Wilms et al., 2001a,b). Locations of eRFs were near to vRFs, confirming the retinotopic distribution of electrically evoked cortical activity. The estimation of eRFs can be improved with retinal stimulation arrays with many densely spaced electrodes.

4.4   Estimate of spatial resolution with retinal implants

Cortical cells can only contribute to the processing of stimulus information if their activity is changed in response to the stimulus. Thus the spatial spread of cortical responses to stimuli roughly represents the cortical region dedicated to the processing of stimulus information. The analysis of LFP data yields a conservative measure of cortical spread since it integrates pre-synaptic inputs of a wider cortical area than compared to analyses based on data of single cortical cells (Schanze, 1995). Therefore, the estimation of spatial resolution of electrical retina stimulation was based on the analysis of the width of ePSFs as well as the minimum separabiles for LFP.

Wörgötter et al. (1998) and Wörgötter and Eysel (2000) demonstrated that anesthetized cats show spontaneous transitions from a synchronized EEG-mode similar to the state of drowsiness and sleep to a non-synchronized mode as during alertness. During phases of synchronized EEG, brief high-frequency bursts of spikes in the dLGN resulted in more effective connectivity and lead to a larger point spread of activity and wider RFs. In our case, spatial resolution

was assessed in an anesthetized animal preparation, which often shows synchronized EEG. This is further evidence that our analyses yield a conservative estimate for the spatial resolution in wake animals or blind people.

With a linear recording electrode configuration, separations of ePSFs centered in a line perpendicular to the recording electrode array orientation could only poorly be assessed. The reason is that merely the projection of the connection line onto the recording electrode array orientation could be estimated. However, the measurement of the FWHH was not affected by the recording electrode orientation (equations 2.1–2.4).

The minimum detectable base width of ePSFs was twice the recording electrode spacing. In this case, supra-threshold activity was detected by only one recording electrode. For Gaussian fits to ePSFs this constraint lead to a minimum detectable FWHH of about one recording electrode spacing (305 μm or 500 μm). The upper bound for FWHHs was constrained by the size of the recording array (up to 4.3 mm) and was about half the total extent of electrodes (i.e. approximately 2.15 mm) in order to capture the base width of the activity distribution.

4.4.1   Width of cortical ePSFs

We calculated the average FWHH of ePSFs for LFP to 1.28 $mm \pm 0.33$ mm cortex (Fig. 3.10). This corresponds to $1.4° \pm 0.4°$ visual angle (mean cortical magnification factor 0.9 mm cortex/deg at $5°$ eccentricity; Tusa et al., 1979). The FWHH increased with the stimulation current amplitude. It was $0.92° \pm 0.15°$ (N=7) near threshold stimulation and $1.58° \pm 0.49°$ (N=121) at about tenfold threshold stimulation.

The width of ePSFs was influenced by the stimulation current amplitude and the frequency band analyzed (different integration fields for SUA, MUA, and LFP). Additionally, the stimulation and recording electrode diameter, electrode-to-tissue distance, and depth of anesthesia further affect the amplitude and width of ePSFs. The amplitude and width of ePSFs increased with increasing stimulation current (Fig. 3.10) and differed between stimulation electrodes. This was also reported for sub-retinal electrical stimulations in in-vitro chicken preparations (voltage pulse stimulation with a micro-electrode array, individual electrode diameters 10 μm; Stett et al., 2000). Here, the width of retinal activity distributions was about 0.2 mm and was smallest for low stimulation voltages. Based on LFP data from cat visual cortex we found an average FWHH of 1.28 mm cortex corresponding to $1.4°$ visual angle and to 0.28 mm retina ($5°$/1 mm retina). Given the extended spatial integration window of LFP data compared to single unit recordings, the data from chicken retina and cat cortex give comparable results.

In psychophysical experiments, blind volunteers perceived phosphenes of

increasing size and brightness, when the amplitude and the duration of applied electrical epi-retinal stimuli were increased (biphasic current stimuli of 1–4 ms duration and 300–800 μA amplitude, electrodes were positioned 0.5 mm distant from the retinal surface; Humayun et al., 1996). In the auditory domain, cochlear implant stimulation in the cat yielded increasingly broader cortical response areas, hence diminished spatial resolution if the stimulation current amplitudes were increased (Dinse et al., 1997). The adjustment of the ePSF width and hence, spatial resolution, may be achieved by means of fine tuning of the stimulation currents for individual retinal electrodes.

The amount of overlap between ePSFs was analyzed for N=154 pairs of ePSFs. It was smallest (i.e. spatial resolution highest) for low stimulation currents that were just above stimulation threshold. Minimum separabiles were $0.8° - 2.0°$ for near threshold stimulation and $1.6° - 4.3°$ for about ten-fold threshold stimulation. The analyses of FWHHs and minimum separabiles therefore give similar results for the spatial resolution. In particular, the best spatial resolution based on LFP responses is in the range of $0.8°$ visual angle.

4.4.2 Dynamics of cortical ePSFs

The temporal evolution of ePSFs often shows two phases. With near-threshold stimulation, localized activity appears in isolation within 10–20 ms latency. This first volley of activity probably reflects mono-synaptic cortical responses in layer 4 directly driven by the dLGN (Mitzdorf, 1985). When stimulated with higher current amplitudes, cortico-cortical interactions become supra-threshold for more distant sites at a temporal offset of about 20 ms after the initial response (Fig. 3.12). The dynamic broadening of ePSFs results either from two parallel inputs (a fast, locally projecting and a slow, broadly projecting) or one local input to the cortex followed by a radial spread of activity. Most probably, the broadening of ePSFs takes place at the cortical level rather than in the retina or dLGN and is mediated by lateral interactions like thalamo-cortical feedback, the intra-cortical feedback and the feedback from higher areas (Dinse and Krüger, 1994). For the estimation of cortical spread evoked by retinal stimulation, the first response component was chosen. At this moment of retino-cortical signal transduction, intra-cortical processing has not shaped spatial activity distributions, yet. Later response components reflect subsequent processing of activity.

4.4.3 Multi-peaked cortical ePSFs

Cortical ePSFs are single- or multi-peaked (Fig. 3.9). These peaks are fixed to cortical positions. Shifting the retinal stimulation sites resulted only in slight shifts or in formation of adjacent peaks. Therefore, multi-peakedness

is probably of cortical origin and might reflect the structured organization of the visual cortex, including its inhomogeneous input (Hubel and Wiesel, 1977; Horton and Hubel, 1981; Cynader et al., 1987). Since electrical stimulation was applied monocularly, multi-peaked ePSFs might result from ocular dominance columns found in cat area 17 and 18. In cat area 18 Cynader et al. (1987) found bands of cells with similar preferred eye input. The stripes roughly extended perpendicular to the vertical meridian. The cortical distance between these bands was 1.86 ± 0.75 mm. This roughly matches the separation of peaks in the ePSFs in area 18.

4.4.4   Comparison of cortical vPSFs and ePSFs

The analysis of vPSFs suggests that spatio-temporal resolution may be underestimated by analyzing the width of ePSFs. Cortical vPSFs are often broader ($2-3$ mm FWHH; Fig. 3.6) than ePSFs (1.28 mm ± 0.33 mm). Since visual stimulation was multi-focal (with 1° visual stimuli) one should not compare the vPSFs directly with ePSFs that were produced with uni-focal stimuli (ca. 0.25° stimulation electrode diameter).

The visual input activates retinal networks in a more natural way than an (epi-retinal) electrical stimulus does. On parallel magno-, parvo-, and coniocellular pathways with distinct latency ranges, connectivity patterns and visual tuning properties, different stimulus features ("ON", "OFF") are encoded separately (Kuffler, 1953). With visual stimuli, the spatio-temporal input to the cortex is more complex and "rich" and can specifically activate specialized cortical units. In contrast, with electrical stimulation, intra-retinal processing is partly or totally bypassed. Electrical stimuli synchronously activate retinal cells or fibers regardless of their visual function. However, magno-cellular neurons might be stimulated more efficiently than parvo- or conio-cells because they are larger and activation thresholds are low for neurons with large diameters (Ranck, 1975). The lack of complexity of cortical input after electrical stimulation leads to an inefficient stimulation of the cortex. Summarizing, one might expect that visual point stimuli are more efficient and hence activate a larger cortical area than electrical point stimuli of the same retinal extent.

Grinvald et al. (1994) reported how after visual stimulation onset, cortical activity spread from the site of initiation over an area at least ten times larger in upper cortical layers (real-time optic imaging after visual stimulation with small drifting gratings). The space constant for this spread was 1.5 mm perpendicular and 2.7 mm parallel to the V1/V2 border in macaque monkey. The activity spread at velocities of 0.10–0.25 m/s.

Cynader et al. (1987) estimated the width of vPSFs in area 18 of the cat to 0.8–2.35 mm (FWHH) along the anterio-posterior axis (approximately along the vertical meridian). As a possible reason for broad vPSFs they suggested

a "compromise between the contradictory demands for high precision of localization of multiple stimuli and representation of many response features for each point in visual space."

Jancke et al. (1999) and Dinse and Jancke (2001) transformed cortical activity maps of cats to visual space. The projection was performed according to the visual RFs of the cortical recording sites in order to study cortical responses to visual stimuli in a common metric space. In the context of retinal electrical stimulation, this transformation would facilitate an impression of what electrical stimuli might "mean" for an observer, since cortical responses would be assessed in visual space rather than in cortical coordinates. However, a prerequisite for this approach is the existence of retinotopic cortical maps that do not alter in response to long-term electrical stimulation. This cannot be expected in blind people, especially after a prolonged deprivation of meaningful physiological input to the cortex. Instead, is has been reported that adult cortical connectivity adapts to the lack of sensory input by substantially rearranging RF-maps (Pons et al., 1991; Rauschecker, 1995). The rather stereotype and highly synchronized cortical input after electrical stimulation with a retinal implant is expected to evolve a much simpler cortical representation of the visual world ("Hebbian learning"). With a retinal implant, visual objects will be cortically represented in an one-to-one retinotopic fashion (Wilms et al., 1999). Thus, in the framework of predicting the spatial resolution of electrical retina stimulation in deprived visual cortices, it is sufficient to analyze the cortical representation of electrical stimuli rather than their transformation to visual space.

4.5 Estimate of temporal resolution with retinal implants

4.5.1 Analysis of response rise times

Temporal resolution achievable with electrical retina stimulation was assessed by estimating the signal rise time at the initial phase of cortical LFP responses to electrical stimuli. As expected, the rise time declined with increasing stimulation strength. Since the electrical field produced by the retina electrode extends to a retinal area that is larger for higher stimulation currents, an increasing number of retinal ganglion cells can be activated synchronously. As a result, spatial integration at subsequent synaptic connections (dLGN and layer 4 of the cortex) requires less time for the post-synaptic neurons to become supra-threshold. In this way, the first volley of activity is conveyed faster to the cortex. Rise times were in the range of 8–12 ms, depending on the stimulation current amplitude. Taking twice the rise time as a measure for the

temporal resolution, electrical stimulation at 40–60 imp/s will probably be resolved by the cortex. Strong electrical stimuli yield higher temporal resolutions since response rise times are shorter.

4.5.2 Dependency between stimulation rate and efficacy

The temporal resolution for visual stimuli can be defined as the smallest perceivable temporal interval between visual stimuli. This interval is estimated in psychophysical tests by presenting visual stimuli at various repetition rates (van de Grind et al., 1973; Ripps and Weale, 1976). The maximum perceivable repetition rate, the "critical flicker frequency" (CFF) is limited by the refractory period of activated neurons along the visual pathway and depends on the light intensity of the test stimulus. Stimulation at repetition rates exceeding the CFF leads to a perceived fusion of individual stimuli resulting in the percept of continuous illumination (Kelly, 1972). In the photopic range, the CFF increases with the logarithm of the stimulus luminance and typically is between 10–50 imp/s ("Ferry-Porter-law"; van de Grind et al., 1973). Grüsser and Creutzfeld (1957) reported that in cat visual cortex, individual neurons can follow visual stimuli at up to about 47 imp/s at 500 lux luminance. The average cortical CFF in their preparation was 18.8 imp/s. At stimulus repetition rates beyond the CFF, retinal and cortical neurons fail to respond to every flicker but still exhibit increased stimulus-locked activity.

In analogy to the visual CFF, flicker fusion frequencies were also examined for phosphenes evoked by electrical stimuli to the eye. In psychophysical experiments with human observers, one electrode was placed on the forehead, the other on the temporal bone near the eye (van de Grind et al., 1973). Similar to visual stimulation, the CFF increases with electrical stimulus intensity. The minimum threshold in the light-adapted eye amounts to about 20 imp/s. Generally, electrical CFFs were found to be higher than visual CFFs (van de Grind et al., 1973).

In this study, the maximum frequency of epi-retinal electrical stimulation capable of evoking significant neuronal activity was estimated. Stochastic stimuli were used in order not to overstate temporal resolution by the analysis of responses to continuously oscillating stimuli (Boynton, 1972). In a series of measurements, the mean stimulation rate of electrical stimuli with Gamma distributed inter-stimulus intervals was varied systematically. Electrical stimulation at mean rates of 60–80 imp/s were efficient in evoking a significant number of spikes ($S/N > 2$, Fig. 3.15 A) if retinal stimulation sites matched the RFs of the cortical recording sites. Obviously, these rapid sequences of electrical stimuli with natural interval statistics can modulate cortical activity. This suggests that coding of visual stimulus information is possible at a temporal resolution of 12.5 ms.

According to the data, the maximum efficient electrical stimulation frequency is in the same range or higher than the psychophysical CFF for visual stimulation. This is not astonishing, because the slow intra-retinal signal processing is by-passed by epi-retinal electrical stimulation.

4.5.3   Analysis of response duration

As a rough estimate of the temporal resolution achievable, the durations of the excitatory phase of LFP responses were examined. Response durations were 20–50 ms in most cases. Shortest durations, hence best temporal resolutions, result with stimulation just above threshold level. However, the excitatory response duration can rise significantly for stimulation at higher amplitudes (Fig. 3.1). The response durations suggest that electrical stimulation at about 20–50 imp/s should be possible. When SUA is concerned, response durations dramatically shrink to 0.5 ms (absolute width of spike latency distributions in Fig. 3.17). However, this does not imply that temporal resolution of electrical stimulation is in the range of 0.5 ms. Electrical stimulation at a rate of 2000 imp/s is certainly not efficient. Although retinal ganglion cells can discharge at rates of 200–800 imp/s in burst mode (Kuffler, 1953) and optic nerve fibers can convey spikes at a maximum rate of 400–800 imp/s (Enroth, 1952), the maximum perceivable rate is much lower. The data shows that response S/N–ratios drop to chance level at electrical stimulation rates beyond 100 imp/s (Fig. 3.15 A). Therefore, the response duration affects the precision rather than the achievable temporal resolution of retina stimulation.

Eger (2001) analyzed LFP and MUA in response to electrical stimuli with Gamma distributed inter-stimulus intervals. He reported that stimuli conveyed a maximum of transinformation in the range of 20–140 bit/s at mean stimulus rates of 20–40 imp/s suggesting a temporal resolution of 25–50 ms. Due to the high S/N–ratios for first spike responses (Fig. 3.15 A), the maximum amount of transinformation conveyed by SUA may be shifted to even higher stimulation rates compared to LFP and MUA.

Summarizing, is is useful to assess temporal resolution by the analysis of stimulation efficacy (S/N–ratios), signal rise times, and transinformation between stimulus and response. These methods yield temporal resolutions of about 40 imp/s, which may be regarded as a lower bound for temporal resolution in the design of a retinal implant. Electrical stimulation at an overall frame rate above the CFF avoids the sensation of a – probably annoying – pseudo-visual flicker.

Cues for visual binding arise from the temporal structure of the stimulus (Lee and Blake, 1999). Since a high precision of cortical responses to electrical retina stimulations is guaranteed (Fig. 3.17), the coding of complex objects

that involves linking of even disjoined object parts seems feasible.

4.6 Cortical plasticity under electrical retina stimulation

The learning capacity ("plasticity") of the visual cortex is expected to play a crucial role in the functioning of any retinal implant (Wilms et al., 1999). In particular, it is expected that the visual cortex reacts in a way to optimize its information processing capabilities for the unfamiliar pseudo-visual electrical input (Joublin et al., 1996; Zeki, 1993). In preliminary experiments we attempted to induce "learning effects" by prolonged electrical stimulation sessions with single or paired stimulation electrodes. Stimulation sessions lasted for up to 25 min of repetitive stimulation with various stimulation current amplitudes and rates. However, no significant changes, neither in RF position, size, nor the coupling strength of pairs of recording channels were observed.

Dinse et al. (1993) reported that significant changes in cooperativity of single neurons parallel RF changes. These effects were observed after several hours of intra-cortical micro-stimulation in the somatosensory cortex of monkeys and rats. Godde et al. (1996) reported that 6–15 hours of tactile coactivation resulted in selective and reversible reorganization of RFs and cortical maps in the hind paw representation of adult rats. Later, they found that tactile coactivation-induced changes in spatial discrimination performance of human volunteers could be evoked with stimulation protocols exceeding 30 min (Godde et al., 2000).

This suggests that experiments addressing the question whether cortical plasticity may be mediated by electrical retina stimulation should use longer stimulation sessions of several hours. To keep experimental conditions stable over such long periods of time, the long term implantation of retinal implants is necessary. The time course of potential learning effects can be uncovered by monitoring the cortical responses to test stimuli.

Klinke et al. (1999) reported that congenitally deaf cats showed improved hearing ability when exposed to months of meaningful electrical stimuli by an implanted cochlear stimulator. In particular, "chronically implanted cats produced field potentials of higher amplitudes, expanded area, developed long latency responses indicative of intra-cortical information processing". However, when congenitally or pre-lingually deaf adult humans received cochlear implants, the results were disappointing.

Long-term exposure to spatio-temporal input patterns leads to a reorganization of cortical connectivity. In blind people with profound practice in Braille reading, visual areas V1 and V2 exhibit an increased cerebral blood flow when subjects were instructed to perform discriminative Braille or non-

Braille reading tasks. In contrast sighted subjects showed a decreased regional cerebral blood flow in the same task (Sadato et al., 1996). Similarly, string players who started playing in early childhood, exhibited an increased cortical representation of the fingers of their left hand (Elbert et al., 1995).

Lack of spatio-temporal input patterns due to visual scotoma (e.g. retinal injury) or after deafferentiation of sensory input (Pons et al., 1991; Rauschecker, 1995) can lead to long-term reorganizational changes that allow adjacent afferents, even of other modalities, to take over idle cortical area for information processing.

Experiments on the spatio-temporal resolution were performed in cats with intact visual systems. Although the cat was chosen for its similar visual system, it still remains unclear whether conclusions drawn from these experiments have significance for the assessment of spatio-temporal resolution in blind human patients. Studies in blind volunteers including rehabilitation training methods for fine tuning of the visual implant will further improve predictions on the benefit of a visual prosthesis based on electrical retina stimulation.

4.7 Outlook on visual prostheses

Our data show that best spatial resolutions of electrical retina stimulation were in the range of $0.8° - 2.0°$. The methods used were chosen to obtain a conservative measure for the spatial resolution. Thus higher spatial resolutions are probably possible. Cha et al. (1992a) reported that a pixelized vision system based on a 25x25 square grid spanning 30° visual angle is sufficient to allow sighted volunteers to navigate in complex visual environments with nearly normal speed. In order to equip the implant patient with such a pixelized vision one requires an angular resolution of 1.2° at 625 stimulation sites. Unfortunately, this does not suffice for normal reading. Cha et al. (1992b) demonstrated that 625 pixels with a spacing of 4 min of arc (1.7° of central visual field) was needed to allow sighted volunteers reading at 2/3 normal speed (170 words/min with scrolled text or 100 words/min with fixed text). The epi-retinal approach, however, facilitates optical zooming into the visual field and is therefore capable of adjusting angular resolution at the expense of the size of the simultaneously represented visual field. This feature is not supposed for the current sub-retinal approach, which is constrained to a fixed angular resolution.

An angular resolution of 0.8° provides the potential implant patient with an artificial visus of 1/48. Equipped with a sufficient number of stimulation electrodes, the patient will still be legally blind but probably be able to discriminate large objects for navigation in visual environments (Cha et al., 1992a).

From the neurophysiological point of view, temporal resolution is a minor

problem. Stimulation rates of 80 imp/s evoke significant cortical single unit activity. The analysis of LFP rise times suggests temporal resolutions in the range of 40–60 imp/s. Eger (2001) found a maximum of transinformation in population activity at mean stimulus rates of 20–40 imp/s. Thus, electrical stimulation beyond the psychophysical CFF should be feasible and avoid the perception of pseudo-visual flicker.

There is some evidence that epi-retinal stimulation with flat electrode contacts tends to activate ganglion cell axons rather than somata. This means that the spatial resolution of electrical retina stimulation is better perpendicularly, than in parallel to axon fibers. In order to overcome this asymmetry, one should aim at stimulating somata or axons that originate in proximal somata rather than in distal ones. This may be achieved by stimulation electrodes that impinge on the membrana limitans interna and traverse the axonal layer towards the somata ("quasi-intra-retinal stimulation"; Eckhorn, 1997). The study of LFP- and MUA-vRFs for retinal fiber electrodes may shed light on the benefits of the quasi-intra-retinal stimulation approach (cf. 3.3): the angular separation of LFP- and MUA-vRFs should decrease with the penetration depth of the recording electrode into the retina. As the electrode tip traverses several layers of axons, the MUA signal contains spikes originating from increasingly proximal ganglion cell somata. If the electrode tip is in the vicinity of a ganglion cell soma, MUA-vRFs and LFP-vRFs should become congruent. However, it is still not clear, whether the retinal neurons activated by electrical stimulation are located within vRFs of the retinal electrodes. Soma spikes are larger in amplitude and duration and therefore more likely to be detected in vRF measurements (Kuffler, 1953). On the other hand, retinal axons of more distal somata might be more likely to be electrically stimulated since they have lower stimulation thresholds than somata (Nowak and Bullier, 1997b,a).

The sub-retinal approach elegantly evades the axon stimulation problem by stimulating the retinal network at its natural input level near the photoreceptor layer. However, the proposed sub-retinal concept relies more strongly on a more or less intact intra-retinal circuitry than the epi-retinal approach. Moreover, state-of-the-art photodiode stimulation arrays are not capable of extracting enough stimulation energy out of the naturally occurring levels of retinal illumination, yet. Equipping the sub-retinal implant with an external power supply as proposed by Zrenner et al. (1999) might overcome this limitation.

Further research should concentrate on the influence of electrical multi-focal stimulation on the spatio-temporal resolution feasible with electrical retina stimulation, since this will be the normal working condition of a retina implant. Within the framework of this study, Eger (2001) already applied information theoretical analyses to this problem.

The use of an implant to bypass the degenerated retinal layers mirrors the successful cochlear implant in the auditory domain, which has restored useful hearing to many deaf patients. Post-implantation training and rehabilitation concepts for the cochlear implant patient should be adapted to the needs of retina implant patients. The brain and – ultimately – the patient must become familiar with a spatio-temporal pseudo-sensory input that he or she has not yet learned to identify as the perception of a visual object.

5 Appendix
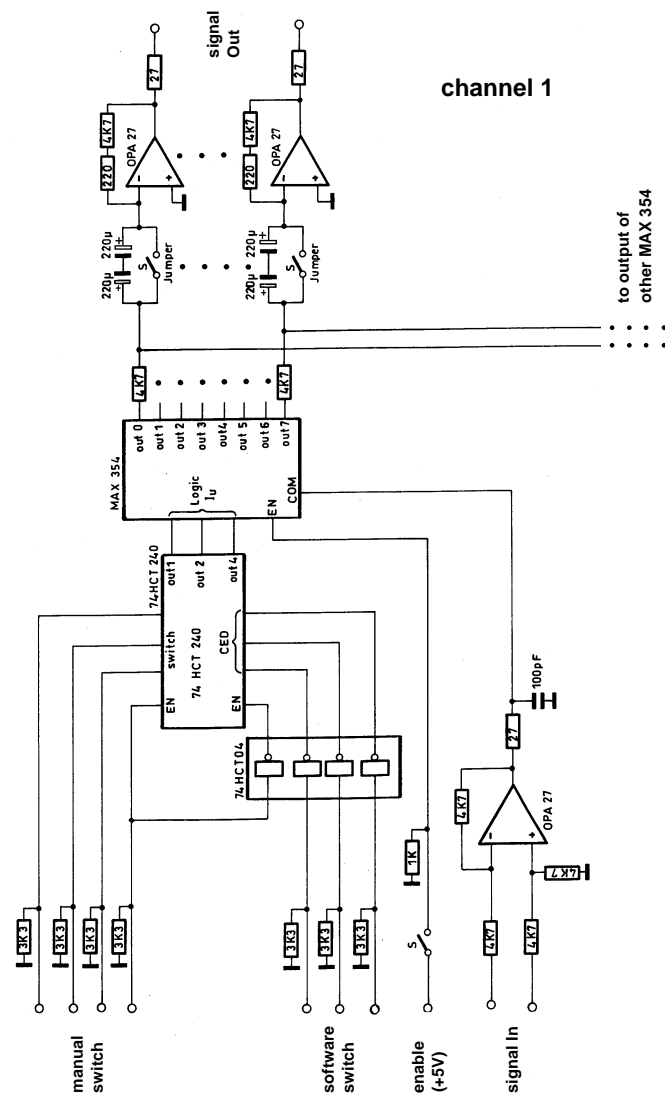
Figure 5.1: Logical circuit of the multiplexer ("4-out-of-8 selector") used for generating spatio-temporal electrical stimuli. One of four parallel channels is depicted.
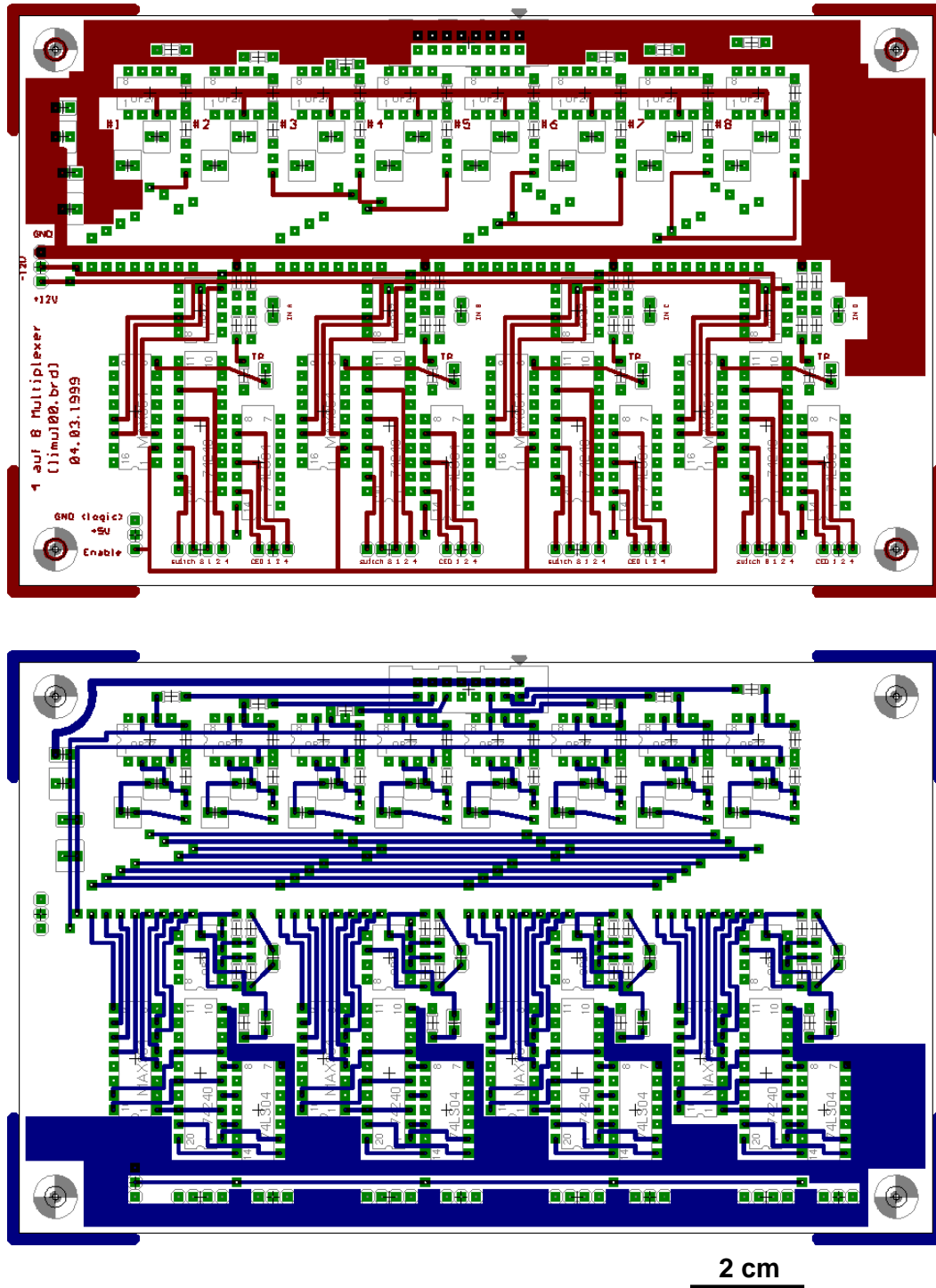
Figure 5.2: Final printed-circuit board layout for the multiplexer ("4-out-of-8 selector") used for generating spatio-temporal electrical stimuli. The front view is shown on top; below is the backside view of the board. The layout was designed using a CAD software (*EAGLE*).

Abbreviations

CFF	critical flicker frequency
FWHH	full width at half height: the widths of ePSFs were defined as the FWHH of the Gaussian fits
LFP	local field potentials
dLGN	dorsal lateral geniculate nucleus
MUA	multi unit activity
ePSF	electrical point spread function
vPSF	visual point spread function
PSTH	peri stimulus time histogram
cRF	classical receptive field
eRF	electrical receptive field
vRF	visual receptive field
SNR	signal–to–noise ratio
SUA	single unit activity
V1	primary visual cortex
W	denotes the W pathway of the visual system originating in the conio-cellular retinal cells
X	denotes the X pathway of the visual system originating in the parvo-cellular retinal cells
Y	denotes the Y pathway of the visual system originating in the magno-cellular retinal cells

Glossary

Action potential A rapid, transient, all–or–none* change in electrical potential between the inside of a nerve cell and the extracellular medium that can occur when a cell has been activated by a stimulus. The action potential is followed by a period of unresponsiveness (*absolute refractory period*) or reduced responsiveness (*relative refractory period*) to further stimuli.

Afferent Heading towards. In sensory systems, afferent signals are those carrying sensory information to the central nervous system. cf. Efferent

All–or–none When activated by a stimulus, a nerve cell's response is marked either by a stereotype operation or by none at all.

Area 17 Part of the primary visual cortex*.

Area 18 Part of the cat primary visual cortex*.

Area centralis Area in a vertebrate retina rich in cones. The area centralis denotes the central region of the retina enabling the highest spatial resolution. In the human eye the area centralis corresponds to the fovea.

Axon Single and usually long nerve cell process that conducts action potentials away from the cell body. The velocity for traveling action potentials is between 1 and 100 meters per second. Conduction velocity is bigger in axons with a large diameter. Retinal ganglion cell* axons are translucent and cross over the retina towards the optic disk*. They form the innermost retinal layer and thus can be electrically stimulated with epi-retinal electrodes.

Chronaxie The stimulus duration necessary to stimulate a neuron above threshold, if the stimulation amplitude is twice the rheobase*. The chronaxie is useful as an index of the excitability of a preparation.

Critical flicker frequency, CFF The maximum perceivable repetition rate. Visual stimulation at repetition rates exceeding the CFF leads to a perceived fusion of individual stimuli, resulting in the perception of continuous illumination.

Classical receptive field The visual classical receptive field is defined as the retinal area which is capable of modulating the activity of a cortical neuron if visually stimulated. In this study visual receptive fields ("vRF") were analyzed mostly for populations of cortical neurons. In analogy to this receptive field concept in the visual domain, "electrical receptive fields" ("eRFs") were estimated as well. Accordingly, eRFs were defined as the retinal area capable of modulating cortical activity when stimulated electrically.

Efferent Heading away. In sensory systems efferent signals carry information to the peripheral motor system. cf. Afferent.

Electrical receptive field cf. Classical receptive field.

ePSF cf. PSF.

Epi-retinal stimulation Electrodes are lowered onto the inner retinal surface (epi-retinal positioning). Electrical stimuli can evoke spikes* in retinal ganglion cells and axons. Typically, threshold currents for biphasic current-balanced impulses of 0.4 ms duration are in the range of $20 - 40\mu A$.

Excitatory post-synaptic potential, EPSP In excitatory chemical synapses, a pre-synaptic neuron releases transmitters into the synaptic gap. This causes an inward current into the post-synaptic cell, leading to a voltage drop, the EPSP. Temporal integration of many EPSPs can drive the post-synaptic neuron towards its threshold level for generating an action potential*.

Ganglion cells Output neuron of the retina. Ganglion cell axons* form the optic nerve. Ganglion cells can be classified by different morphological and physiological features (cf. X-, Y-, W-cells). Ganglion cells have concentric receptive fields* (RF) with antagonistic center-surround properties. ON-ganglion cells respond best to a spot of light focused on the RF center, whereas OFF-ganglion cells prefer a dark spot with bright surround.

Inhibitory post-synaptic potential, IPSP In contrast to the excitatory post-synaptic potential*, other types of transmitters cause an outward current in the post-synaptic cell, leading to its hyperpolarization.

dLGN A sub-cortical, thalamic structure receiving direct input from the retinae via the optic nerves. The dLGN comprises several layers that distinctly process information from retinal cells. The dLGN relays incoming activity to the primary visual cortex*.

Local field potentials, LFP Signals resulting from bandpass filtering of extracellularly recorded signals (1–140 Hz) mainly capturing slow potentials, such as EPSPs* or IPSPs*.

Magno cells Type of ganglion cells in the primate retina which correspond to Y-cells* in the cat.

Multi unit activity, MUA Spiking activity of a population of neurons. Technically, the extracellularly recorded signal is highpass filtered (0.5–10 kHz), subsequently rectified, and then lowpass filtered. Therefore, MUA reflects the envelope of spiking activity, an estimate for the population spike density.

Optic disk The retinal site where the ganglion cell axon fibers leave the retina. Contains no photoreceptors and therefore creates a blind spot in the visual field.

Parvo cells Type of ganglion cells in the primate retina which correspond to X-cells* in the cat.

Primary visual cortex, V1 Defined as that part of the cortex that receives direct input from the dLGN*. For primates, primary visual cortex, V1, and area 17

are synonymous terms. In cat, area 18 and 19 also get input from the dLGN and thus belong to the primary visual cortex.

Peri stimulus time histogram, PSTH Cortical responses are averaged over identical stimulus conditions to increase the signal-to-noise ratio of the estimated cortical response.

Point spread function, PSF Cortical activity distributions. The amplitudes of normalized averaged cortical responses to visual stimuli (vPSF) or electrical stimuli (ePSF) were plotted against the cortical recording electrode separations.

Receptive field, RF Defined as the restricted region of the sensory input space (e.g. retina or skin) that influences the activity of a neuron. In analyses of the visual system, the RF is usually projected onto a tangent screen.

Retinotopy A preservation of spatial relationships of retinal locations in higher brain representations.

Rheobase Minimum stimulus amplitude necessary to stimulate a neuron above threshold.

Spike cf. Action potential.

Spike raster plot The spikes detected in each stimulus trial are marked in piled rows.

Single unit activity, SUA Comprises action potentials of single neurons, cf. Action potentials.

Sub-retinal stimulation Electrode arrays are implanted under the neural retina in the sub-retinal space. Electrical stimuli activate outer retinal cells and thus the retinal neural network. cf. Epi-retinal stimulation.

V1 cf. Primary visual cortex.

Visual receptive field cf. Classical receptive field.

Visus Measure for visual acuity. The visus is defined as the reciprocal of the minimal separable visual angle in arc minutes. In normal vision, the visus equals one.

vPSF cf. PSF.

X cells Type of ganglion cells primarily responsible for the cat's contrast sensitivity at high spatial frequencies. X type ganglion cells have small RFs and produce a sustained response. Their axons* have a low conduction velocity for action potentials*. X cells are separated into two classes, ON-center and OFF-center cells. cf. Ganglion cell.

Y cells Type of ganglion cells with larger RFs than X cells. They respond transiently to rapid stimulus motion. Y cells are separated into two classes, ON-center and OFF-center cells. cf. Ganglion cells.

W cells Type of ganglion cells. cf. Ganglion cells.

Bibliography

Abeles M, Goldstein MH: Multispike train analysis. Proceedings of the IEEE, 1977, 65,5: 762–773.

Baseler HA, Sutter EE: M and P components of the VEP and their visual field distribution. Vision Res., 1997, 37,6: 675–690.

Becker M, Hünermann R, Eckmiller R: System identification of a learning retina encoder for a retina implant. Investigative Ophthamology and Visual Science Suppl., 1997, 38,4: 41.

Beers MH, Berkow R, editors: The Merck Manual of Diagnosis and Therapy. Merck & Co., Inc., Whitehouse Station, NJ, USA, 17th edition, 2001 .

Berry II MJ, Meister M: Refractoriness and neural precision. J. Neurosci., 1998, 18,6: 2200–2211.

Bialek W, Rieke F, de Ruyter van Steveninck RR, Warland D: Reading a neural code. Science, 1991, 252: 1854–1857.

Borish J, Angell JB: An efficient algorithm for measuring the impulse response using pseudorandom noise. J. Audio. Eng. Soc., 1983, 31,7: 478–488.

Boycott BB, Dowling JE: Organization of the primate retina. Philos. Trans. R. Soc. Lond. B, 1969, 255: 109–184.

Boynton RM: Discrimination of homogeneous double pulses of light. In D Jameson, LM Hurvich, editors, Handbook of sensory physiology, volume 7, Springer, 1972 .

Brindley GS, Lewin WS: The sensations produced by electrical stimulation of the visual cortex. J. Physiol., 1968, 196: 479–493.

Celebrini S, Thorpe SJ, Trotter Y, Imbert M: Dynamics of orientation coding in area V1 of the awake primate. Vis. Neurosci., 1993, 10: 811–825.

Cha K, Horch KW, Normann RA: Mobility performance with a pixelized vision system. Vision Res., 1992a, 32,7: 1367–1372.

Cha K, Horch KW, Normann RA, Boman D: Reading speed with a pixelized vision system. J. Opt. Soc. Amer. A, 1992b, 9.5: 673–677.

Chow AY, Chow VY: Subretinal electrical stimulation of rabbit retina. Neuroscience Letters, 1997, 225: 13–16.

Cleland BG, Dubin MW, Levick WR: Simultaneous recording of input and output of lateral geniculate neurones. Nature New Biology, 1971, 231: 191–192.

Cynader M, Swindale N, Matsubara J: Functional topography of cat area 18. J. Neurosci., 1987, 7.5: 1401–1413.

Das A, Gilbert C: Distortions of visuotopic map match orientation singularities in primary visual cortex. Nature, 1997, 387: 594–598.

Dawson WW, Radtke ND: The electrical stimulation of the retina by indwelling electrodes. Investigative Ophthamology and Visual Science, 1977, 16,3: 249–252.

Dinse H, Godde B, Hilger T, Haupt S, Spengler F, Zepka R: Short-term functional plasticity of cortical and thalamic sensory representations and its implication for information processing. Brain Plasticity, 1997, 73: 159–178.

Dinse H, Jancke D: Progress in Brain Research. Ed. Nicolelis, M.A.L., volume 130. Elsevier Science B.V., 2001 pages 155–173.

Dinse H, Krüger K: The timing of processing along the visual pathway in the cat. NeuroReport, 1994, 5: 893–897.

Dinse HR, Recanzone GH, Merzenich MM: Alterations in correlated activity parallel ICMS-induced representational plasticity. NeuroReport, 1993, 5: 173–176.

Dobelle W: Artificial vision for the blind by connecting a television camera to the visual cortex, 2000, 46: 3–9.

Dobelle WH, Mladejovsky MG, Girvin JP: Artificial vision for the blind: Electrical stimulation of visual cortex offers hope for a functional prosthesis. Science, 1974, 183: 440–444.

Eckhorn R: "Quasi-intra-retinal stimulation", 1997, personal communication.

Eckhorn R, Krause F, Nelson JI: The RF-cinematogram. A cross-correlation technique for mapping several visual receptive fields at once. Biol. Cybern., 1993, 69: 37–55.

Eckhorn R, Thomas U: A new method for the insertion of multiple microprobes into neural and muscular tissue, including fiber electrodes, fine wires, needles and microsensors. J. Neurosci. Methods, 1993, 49: 175–179.

Eckmiller R: Learning retina implants with epiretinal contacts. Ophthalmic Research, 1997, 29: 281–289.

Eger M: Information theoretical methods for the functional adjustment of retina implant parameters. Ph.D. thesis, Philipps-University Marburg, Germany, 2001.

Elbert T, Pantev C, Wienbruch C, Rockstroh B, Taub E: Increased cortical representation of the fingers of the left hand in string players. Science, 1995, 270: 305–307.

Elliott D, Rao K: Fast transforms. Algorithms, analyses, applications. Academic press, 1982.

Enroth C: The mechanism of flicker and fusion studied on single retinal elements in the dark-adapted eye of the cat. Acta physiol. scand., 1952, 27: suppl. 100.

Ferster D, Lindström S: An intracellular analysis of geniculo-cortical connectivity in area 17 of the cat. J. Physiol., 1983, 342,1: 181–215.

Godde B, Spengler F, Dinse HR: Associative pairing of tactile stimulation induces somatosensory cortical reorganization in rats and humans. NeuroReport, 1996, 8: 281–285.

Godde B, Stauffenberg B, Spengler F, Dinse H: Tactile coactivation-induced changes in spatial discrimination performance. J. Neurosci., 2000, 20.4: 1597–1604.

Grinvald A, Lieke E, Frostig R, Hildesheim R: Cortical point spread function and long-range lateral interactions revealed by real-time optical imaging of macaque monkey primary visual cortex. J. Neurosci., 1994, 14: 2545–2568.

Grüsser OJ, Creutzfeld O: Eine neurophysiologische Grundlage des Brücke-Bartley-Effektes: Maxima der Impulsfrequenz retinaler und corticaler Neurone bei Flimmer-Licht mittlerer Frequenzen. Pflügers Arch. ges. Physiol., 1957, 263: 668–681.

Hesse L, Schanze T, Wilms M, Eger M: Implantation of retina stimulation electrodes and recording of electrical stimulation responses in the visual cortex of the cat. Graefe's Arch. Clin. Exp. Ophthalmol., 2000, 238: 840–845.

Horton J, Hubel D: Regular patchy distribution of cytochrome oxidase staining in primary visual cortex of macaque monkey. Nature, 1981, 292: 762–764.

Hubel D, Wiesel T: The Ferrier Lecture: Functional architecture of macaque monkey visual cortex. Proc. R. Soc. Lond. B, 1977, 198: 1–59.

Humayun M, Probst R, Juan E. de J, McCormick K, Hickingbotham D: Bipolar surface electrical stimulation of the vertebrate retina. Arch. Ophthalmol., 1994, 112: 110–116.

Humayun MS, Juan E. de J, Dagnelie G, Greenberg RJ, Probst RH, Phillips DH: Visual perception elicited by electrical stimulation of retina in blind humans. Arch. Ophthalmol., 1996, 114: 40–46.

Humayun MS, Juan Jr Ed, Weiland JD, Dagnelie G, Katona S, Greenberg R, Suzuki S: Pattern electrical stimulation of the human retina. Vision Res., 1999, 39: 2569–2576.

Jancke D, Erlhagen W, Dinse H, Akhavan A, Giese M, Steinhage A, Schöner G: Parametric population representation of retinal location: neuronal interaction dynamics in cat primary visual cortex. J. Neurosci., 1999, 19: 9016–9028.

Joublin F, Spengler F, Wacquant S, Dinse HR: A columnar model of somatosensory reorganizational plasticity based on Hebbian and non-Hebbian learning rules. Biol. Cybern., 1996, 74: 275–286.

Kelly DH: Flicker. In D Jameson, LM Hurvich, editors, Handbook of sensory physiology, volume 7, Springer, 1972 .

Kirk D, Cleland B, Levick W: Axonal conduction latencies of cat retinal ganglion cells. J. Neurophysiol., 1975, 38: 1395–1402.

Klinke R, Kral A, Heid S, Tillein J, Hartmann R: Recruitment of the auditory cortex in congenitally deaf cats by long-term cochlear electrostimulation. Science, 1999, 285: 1729–1733.

Klistorner A, Crewther DP, Crewther SG: Separate magnocellular and parvocellular contributions from temporal analysis of the multifocal VEP. Vision Res., 1997, 37,15: 2161–2169.

Kobuch K, Sachs H, Zrenner E, Gabel V: Ab externo transchoroidal access to the subretinal space for implantation of microphotodiodes. Investigative Ophthamology and Visual Science, 1998, 39,4: S903.

Kohler K, Hartmann JA, Werts D, Zrenner E: Histologische Untersuchungen zur Netzhautdegeneration und zur Gewebeverträglichkeit subretinaler Implantate. Der Ophthalmologe, 2001, 98: 364–368.

Kossler R: Reversible Ladungsübertragung von Mikroelektroden zur Stimulation des neuronalen Gewebes. Master's thesis, Neurophysics Department, Philipps University Marburg, 1998.

Kuffler SW: Discharge patterns and functional organization of mammalian retina. J. Neurophysiol., 1953, 16: 37–68.

Lee BB, Cleland BG, Creutzfeld OD: The retinal input to cells in area 17 of the cat's cortex. Exp. Brain Res., 1977, 30: 527–538.

Lee SH, Blake R: Visual form created solely from temporal structure. Science, 1999, 284: 1165–1168.

Loeb GE: Neural prosthetic interfaces with the nervous system. Trends Neurosci., 1989, 12,5: 195–201.

McCreery DB, Agnew WF, Yuen TGH, Bullara LA: Relationship between stimulus amplitude, stimulus frequency and neural damage during electrical stimulation of sciatic nerve of cat. Eng. and Comput., 1995, 33: 426–429.

McCreery DB, Yuen TGH, Agnew WF, Bullara LA: A characterization of the effects on neuronal excitability due to prolonged microstimulation with chronically implanted microelectrodes. IEEE Transactions On Biomedical Engineering, 1997, 44,10: 931–939.

Meister M, Berry MJ: The neural code of the retina. Neuron, 1999, 22: 435–450.

Mitzdorf U: Current source-density method and application in cat cerebral cortex: Investigation of evoked potentials and EEG phenomena. Physiological Reviews, 1985, 65,1: 37–100.

Mitzdorf U, Singer W: Prominent excitatory pathways in the cat visual cortex (A 17 and A 18): A current source density analysis of electrically evoked potentials. Exp. Brain Res., 1978, 33: 371–394.

Mountcastle VB, Poggio GF, Werner G: The neural transformation of the sensory stimulus at the cortical input level of the somatic afferent system. In Information processing in the nervous system, volume 3 of *Exerpta Medica International Congress No. 49*, Leiden, 1962 pages 196–217.

Nicholls JG, Martin AR, Wallace BG: From neuron to brain. Sinauer Associates, Inc., 3rd edition, 1992.

Nisch W: Impedances of TiN-polyimide electrode arrays, 2001, personal communication.

Normann R, Maynard E, Guillory K, Warren D: Cortical implants for the blind. IEEE Spectrum, 1996, 33: 54–59.

Normann RA, Maynard EM, Rousche PJ, Warren DJ: A neural interface for a cortical vision prosthesis. Vision Res., 1999, 39: 2577–2587.

Normann RA, Warren DJ, Ammermüller J, Fernandez E, Guillory S: High-resolution spatio-temporal mapping of visual pathways using multi-electrode arrays. Vision Res., 2001, 41: 1261–1275.

Nowak L, Bullier J: Axons, but not cell bodies, are activated by electrical stimulation in cortical gray matter. Exp. Brain Res., 1997a, 118: 477–488.

Nowak LG, Bullier J: The timing of information transfer in the visual system. Cereb. Cortex, 1997b, 12: 205.

Orban GA: Neuronal operations in the visual cortex. Springer, Berlin, 1st edition, 1984.

Pons TP, Garraghty PE, Ommaya AK, Kaas JH, Taub E, Mishkin M: Massive cortical reorganization after sensory deafferentation in adult macaques. Science, 1991, 252: 1857–1860.

Ranck J. B. J: Which elements are excited in electrical stimulation of mammalian central nervous system: A review. Brain Res., 1975, 98: 417–440.

Rauschecker JP: Compensatory plasticity and sensory substitution in the cerebral cortex. Trends Neurosci., 1995, 18,1: 36–43.

Reich D, Mechler F, Purpura K, Victor J: Interspike intervals, receptive fields, and information encoding in primary visual cortex. J. Neurosci., 2000, 20: 1964–1974.

Reid RC, Victor JD, Shapley RM: The use of m-sequences in the analysis of visual neurons: Linear receptive field properties. Vis. Neurosci., 1997, 14: 1015–1027.

Reitböck H: Fiber microelectrodes for electrophysiological recordings. J. Neurosci. Methods, 1983, 8: 249–262.

Rieke F, Warland D, de Ruyter van Steveninck R, Bialek W: Spikes: Exploring the Neural Code. The MIT Press, Cambridge, 2nd edition, 1997.

Ripps H, Weale RA: Visual function in man. - Temporal analysis and resolution., volume 2A of *The Eye*. Academic Press, 2nd edition, 1976 .

Rodieck RW: The vertebrate retina. Principles of structure and function. W. H. Freeman and Company, U.S.A., 1st edition, 1973 page 603.

Rullen Rv, Thorpe SJ: Rate coding versus temporal order coding: what the retinal ganglion cells tell the visual cortex. Neural Comput., 2001, 13: 1255–1283.

Sachs H, Kobuch K, Zrenner E, Gabel V: Ab interno implantation of subretinal microphotodiodes in rabbit and micropig. Investigative Ophthamology and Visual Science, 1998, 39,4: S–903.

Sadato N, Pascual-Leone A, Grafman J, Ibanez V, Deiber MP, Dold G, Hallet M: Activation of the primary visual cortex by Braille reading in blind subjects. Nature, 1996, 380: 526–528.

Santos A, Humayun M, de Juan E, Greenburg R.J. Marsh M, Klock I, Milam A: Preservation of the inner retina in retinitis pigmentosa. Arch. Ophthalmol., 1997, 115: 511–515.

Schanze T: Struktur und Kopplung reizabhängiger rhythmischer Aktivität der Sehrinde. Ph.D. thesis, Philipps-University Marburg, 1995.

Schanze T, Eckhorn R, Hesse L, Eger M, Wilms M, Kossler R, Nebeling B: Experimental setup for assessing the efficacy and quality of retina implant stimulations by retinal and cortical recording in cat. In N Elsner, R Wehner, editors, Göttingen Neurobiology Report 1998, volume 2, Thieme, 1998 .

Schanze T, Kremper A, Eckhorn R: Modelling the electrical stimulation of retinal ganglion cells as required for the development of retina implants. In N Elsner, H Wässle, editors, Göttingen Neurobiology Report 1997, volume 2, Thieme, 1997 .

Schanze T, Wilms M, Eger M, Eckhorn R: Methods for testing the quality of electrical retina stimulation by recordings in cat visual cortex for the development of a retina implant. Vision Res., 2001, submitted.

Schmidt EM, Bak MJ, Hambrecht FT, Kufta CV, O'Rourke DK, Vallabhanath P: Feasibility of a visual prosthesis for the blind based on intracortical microstimulation of the visual cortex. Brain, 1996, 119: 507–522.

Seiler MJ, Aramant RB, Ball SL: Photoreceptor function of retinal transplants implicated by light-dark shift of S-antigen and rod transducin. Vision Res., 1999, 39: 2589–2596.

Stanford LR: Conduction velocity variations minimize conduction time differences among retinal ganglion cell axons. Science, 1987, 238: 358–360.

Stett A, Barth W, Weiss S, Haemmerle H, Zrenner E: Electrical multisite stimulation of the isolated chicken retina. Vision Res., 2000, 40: 1785–1795.

Stieglitz T, Beutel H, Schuettler M, Meyer J: Micromachined, polyimide-based devices for flexible neural interfaces. Biomedical Microdevices, 2000, 2:4: 283–294.

Stone J, Hoffmann KP: Conduction velocity as a parameter in the organisation of the afferent relay in the cat's lateral geniculate nucleus. Brain Res., 1971, 32: 454–459.

Stone J, Holländer H: Optic nerve axon diameters measured in the cat retina: some functional considerations. Exp. Brain Res., 1971, 13: 498–503.

Sutter EE: Advanced methods in physiological system modeling. Ed. V.Z. Marmarelis, volume 1. Los Angeles, California, University of Southern California, 1987 pages 303–315.

Sutter EE: Nonlinear vision: determination of neural receptive fields, function, and networks. Ed. Pinter, R.B. and Nabet, B. Boca Raton, FL: CRC, 1992 pages 171–220.

Sutter EE: Imaging visual function with the multifocal m-sequence technique. Vision Res., 2001, 41: 1241–1255.

Troy J, Lennie P: Detection latencies of X and Y type cells of the cat's dorsal lateral geniculate nucleus. Exp. Brain Res., 1987, 65: 703–706.

Tusa RJ, Palmer LA, Rosenquist AC: The retinotopic organization of area 17 (striate cortex) in the cat. J. Comp. Neurol., 1979, 177: 213–236.

van de Grind WA, Grüsser OJ, Lunkenheimer HU: Central Processing of Visual Information. A: Integrative Functions and Comparative Data, volume VII/3 of *Handbook of Sensory Physiology*. Springer, Berlin, Heidelberg, New York, 1973 .

Veraart C, Raftopoulos C, Mortimer JT, Delbeke J, Pins D, Michaux G, Vanlierde A, Parrini S, Wanet-Defalque MC: Visual sensations produced by optic nerve stimulation using an implanted self-sizing spiral cuff electrode. Brain Res., 1998, 813: 181–186.

Wald G: The molecular basis of visual excitation. Nature, 1968, 219: 800–807.

Williams FJM, Sloane NJA: Pseudo-random sequences and arrays. Proceedings of the IEEE, 1976, 64,12: 1715–1729.

Wilms M, Eger M, Schanze T, Eckhorn R: Distributions of cortical activities in cat area 17/18 in response to visual and electrical retinal point stimuli: Investigations for a retina-implant. In 4. Tübinger Wahrnehmungskonferenz, Knirsch, 2001a .

Wilms M, Schanze T, Eger M, Eckhorn R: Assessing potential changes in cortical receptive field properties after electrical stimulation of the cat's retina. Development of an epi-retinal prosthesis. In N Elsner, U Eysel, editors, Göttingen Neurobiology Report 1999, volume 2, Thieme, 1999 .

Wilms M, Schanze T, Eger M, Eckhorn R: Cortical activity distributions in cat area 17/18 elicited by short visual and electrical retinal point stimuli: Investigations for a retina-implant. In N Elsner, GW Kreutzberg, editors, Göttingen Neurobiology Report 2001, volume 2, Thieme, 2001b .

Wörgötter F, Eysel U: Context, state and the receptive fields of striatal cortex cells. Trends Neurosci., 2000, 23.10: 497–503.

Wörgötter F, Suder K, Zhao Y, Kerscher N, Eysel U, Funke K: State-dependent receptive field restructuring in visual cortex. Nature, 1998, 396: 165–168.

Wyatt J, Rizzo J: Ocular implants for the blind. IEEE Spectrum, 1996, 33: 47–53.

Zeki S: A vision of the brain. Blackwell, 1st edition, 1993 pages 222–225.

Zrenner E, Miliczek KD, Gabel V, Graf H, Guenther E, Haemmerle H, Hoefflinger B, Kohler K, Nisch W, Schubert M, Stett A, Weiss S: The development of suretinal microphotodiodes for replacement of degenerated photoreceptors. Ophthalmic Research, 1997, 29: 269–280.

Zrenner E, Rüther K, Apfelstedt-Sylla E: Retinitis pigmentosa - Klinische Befunde, molekulargenetische Ergebnisse und Forschungsperspektiven. Der Ophthalmologe, 1992, 89: 5–21.

Zrenner E, Stett A, Weiss S, Aramant RB, Guenther E, Kohler K, Miliczek KD, Seiler MJ, Haemmerle H: Can subretinal microphotodiodes successfully replace degenerated photoreceptors? Vision Res., 1999, 39: 2555–2567.

Acknowledgements

It is a great pleasure to thank all those who made this dissertation possible.

Scientific CV of the author

Name:	Marcus Wilms
Date of Birth:	13th September 1970
Place of Birth:	Viersen, Germany
Nationality:	German
Marital Status:	Married
Present Address:	Georg-Voigt-Strasse 21 b
	35039 Marburg
	Tel: (06421) 96 4747
	eMail: derwilms@web.de

EDUCATION:

1996 - 2001	**Research Associate** in BMBF-funded Retina-Implant project Dept. of Neurophysics Philipps-University Marburg
2000	**Course on Laboratory Animal Science** School of Veterinary Medicine Hannover
1989 - 1996	**Diploma in Physics** at Rheinisch-Westfälische Technische Hochschule Aachen *Subjects studied:* Theoretical Physics, Experimental Physics, Solid State Physics, Biomedical Engineering. *Diploma thesis:* "Physical Properties of Single Photon Responses of the Ventral Nerve Photoreceptor Cell of Limulus Polyphemus". Dept. of Biology
1993	**Summer school** on "Experimental Methods on the Physics of Thin Films and Surfaces" at the Forschungszentrum Jülich
1989	**Abitur** Albertus-Magnus Gymnasium Dülken